SCIENTIFIC APPLICATIONS OF THE MOBILE TERRESTRIAL LASER SCANNER (M-TLS) SYSTEM

By

JUAN CARLOS FERNANDEZ DIAZ

A THESIS PRESENTED TO THE GRADUATE SCHOOL
OF THE UNIVERSITY OF FLORIDA IN PARTIAL FULFILLMENT
OF THE REQUIREMENTS FOR THE DEGREE OF
MASTER OF SCIENCE

UNIVERSITY OF FLORIDA
2007

To my parents and to my siblings. Who I am and what I have achieved is a result of your dedication, hard work and motivation. Also, to all the close friends who believed in me, encouraged me, and provided their support.

ACKNOWLEDGMENTS

First, DEO GRATIAS. Second, I want to acknowledge the great support and guidance from Ramesh Shrestha, William Carter and K. Clint Slatton. I thank them for sharing with me their knowledge, experience, and spirit, and for their continued motivation and commitment to make the geosensing graduates leaders in the field.

I gratefully acknowledge the persons and institutions that make the J.William Fulbright Foreign Scholarship program a reality. Through them I had the unique opportunity to achieve higher education in one of the top universities of the United States of America.

To all my friends, classmates and colleagues from the Geosensing Systems Engineering program and the NSF supported National Center for Airborne Laser Mapping, who provided me with invaluable support to complete this work.

Finally to the countless persons and institutions who in some way or another have contributed to my success in the UF Geosensing Graduate Program.

TABLE OF CONTENTS

page

LIST OF TABLES

LIST OF FIGURES

Abstract of Thesis Presented to the Graduate School
of the University of Florida in Partial Fulfillment of the
Requirements for the Degree of Master of Science

SCIENTIFIC APPLICATIONS OF THE MOBILE TERRESTRIAL
LASER SCANNER (M-TLS) SYSTEM

By

Juan Carlos Fernandez Diaz

August 2007

Chair: Ramesh Shrestha
Cochair: K. Clint Slatton
Major: Civil Engineering

Terrestrial Laser Scanners (TLS) are mapping instruments composed of a Laser rangefinder and an optical-mechanical system used to steer the laser beam across the surface of interest. The University of Florida Geosensing Engineering and Mapping (GEM) Research Center is working towards developing a Mobile Terrestrial Laser Scanner (M-TLS) system. The core of the M-TLS is a commercial 2-axis ground based laser scanner which is integrated to a mobile telescoping, rotating, and tilting platform which provides up to 6 degrees of freedom for performing scanning operations. A scanner built-in 6 megapixel digital camera and a digital video camera provide the M-TLS moving and still imaging capability. At the final stage of development the M-TLS positioning and navigation system will include a differential GPS array, tilt sensors and an inertial measuring unit which will allow data collection and georeferencing in both static and dynamic modes.

The M-TLS laser scanner is capable of generating 3D spatial and multispectral data sets. A typical dataset is composed of a cloud of millions of points for which 3D coordinates, laser intensity and/or RGB information are available for each one. Data can be collected in a range from 3m to 1500m for a target with an 80% reflectivity or 3m to 350m to targets with a 4%

reflectivity. The laser operates at a wavelength of 1535 nm, with a pulse width less than 10 ns and energy of less than 10 μjoules. The sampling separation can be adjusted down to 0.00115°, and the scanning speed is 2,000 points per second.

The M-TLS is a unique tool that enables GEM researchers to acquire high density point clouds from an advantageous terrestrial geometry, being a very valuable complement for Airborne Laser Scanner data sets. The applications of the M-TLS data sets are numerous in both the fields of science and engineering. Tested applications by the GEM center include urban mapping, as-built surveying, building damage assessment, bridge load analysis, forestry metrics extraction, beach erosion mapping, paleontology and archeology dig mapping, structural geology mapping, forest fire fuel estimation, soil spatial characterization and vehicle 3D modeling. This thesis centers around the novel applications of the M-TLS to specific scientific problems: thoroughly analyzing the applications to beach erosion hot spot mapping, soil roughness metrics extraction, and forestry metrics extraction.

CHAPTER 1
INTRODUCTION TO TERRESTRIAL LASER SCANNING

1.1 Geodesy and the Need for Measurements

Since early history mankind has had questions about nature, many of which can be answered if the proper measurements are made. The shape and size of the Earth was one of the first questions that humans asked. The earliest answers to those questions were based on folklore, common sense or primitive scientific method. These earliest conceptions had to do with supernatural creatures or deities and varied from culture to culture. The Greek philosophers did a lot of thinking about this issue. Homer, the epic Greek writer, popularized the conception that the Earth was a flat disk. It was around the time of Pythagoras, the Greek Mathematician who lived between 580 and 500 BC, that the idea that the Earth must be a sphere, the most perfect three dimensional geometric figure, took form. Following this Pythagorian principle other philosophers such as Aristotle and Archimedes tried to estimate the size of the Earth (Burkard, 1983; Smith, 1996).

The first scientific approach to measure the size of the Earth is credited to Eratosthenes (Burkard, 1983; Ewing & Mitchell, 1970; Smith, 1996), a Greek philosopher who also was a librarian in Alexandria. By studying the difference in the lengths of shadows cast by the Sun on the same day in the cities of Alexandria and Syene, and assuming that the Earth was a sphere, he was able to determine the angular separation between these two cities. Then by measuring the linear distance along the surface between the two cities he was able to estimate the size of the spherical Earth. The thoughts and works of these Greek philosophers led to the birth of the discipline that is called geodesy. Modern geodesy is defined as a branch of applied science that deals with the determination of the size, shape and orientation of the Earth and its gravitational field, and the variations of these parameters with time (Ewing & Mitchell, 1970).

A central focus of geodesy is determining the locations of points on the Earth, i.e., determining the coordinates of points relative to a well defined origin and reference frame. The evolution of surveying techniques and instrumentation led geodesists to treat positioning as two separate but related problems (Shrestha, 1983). For determining the horizontal position components, astronomical observations, triangulation, trilateration and traversing were some of the techniques employed. For determining the vertical position geodetic leveling, trigonometric leveling, barometric leveling or echo sounding techniques are employed (Smith, 1996).

As described in this introduction, the foundations of geodesy are math and physics, however, these rely on real measurements to model the world. The most basic geodetic measurements are the ones pertaining to time, distances and angles. If close attention is given to the history of geodesy it becomes clear that great leaps in knowledge came when new technology and its attendant instrumentation permitted leaps in the accuracy and precision of the measurements. Measuring the distance between widely separated points on Earth has always presented a challenge. One of the earliest successful methods of connecting widely separated points is a method known as triangulation. In a triangulation network, the angles of a chain of triangles are observed, along with one relatively short “baseline” length. From this single distance observation, and using trigonometry, all the sides of the triangles are computed.

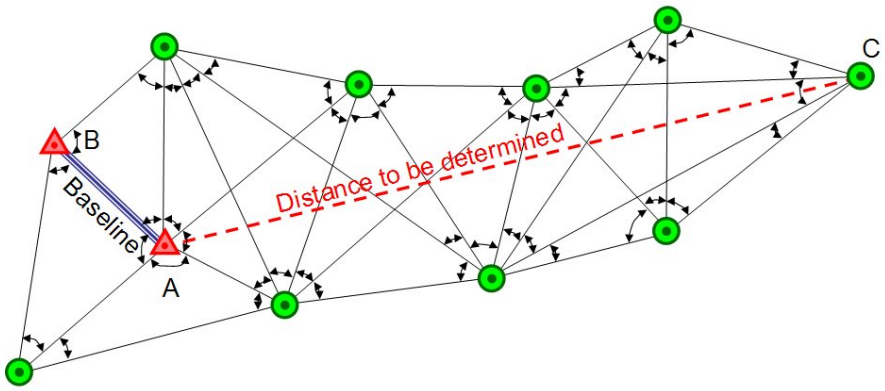

Figure 1-1. Triangulation network. The baselines A to B, as well as all the internal angles need to be measured to determine the A-C distance.

Triangulation is a time consuming method and errors in the angular and distance measurements propagate all along the network, reducing the precision and accuracy of the desired A to B distance. A breakthrough in distance measurements came in 1941, when a Swedish geodesist named Eric Bergstrand conceived a new technique to measure the time it took a beam of light to travel a known distance to determine the speed of light. He then realized that if the speed of light were accurately known, he could invert that technique and measure the distance between two points (Carter, 1973). This was the dawn of Electronic Distance Measurement or EDM. Because of the curvature of the Earth, it still remained necessary to determine the distance between widely separated points with a series of shorter distance measurements, in a method known as trilateration. The ease of use, accuracy and productivity of EDM instruments allowed trilateration to quickly displace triangulation.

Since 1941 EDM has evolved from a concept to a proven technology. Today there are many different forms of EDM instruments; some use radio frequencies, while others use light waves. EDM is used to measure distances small and astronomical, from micro structures to the distance between the Earth and the Moon, and even to neighboring planets. EDM has fulfilled the need for accurate distance measurements and has provided scientists and engineers with the data they need to build a model of our world.

During the past decades EDM instruments have been developed that include opto-mechanical scanners which steer the measuring beam over a selected pattern to collect a set of surface coordinates that can be used to create a mathematical representation of any surface in three-dimensional space. This thesis will present the experiences and results of almost two years of experimenting with a terrestrial LASER scanner to fulfill the need for measurements in several scientific fields such as forestry, soil science, geology and beach morphology.

1.2 History of LASER EDM and Scanners

In tracing the origins of LASER EDMs and scanners one can dig as deep as to the early astronomical observations aimed to estimate the velocity of light, performed by Romer and Huygen, or the ground-based experiments conducted by Hippolyte Fizeau, Leon Foucault, Simon Newcomb and Albert A. Michelson. However, most historians will set the origins of the EDM technique and instruments around the 1940s, highly influenced by the wartime efforts to develop the RADAR (Radio Detection and Ranging).

The origin of the first EDM instrument began in 1938 when the physicist and geodesist Erik Bergstrand, of the Swedish Geographical Survey Office, began to investigate the possibilities of using a Kerr cell as an electro-optical shutter to modulate a beam of light in an attempt to measure of the speed of light. Bergstrand's first operational instrument was reported to work in 1941. It used a Kerr Cell controlled by a crystal oscillator to modulate light from an ordinary incandescent light bulb. The light beam was collimated and projected by a parabolic mirror to a reflective corner cube array, the returning waveform was detected by a photomultiplier tube (PMT), and the round trip travel time was determined from the difference in phase of the transmitted and reflected modulated light beam (Carter, 1973; Smithsonian, N.D.).

In 1947 Bergstrand took his instrument to a 6 km baseline in Orland and obtained a measurement of the speed of light of 299,793.1 ±0.2 km per second. A year later in August 1948, Bergstand read a paper at the meeting of the International Association of Geodesy(IAG) held in Oslo, Norway. In that paper he explained that one could reverse the process, measure the light time of flight and use the value of the speed of light to compute the distances between two points. Soon after the meeting, Bergstand licensed the concept to the Swedish AGA (Svenska Aktiebolaget Gasacumulator) company to develop a commercial instrument.

AGA produced the first EDM instrument in the early 1950s, and marketed it as the "Geodimeter", short for "geodetic distance meter". The instrument used a Kerr cell to modulate the light, but the incandescent light bulb used by Bergstand was replaced with a mercury vapor light. The development of the Geodimeter by AGA continued through the 1950s and 1960s. The last model to use mercury lamps was the Geodimeter Model 6 introduced in 1964. Figure 1-2 shows an early production Geodimeter and its required corner cube reflector array. (NOAA, N.D.; Smithsonian, N.D.)

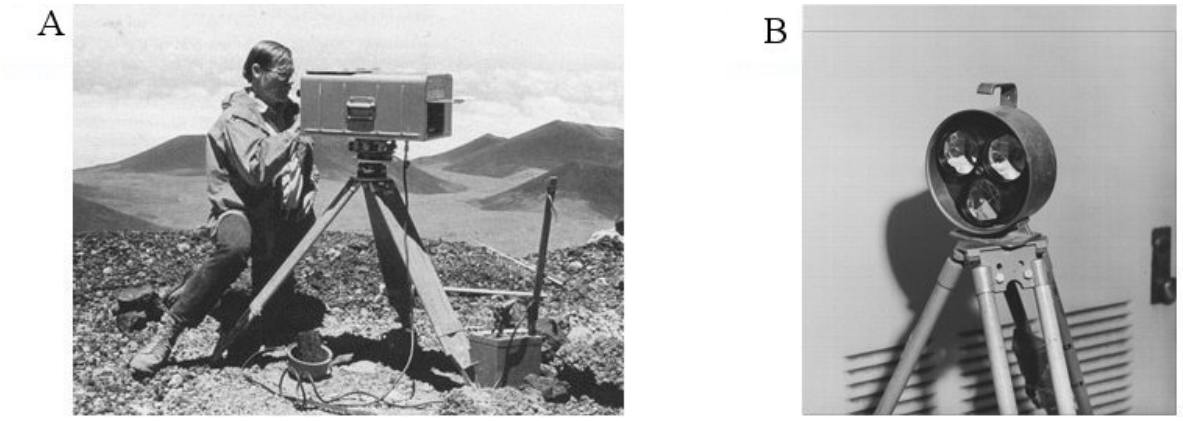

Figure 1-2. Early EDM equipment. A) AGA Geodimeter B) Corner cube reflectors. (Source: http://pubs.usgs.gov/gip/monitor/techniques.html , Last accessed March 16th, 2007)

Around the same time that AGA was producing the first Geodimeter, Harry A. Baumann of the South African Trigonometrical Survey and Trevor Lloyd Wadley of the Telecommunications Research Laboratory of the South African Council for Scientific and Industrial Research (CSIR) were developing the Tellurometer. The Tellurometer was the first commercial EDM instrument to use microwave beams to measure long distances with geodetic accuracy. The first model appeared in 1954, marketed as the Micro-Distancer M/RA 1. It was composed of two units, designated as master and remote, each set on the extreme points of the distance to be measured. Its range was between 30 and 50 km. The system used a continuous 3 GHz carrier frequency modulated by 10 megahertz and three other nearby frequencies. The

remote station retransmitted the incoming wave in a similar wave of more complex modulation, and the resulting phase shifts of the carrier and the modulating signals was used to unambiguously determine the distance traveled(NOAA, N.D.; Smithsonian, N.D.). The Tellurometer had the disadvantage that propagation of the microwave energy caused multipath reflections that degraded the system precision and accuracy.

Between 1938 to 1960 EDM evolved from a concept to widely used operational technique. However, its greatest leap in range and accuracy was yet to be realized. In 1954, Charles Townes at the University of Columbia invented the MASER (Microwave Amplification by Stimulated Emission of Radiation). (IEEE, N.D.) A maser is a cavity filled with gas (the first used ammonia gas) that when "pumped" with microwave radiation generates more microwave radiation.

1957 will always be remembered as the year that the Soviet Union launched the first artificial satellite – Sputnik I. But in November of 1957 Gordon Gould, a graduate student at Columbia University working with Townes, coined the acronym LASER, for Light Amplification by Stimulated Emission of Radiation, and described the principal components of the LASER. However, Gould did not publish his work, focusing his efforts in finding a position and the resources to try to build the LASER (IEEE, N.D.; Taylor, 2000).

In March 1958, Arthur Schawlow, apparently independently, also realized that the secret to the LASER involved an optical cavity, along the lines of a Fabry-Perot interferometer. Schawlow shared his idea with Charles Townes, his brother-in-law, and together they wrote a paper entitled "Infrared and Optical Masers" published in Physical Review Volume 112, number 6. (Schawlow & Townes, 1958)

The paper by Schawlow and Townes encouraged widespread thinking about how a Maser at optical wavelengths or LASER might be built. In 1960 Theodore Maiman and his colleagues

at Hughes Aircraft Company, succeeded in building the first solid state pulsed LASER, using a Ruby Rod. The LASER light was red with a wavelength of 0.6943 micrometers. That same year, Ali Javan and his colleagues from Bell Laboratories succeeded in building the first gas LASER. The HeNe LASER produced a continuous beam at five different wavelengths, achieving the highest power of 15 miliwatts at 1.153 micrometers (Javan et al., 1961 & Bennett, 2000).

The gas LASER was well suited for use in terrestrial EDM instruments. The light produced by a LASER is highly mono-chromatic and coherent (the photons of a LASER beam have a single wavelength, phase and move in the same direction). These attributes allow a LASER beam to have a small divergence, which means that the energy does not spread in the typical large spherical pattern of other light sources. Replacing the mercury vapor light with a HeNe LASER dramatically increased the operating range of the Geodimeter, and enabled the development of other smaller EDM instruments that quickly took over many aspects of surveying. The solid state pulsed ruby LASERs were not very energy efficient, and even the best “Q-switched” devices produced light pulses meters in length, making them poorly suited for short range geodetic surveying, but they could produce large quantities of energy, however, they would soon find a role in space geodesy (Carter, 1973).

For geodesists the main limitation of the improved LASER based EDM instruments was not the technical capabilities of the instruments themselves, but rather that the curvature and topography of the Earth limited the line of sight distances. As soon as the first artificial satellite was put in orbit in 1957, geodesist start to realize that a spaceborne “target” could greatly extend the measured baseline distances. At the same time scientists interested in the fields of gravity and relativity (which also are of great importance to geodesy) started working on a concept to employ a high density and high altitude artificial satellite to measure slow changes in the

universal gravitation constant (G) by accurate tracking the satellite path using retroreflectors and pulsed search lights (Bender et al; 1973).

In 1964 the first geodetic satellite (Beacon Explorer 22-B) was put in orbit, it had an array of corner cube reflectors that were illuminated using pulsed ruby LASER beams, the first ranging measurements obtained on Oct 31, 1964 (Carter, 1973; McGarry & Zagwodzki, 2005). However, even before the satellite was launched scientist realized that low orbiting satellites imposed several challenges such as very short visibility times and Earth's gravitational perturbations that would limit the quality of the relativist experiments.

As early as 1962 J.E. Faller had proposed the idea of placing a retroreflector on the surface of the Moon, which could be used to bounce back a LASER beam shot from the Earth. Between 1962 and 1964 experiments that included the detection of LASER beams bounced from the moon's surface were performed, and in 1965 the Lunar Ranging Experiment (LURE) multi-institutional team was formed. From 1965 to 1969 the LURE team focused their efforts to develop the largest and most sophisticated EDM system to date. Their first great milestone was reached on July 21st, 1969, when Neil Armstrong aligned and leveled the first corner cube reflector array on the surface of the moon.

Shortly after the installation of the array on the surface of the Moon, scientists on the Earth used the Lick Observatory's 3.05 meter telescope and a Q switched pulsed ruby LASER to aim a 2 arc minute divergence beam to the array. The first successful return signal from the array was obtained on August 1, 1969 at Lick Observatory, shortly after, on August 20th the McDonald Observatory reported success obtaining returns. Successful results were also reported that same year by the Air Force Cambridge Research Laboratories (AFCRL) Lunar Ranging Observatory in Arizona (Bender et al., 1973; Carter, 1973).

Down on Earth, AGA continued its development of the Geodimeter, introducing its Model 8 in 1967, which was its first instrument to use a helium-neon LASER. The LASER allowed the extension of the measuring range of the lamp units of 20 to 30 km to a range of 60 km in both day and night conditions. (Smithsonian, N.D. & Cheves, M; 1999)

In 1965 LASER Systems & Electronics, Inc. was established by a team of physicists and engineers who had worked at the Engineering Development Center at Arnold Air Force Base in Tullahoma, Tennessee. In 1970, LASER Systems & Electronics unveiled their first electronic distance measuring instrument: the Ranger. This was the first competition AGA faced; it used a red visible LASER and was capable of ranging distances from 1 meter to 6 km with an accuracy of ±5 mm +2 ppm. The EDM side of LASER Systems & Electronics was sold to Keuffel & Esser in 1971, which continued to manufacture the Ranger, RangeMaster and AutoRanger (1977) series. (NOAA, N.D.; Smithsonian, N.D.)

Figure 1-3. K+E RangeMaster III EDM unit. (Source: http://celebrating200years.noaa.gov/distance_tools/ranger.html, last accessed March 20th, 2007)

During the 1970's several surveying and electronic instrument companies developed EDM equipment. Among those companies were Cubic Corporation, Hewlett-Packard, Wild and Zeiss. One of the trends of this period was to combine an angular measuring device with an EDM into what was, and still is called a total station. These instruments continued to evolve into the simpler, more compact, accurate and cheaper units that can be found today. Most of these units

require the use of corner cube reflectors to get a strong return signal that enable a computation of the distance. Some EDM devices followed a different evolutionary path, and they are able to use weak return signals that are bounced back from natural targets such as the surface of the Earth or man made structures to compute the range from the instrument to the surface.

Between 1964 and 1966 Spectra-Physics, a company based in Mountain View, California developed a series of precise LASER-based EDMs. Its first prototype model, the Mark I, was designed as an airborne profile recorder (1964). The Mark II model was mounted in a Douglas A-26 and used to record a height profile across a stadium from a flying altitude of 300 meters. The Mark III model introduced in 1966 was marketed as a "Geodolite", its development was funded by the United States Army Engineer Topographic Laboratories. (Smithsonian, N.D.). This concept was further used not only as a profiler but also as a LASER altimeter and for bathymetric measurements.

Figure 1-4. Spectra-Physics Geodolite. (Source: http://historywired.si.edu/object.cfm?ID=22, last accessed March 20th, 2007)

In 1969 Hickman & Hogg were the first to report results on the feasibility of using a pulsed blue-green (frequency doubled NdYAG: Neodynium Yttrium Aluminum Garnet) LASER from an airborne platform for near-shore beach reconnaissance surveys over the shores of Lake Ontario. The concept was employed on the LASER altimeter experiment which was flown on the

Apollo 15, 16 & 17 (1971, 1972 & 1972) to the Moon. The LASER altimeter experiment obtained data on the altitude of the Command Service Module (CSM) above the lunar surface. The altimeter was used to support mapping and panoramic camera photography. It operated in two modes. In the independent mode it performed ranging measurements every 20 sec. In the slave mode when the metric camera was operated, it automatically emitted a LASER pulse to correspond to a midframe range for each frame (NASA, N.D.).

Also between 1971 and 1972 U.S. Naval Oceanographic Office (NAVOCEANO) performed flight tests of a prototype airborne LASER bathymetry profiler known as Pulsed Light Airborne Depth Sounder (PLADS). Even though those tests proved that airborne LASER bathymetry was feasible they were not conclusive in terms of operational system performance and cost benefit ratio. In 1973 a joint project between NASA and the Naval Oceanographic Office was established to develop and thoroughly test an Airborne LASER Bathymeter (ALB) System. The construction of the system was concluded in 1975. Using two pulsed LASER sources: a 2 kW 540 nm 6 nsec 10-200 pps Neon Ion LASER and a 2MW 532 nm 8 nsec 10-50 pps frequency doubled Nd Yag LASER. The receiver consisted of a 28 cm Cassegrain telescope, two narrowband 0.4 nm filters and an 8575 RCA photomultiplier tube. Over 200 hours of fight test were used to collect bathymetric data on Chincoteaque, VA, the Chesapeake Bay and Key West, FL. (Kim, Cervenka, Lankford; 1975)

In 1975 NASA Wallops Flight Center and AVCO Everett Research Laboratory proposed a bathymetric LIDAR Airborne system building on the previous experiences of the ALB. The proposal passed in 1977, and the new instrument was built in the same year by the AVCO Everette Corporation. The system became known as Airborne Oceanographic LIDAR (AOL). The program was sponsored by NASA, NAVOCEANO, and NOAA as an advanced testbed

sensor for altimetry, bathymetry, hydrography, and fluorosensing research. (Guenther et al., 1978; Mitchell, N.D.).

The first implementation of AOL was based on AVCO C-5000 gas (neon/nitrogen) 540.1 nm 2 kW 400 pps LASER, a 56 cm nutating scanner mirror, a 30.5 cm diameter Cassegranian f/4 telescope, a narrow band 0.4nm filter and a photomultiplier tube. This was the first implementation of a scanning airborne LIDAR altimeter. (Guenther et. al., 1978) The AOL was improved and redesigned several times over two decades. Improvements in enabling technologies such as differential GPS, Inertial Measuring Units (IMU) and best estimate trajectory algorithms continually enhanced the precision, accuracy and productivity of the AOL system. In 1994 the AOL underwent major hardware renovation and its topographic mapping and ocean fluorosensing functionalities were separated in to two new systems: The Airborne Topographic Mapper (ATM) and the AOL.

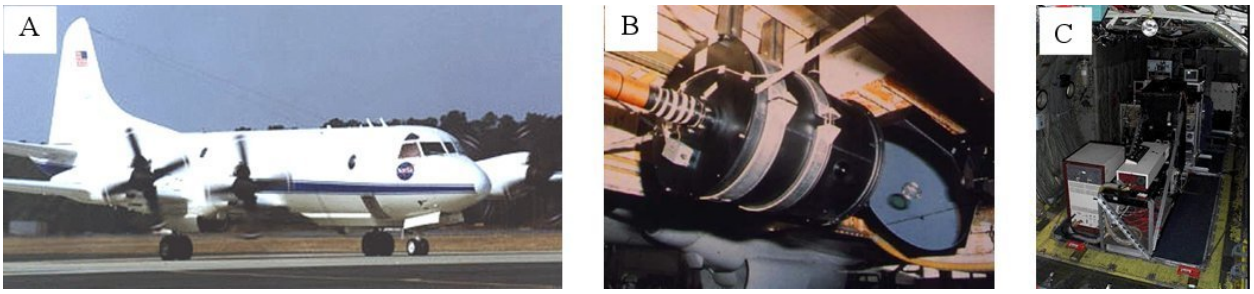

Figure 1-5. NASA AOL system. A) P3 Orion platform. B) Scannig mirror. C) Instrument rack. (Source http://sealevel2.jpl.nasa.gov/jr_oceanographer/oceanographer-williams.html, last accessed March 20, 2007)

The key technological advances that enabled the simple LASER profilers to become scanners were the development of more sensitive photodetectectors in the form of photomulipliers and avalanche photo diodes (which enabled the recovery of the reflected LASER pulses at lower signal-to-noise-ratios), LASER beam steering mechanisms (scanners and their respective encoders), and finally the the highly accurate Integrated Navigation Systems (INS).

The greatest advantage of airborne LASER scanning over original profiling methods is the dramatic increase in mapping coverage per unit of flight time.

Before 1995 all airborne LIDAR systems were custom built, highly expensive, and were only available for big research institutions and companies. However in 1995 Optech Inc., a company based in Toronto, Canada, offered the first commercial-off-the-shelf Airborne LIDAR Mapping System. Soon after other companies started offering their own systems: Riegl in 1996 with its low altitude scanner, Saab Survey Systems in 1997, and the Top Eye and Azimuth Corporation in 1998 with its Aeroscan system (which later was bought by Leica) (Baltsavias,1999; Flood,2001; Cheves, 2002).

As technology advanced the receiving electronics increased in sensitivity and timing accuracy, LASERs became smaller yet more powerful and robust, scanners became smaller and their encoders more precise. The continued miniaturization and improvements of the airborne LASER scanners led the manufacturers to consider the construction of small, short range LASER scanners that could be mounted on tripods or small vehicles. The first units were introduced in the late 1990's. Some referred to these units as terrestrial LASER scanners to differentiate them from their airborne counterparts. Today there is no universally accepted nomenclature as each manufacturer has created its own terminology. Riegl names them "3D Imaging Sensor", Optech calls them "LASER Ranging and Imaging Systems", Leica labels them "High-Definition Surveying Systems", but in the government and academic literature they are mainly referred as terrestrial LIDAR scanners.

Over the last 8 years Terrestrial LASER Scanners (TLS) have become very common and useful tools, mainly used in the areas of architecture, civil engineering, surveying and mapping. As mentioned earlier, science is always in need of measurements to model the world. Just as

their predecessor, the Airborne LASER Scanner, proved to be useful to different braches of natural science, TLS systems have great potential to provide dense and accurate range sampling of the environment in an efficient fashion.

1.3 TLS Subsystems and Principles of Operation

Terrestrial LASER Scanners are complex and very precise instruments; they are composed of two basic subsystems. The first subsystem is a LASER ranging device commonly called LIDAR for (Light Detection And Ranging) or LADAR (LASER Detection And Ranging). The latter is the nomenclature generally used by the military. The second subsystem is an optical and or mechanical device capable of steering the LASER beam in a scanning fashion over the area of interest. (Fröhlich & Mettenleiter, 2004) Even though TLS have these common elements, there are at least a dozen different types of instruments in the current market. This is due to the fact that there are 3 different ways a LIDAR can work and more than 3 ways to do scanning in two dimensions.

1.3.1 LIDAR Ranging Principles

A LIDAR can be used to measure the distance between two points in any of the three following ways: phase difference, time-of-flight and by optical triangulation. Each of these ranging approaches has its own set of strengths and weaknesses. In the phase difference units, the continuous LASER signal can be modulated at very high frequencies, and the numbers of ranges per second is generally limited only by the speed at which the data can be recorded. Thus PD units have the largest point collection throughput of all types of units. Their main limitation is the ambiguity of the range measurement. PD units are ideal in situations where very short acquisition times are desired, with sample collection rates in the order of hundreds of thousands of samples per second and mm level accuracy, but with limited range.

Optical Triangulation units are ideal for measuring distances of a few meters with micrometer level accuracy at high data rates. However, its accuracy depends on the relation between range and baseline distance and falls off rapidly with increasing range. Other limitations are that its performance can be degraded if the surface is not uniform in shape or reflectance and by the presence of noise in the form of exterior illumination from non-coherent light sources.(Curless & Levoy;1995)

Time of Flight units have the advantage that they provide unambiguous ranges from a few meters all the way to thousands of meters. However, because after they emit the LASER pulse they must wait until there is a return signal before they can send the next pulse. The point collection throughputs are relatively low compared to the PD and OT units. However, is worth mentioning that there are some special airborne and long range LIDAR systems that are able to work with multiple pulses at a given time. The other limitation is that the range resolution (the ability to separate proximate object at different ranges) decreases as the pulse width increases. That means that for pulsed LIDAR there is always a tradeoff between range and range resolution. However they are established as the most common type of ranging LIDARs.

1.3.1.1 Phase difference measurement (PD)

Phase Difference was the ranging method used in early geodetic EDMs like the Geodimeter & Tellurometer and on current systems that employ continuous wave (CW) LASERs. In these LIDARs the amplitude of the LASER “wave” is modulated and the phase difference between the outgoing and reflected wave is measured. The problem with this method is that phase differences are not unique, there is always an ambiguity about the number of complete modulating wave cycles that have occurred prior to the phase difference. Most current TLS that work under this modality do not provide ambiguity resolution so they have a limited range usually less than 100 meters (Wehr & Lohr, 1999 ;Fröhlich & Mettenleiter, 2004). It is

important to clarify that the LASER has its own natural frequency and wavelength. Optical LASERs have wavelengths in the range of .4 to 1.5 μm. The phase difference that is used to determine the target range is based on the amplitude modulating signal (not the LASER natural wavelength), which has a wavelength in the order of several to hundreds of meters.

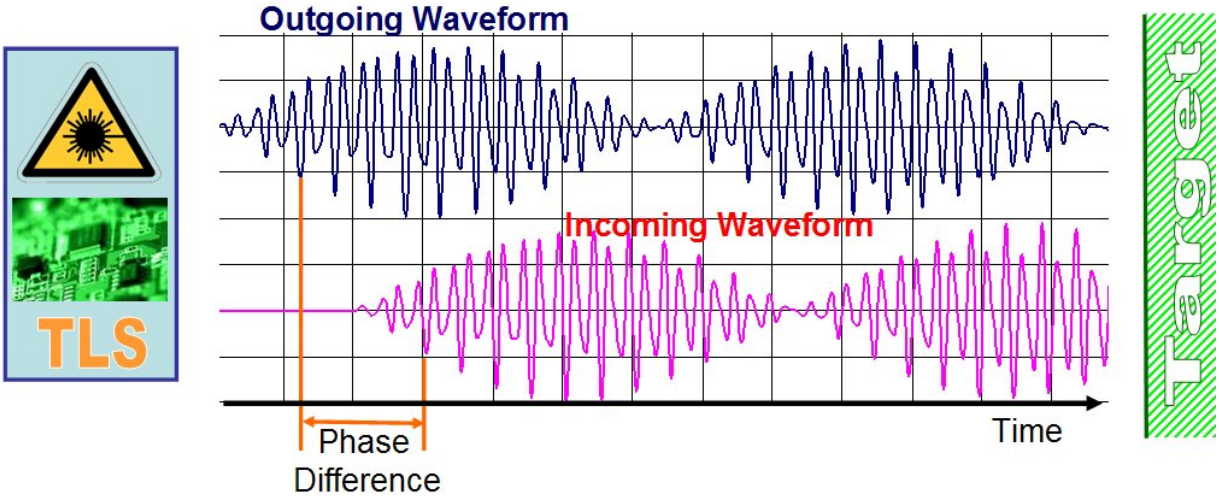

Figure 1-6. Phase difference ranging principle.

Table 1-1. Phase difference ranging principles expressions and equations.

Parameter	Formula
Ambiguous phase difference	$APD = 2\pi \times n + \phi$
Unambiguous phase difference before one full wave cycle	ϕ
2 way travel time before one full wave cycle	$t_{2way} = \frac{\phi}{2\pi} \times f_{carrier} = \frac{\phi}{2\pi} \times \frac{\lambda_{long}}{c}$
Long amplitude modulating signal wavelength	$\lambda_{long} = \frac{c}{f_{carrier}}$
Short amplitude modulating signal wavelength	λ_{short}
Speed of light	c
Signal to noise ratio	s/n
Maximum unambiguous range	$R_{\max} = \frac{\lambda_{long}}{2}$
Range	$R = \frac{1}{2} \times c \times \frac{\phi}{2\pi} \times f_{carrier} = \frac{\lambda_{long}}{4\pi} \times \phi$
Range resolution	$\Delta R = \frac{\lambda_{short}}{4\pi} \times \Delta\phi$
Single shot range accuracy	$\sigma_R \sim \frac{\lambda_{short}}{4\pi} \times \frac{1}{\sqrt{s/n}}$

1.3.1.2 Time of flight (TOF)

In PD LIDARs the phase difference of the continuous LASER is used to determine the 2 way time-of-flight of the modulated signal. As mentioned in the previous section, the main disadvantage of this method is the ambiguous range. An alternative that help overcome this limitation came with the development of Q-switching by McClung and Hellwarth in 1961 (McClung & Hellwarth,1962). This invention enabled the emission of very energetic LASER pulses rather than the continuous wave beams. This allowed to directly measure the 2 way time-of-flight without any ambiguity. However, even when these pulses are relatively short in time, generally in the order of a few nanoseconds, at the high speed that light travels this translates into several centimeters (e.g. 10ns = 3.0 m). In order to obtain the sub-centimeter accuracy an specialized electronic circuit called a Constant Fraction Discriminator (CFD) is used to precisely time a specific point on the pulse (generally the half point of the pulse amplitude). With discrete packets of light and the CFD is a simple matter to measure with high accuracy the time difference between the emission of the pulse and the detection of its reflected return. This method provides unambiguous range measurements of distances limited only by the dispersion of the LASER energy and the sensitivity of the detector (Wehr & Lohr, 1999).

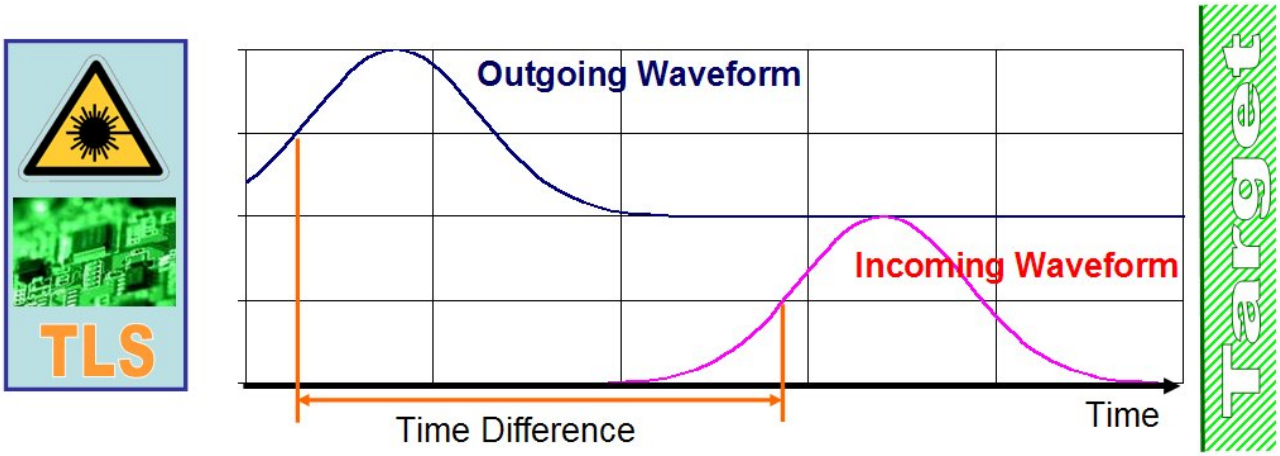

Figure 1-7. Time of flight ranging principle.

Table 1-2. Time of flight ranging principles expressions and equations.

Parameter	Formula
2 way travel time	t
Pulse width	Δt
Speed of light	c
Signal to noise ratio	s/n
Pulse rise time	$t_{pulserise}$
Range	$R = \frac{1}{2} \times c \times t$
Range resolution	$\Delta R = \frac{1}{2} \times c \times \Delta t$
Single shot range accuracy	$\sigma_R \sim \frac{c \times t_{pulse\ rise}}{2} \times \frac{1}{\sqrt{s/n}}$

1.3.1.3 Optical triangulation (OT)

In PD and TOF the outgoing and incoming LASER beam follow the same optical path, however on OT the reflected waveform is observed from a different vantage point. In OT units a LASER beam is steered by a scanning mirror over the target surface and its reflection is collected through a lens that focuses an image on a position sensitive detector such a CCD array. The position of the spot image on the pixels of the camera, the scanner angle and the LASER to lens optic center baseline is then processed using trigonometry to determine the distance to the target. (Beraldin et al., 2003)

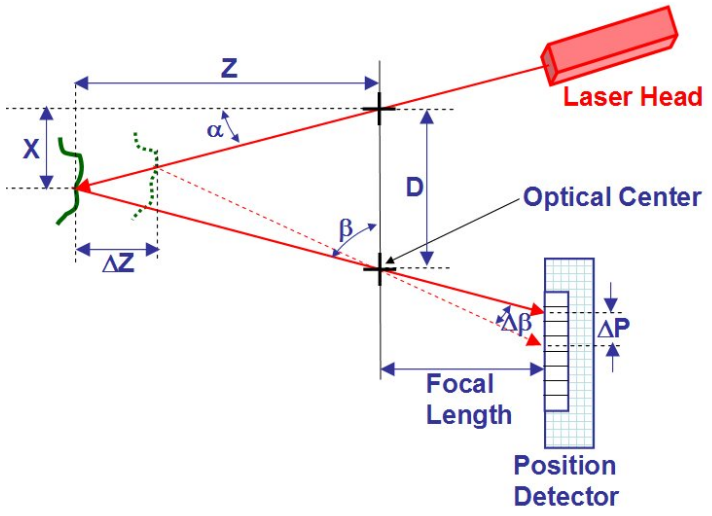

Figure 1-8. Optical triangulation ranging principle.

Table 1-3. Optical triangulation ranging principles expressions and equations.

Parameter	Formula
Baseline distance	D
Deflection angle of the LASER beam	α
Position of the imaged spot	p
Focal length	f
Range	$Z = \frac{D \times f}{p + f \times \tan(\alpha)}$
"Horizontal" position	$X = Z \times \tan(\alpha)$
Position accuracy	σ_p
Single shot ranging accuracy	$\sigma_z \sim \frac{Z^2}{f \times D} \times \sigma_p$

1.3.2 Scanning Mechanisms

Traditionally, geodetic scanning instruments have used reflective optics coupled to a mechanical system, although some newer instruments (CATS & Jigsaw) use refractive scanning elements such as Risley prisms (Carter et al., 2005; Marino & Davis, 2005). Current TLS systems have a 2 axis capability. This is achieved in its simplest implementation by a single line scanner through a rotating or nutating mirror, and the second scanning axis is obtained by rotating the complete instrument as shown in Figure 1-9.

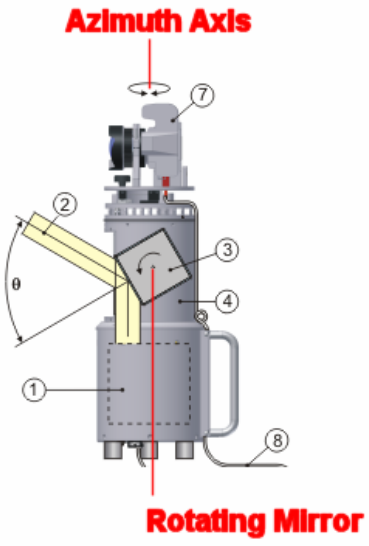

Figure 1-9. Scanning axes on a panoramic view scanner. (Adapted from original source at: http://www.riegl.com/terrestrial_scanners/lms-z390_/390_all.htm, last accessed March 20, 2007)

This type of scanner is usually called a Panoramic View Scanner and is capable of scanning 360° in azimuth and from +75° to -75° in elevation. The other type of scanner is called Camera View Scanner. It is usually implemented by two perpendicular deflection mirrors, one for the azimuth and the other for the elevation. This type of scanner has a fixed field of view typically of 45°x45°, but it can be extended to a panoramic field of view with the aid of optional pan and tilt bases. (Fröhlich & Mettenleiter, 2004)

1.4 Technical Characteristics and Specifications of TLS

Currently there are more than 12 commercial-off-the-shelf TLS systems. With this wide range of options, defining which is the right TLS for a project depends on the careful analysis of the instruments specifications and the project requirements. Appendix A has a description of commercial TLS units. Key specifications of TLS are: range, range resolution, precision, accuracy, azimuth & elevation resolution or point spacing, LASER type & wavelength, and the scan rate, field of view. Subsystem specific characteristics will be described first as they have an impact on integrated system characteristics.

LASER wavelength: Even when the manufacturer won't provide the exact wavelength of the LASER it will generally give a range such as green, red or near infrared. Some consideration must be given to the LASER wavelength of the TLS. Visible LASERS will be best when there is the need for water and glass penetration or when mapping wet surfaces. Most of the energy of infrared LASERs will be absorbed by moist surfaces and the return signal will be very weak.

1.4.1 LASER Type

LASER type will be either pulsed or continuous wave. The advantage or disadvantage of each type was discussed in the previous section.

1.4.2 LASER Class

The Class of a LASER is defined by the American National Standards Institute (ANSI) according to the degree of hazard presented to eye safety based on a maximum permissible exposure (MPE). The class depends on the LASER power and wavelength. TLS must be built to meet eyes safety regulations, and the operator must be aware of what are previsions and precautions that must be taken. Table 1-4 provides a summary of the LASER classification scheme.

Table 1-4. LASER classification

Class	Description
Class I	Safe for use under all reasonably-anticipated conditions of use. It is not expected that the MPE can be exceeded. This class may include LASERs of a higher class whose beams are confined within a suitable enclosure so that access to LASER radiation is physically prevented.
Class IM	This LASERs produce large-diameter beams, or beams that are divergent. The MPE for a Class 1M LASER cannot normally be exceeded unless focusing or imaging optics are used to narrow down the beam. If the beam is refocused, the Class has to be upgraded.
Class II	Emits in the visible region. It is presumed that the human blink reflex will be sufficient to prevent damaging exposure
Class IIM	They emit in the visible region in the form of a large diameter or divergent beam. It is presumed that the human blink reflex will be sufficient to prevent damaging exposure.
Class IIIR	All continuous wave LASERs which may produce up to five times the emission limit for Class 1 or class 2 LASERs. Although the MPE can be exceeded, the risk of injury is low. The LASER can produce no more than 5 mW in the visible region.
Class IIIB	They produce light of an intensity such that the MPE for eye exposure may be exceeded and direct viewing of the beam is potentially serious.
Class IV	High power (typically more than 500 mW if cw, or 10 J/cm² if pulsed). These are hazardous to view at all times, may cause devastating and permanent eye damage, may have sufficient energy to ignite materials, and may cause significant skin damage.

1.4.3 LASER Beam Divergence

The LASER beam divergence will determine the footprint area at a given range. For an accurate mapping one will require the smallest footprint size because the LIDAR computes an average range of the entire illuminated area. The larger the area, the more chance of slope, reflectivity and smoothness variations affecting the range measurement.

1.4.4 Point Spacing

Point Spacing or angular resolution (azimuth and elevation) is the measure of the smallest angular step the scanner mechanism can steer the LASER beam. In other words, it is the measure of the angular or linear separation between adjacent LASER shots.

1.4.5 Range

Range is perhaps the most important characteristic of a TLS, and performance specifications should include both a maximum and minimum ranging distance. Range will vary greatly between units based on the LIDAR principle of operation and the specific design characteristics (pulsed energy and detector sensitivity for TOF, long wavelength for PD and baseline distance for OT).

1.4.6 Range Resolution

Range resolution refers to the ability of the TLS to distinguish between adjacent features in the range direction. Range resolution depends on pulse width on TOF units, of phase measuring resolution on PD, and on baseline distance and the spatial resolution of the position detector in OT units.

1.4.7 Precision and Accuracy

Precision and accuracy are often used usually interchangeably, however, they are not the same concept. Precision is the statistical closeness of a set of repeated measurements while accuracy is closeness of the best estimate value obtained by the measurements to the accepted true “value” of the measured quantity. (DMA, 1991) Baltsavias(1999) states that “ranging precision” is inversely proportional to the square root of the signal to noise ratio and gives expressions for the estimate of the “ranging precision” for TOF and PD LIDARs. Wehr & Lohr (1999) present the same expressions but they refer to them as “ranging accuracy”. What they are in fact are referring is not to either ranging accuracy or precision but rather estimates of ranging

errors as a function of intrinsic electronic parameters which will have some relation to the ranging precision and accuracy.

Before describing TLS precision or accuracy it is necessary to consider that they reconstruct reality by measuring ranges and angles. The final coordinates of points are derived from computations using the observed ranges and angles, and they are subject to a combination of errors from each of the hardware subsystems as well as rounding and other computational errors of the software subsystem. It impossible to derive closed form equations for a TLS precision and accuracy; this parameters must be estimated through extensive laboratory testing.

The overall precision of a TLS system is the degree of repeatability of its range and position measurements. There are two types of precision, single measurement precision and averaged measurement precision. The single measurement precision can be understood as the theoretical error in measuring a single point only once. Averaged measurement precision is obtained if the system takes multiple measurements of a single point and computes a mean and standard deviation from these observations. To determine accuracy a manufacturer has to test the measurements derived from TLS using a higher quality data set to see how well they agree. Manufactures usually quote the modeled accuracy, which is derived from the fitting multiple point measurements to a primitive model. (Iavarone, 2002)

CHAPTER 2
UF MOBILE TERRESTRIAL LASER SCANNING (M-TLS) SYSTEM

2.1 Evolution of the M-TLS Concept

The University of Florida (UF) was a pioneer in the application of commercial airborne laser mapping systems to the fields of environmental and infrastructure surveying. In October, 1996, a demonstration/test project was conducted for the Florida Department of Environmental Protection in collaboration with Optech, the Florida Department of Transportation (FDOT) and the US Geological Survey Center for Coastal Geology. During project LASER (Laser Swath-mapping Evaluation and Resurvey) more than three hundred kilometers of beaches (Mexico Beach, FL, to the western tip of Perdido Key, AL) and a portion of Interstate 10 were mapped using an Optech Inc. ALTM 1020 laser ranging system. (Carter & Shrestha, 1997). Shortly after, in 1998 UF in conjunction with the Florida International University (FIU) purchased its first LIDAR mapping unit, an Optech 1020 ALTM.

In early 2001, the University of Florida (UF), the National Geodetic Survey (NGS), the FAA, and Optech, Inc. conducted a field test to explore using an Airborne Laser Scanner for Detecting Airport Obstructions at the Gainesville Regional Airport. (Parrish et al., 2005) During this research UF personnel tested a preproduction prototype of an Optech's tripod mounted LIDAR unit named "Intelligent Laser Ranging Imaging System" (ILRIS-3D).

After the tragic attacks on September 11, 2001, the Office of the Deputy Under-secretary of Defense approached the US Army's Joint Precision Strike Demonstration (JPSD) to inquire about specific technology capabilities to aid the surveying the NY ground zero. JPSD approached Optech and the University of Florida Geosensing Systems Engineering center for personnel and equipment support. A multi institutional group was established and laser

surveying began on September 18. Besides the airborne unit, two ILRIS-3D systems were deployed to map rubble piles and damaged building structures (Kern, 2001).

These experiences with the Terrestrial Laser Scanner made the UF researches quickly realize the potential of the technology as a valuable complement to the airborne laser unit. During 2002 the UF Geosensing Systems Engineering (GSE) division acquired and fully tested an ILRIS-3D unit. The results of the tests are thoroughly discussed in the 2002 Master thesis "Applications of Laser Scanning and Imaging Systems" by GSE student Devin Robert Drake.

In 2002 UF prepared a proposal for the Florida Department of Transportation of a Mobile Laser Surveying System (MOBLASS). Potential applications of the system were identified to include the precise positioning, the continued evaluation and documentation of the primary components of the transportation infrastructure (center lines, guardrails, signs, bridges maintenance facilities). The proposal consisted on a twelve passenger van equipped with an ILRIS 3D unit mounted on a telescopic pan tilt base, a GPS array for positional and azimuth determination, power leveling and stabilizing units, an auxiliary power generator, an operator control console with display, a PC for data reduction and analysis, a wireless data link for realtime transmission to the operational center and upgrade capabilities for an IMU and other types of sensors (digital imaging, hyperspectral, ground penetrating radar). At that point in time technology just permitted static mapping and the proposal was developed as a Stop-Map-and – Go system, unfortunately FDOT decided not to fund the development of the MOBLASS. Figure 2-1 shows a survey vehicle developed around a concept similar to MOBLASS.

In 2005 the UF Geosensing Systems Engineering division decided to develop the MOBLASS concept with its own resources. The system name was changed to M-TLS for Mobile Terrestrial Laser Scanning system and is based on a new version of the ILRIS 3D system

which enables the interfacing with an Optech produced Pan Tilt base. Other mayor change in the concept is that the vehicle is now a 4x4 truck which extends the terrain operation capabilities and allows an increased instrumental payload. The M-TLS is a unique tool that enables the acquisition of high density point clouds from an advantageous terrestrial geometry, being a very valuable complement for Airborne Laser Scanner data sets.

Figure 2-1. Survey vehicle with a similar concept to MOBLASS.

2.2 M-TLS Subsystems

2.2.1 LIDAR Unit

The core of the M-TLS is a commercial 2-axis ground based laser scanner which is integrated to a mobile telescoping, rotating and tilting platform which provide up to 6 degrees of freedom for performing scanning operations. A scanner built-in 6 megapixel digital camera and a digital video camera provide the M-TLS still and video imagining capability.

The laser scanner is an Optech ILRIS-3_6D, which is capable of generating XYZ with laser intensity or RGB textured point clouds in a range from 3 m to 1500 m for a target with an 80% reflectivity or 3 m to 350 m to targets with a 4% reflectivity. The laser operates at a wavelength of 1535 nm, with a pulse width less than 10 ns and energy of less than 10 μjoules. The sample separation can be adjusted down to 0.00115°, and the scanning speed is 2,000 points per second.

Currently the ILRIS is only capable of performing its scanning and mapping operations on a static mode. In a near future Optech will release a unit with “on-the-move” mapping capabilities, at that point is expected that the M-TLS will perform dynamic mapping operations.

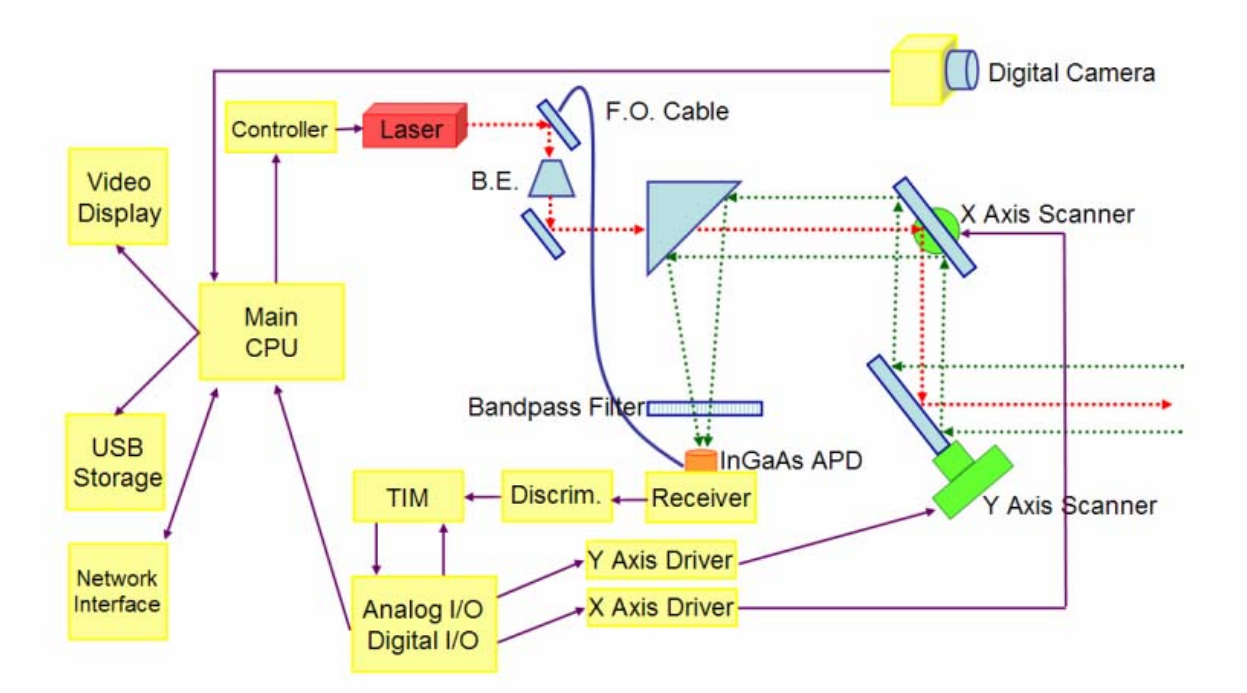

Figure 2-2. OPTECH ILRIS block diagram.

Figure 2-2 shows a block diagram of the ILRIS unit. At a very high level the internal operation of the ILRIS is quite simple. A central microprocessor controls the different subsystems, collect, analyzes and displays data and information. The computer commands a laser controller to fire a pulse, the laser beam generated by a Nd YAG laser is passed thru a non linear crystal that shifts its natural frequency from 1064 nm to 1535 nm. Then the laser beam pass thru a beam expander and a small amount of photons are diverted thru a fiber optic cable to start the time of flight timer.

After the beam is expanded it passes through an optical element that reflects the returning beam to the detector. The beam is then deflected by the vertical and horizontal scanning mirror to the target. The position of each of the mirrors is controlled by the scanner axis drivers and the

central computer. Most of the targets have quasi-Lambertian reflective properties and will reflect the laser beam as a distorted waveform, part of that waveform will return in the same optical path of the outgoing beam. The incoming waveform will be reflected by the scanning mirrors to a fixed parabolic mirror that focus the waveform on to the detector. Prior to entering the detector a narrowband optical filter centered at the 1535 nm limits the noise entering the system. When the returning laser photons arrive at the detector, which is an indium gallium arsenide (InGaAs) Avalanche Photo Diode (APD), a voltage is generated between its terminals. The output voltage is read by an A/D converter where the signal is digitized and sent to a Constant Fraction Discriminator (CFD). The CFD is an electronic device designed to produce accurate timing information from signals of varying amplitudes but the same rise time. CFD usually achieve this by splitting the input signal, attenuating half of it and delaying the other half, then feeding the two halves into a fast comparator with the delayed input inverted. By doing this CFD is capable of triggering a timing signal at a constant fraction of the input amplitude. The CFD trigger is fed into the precise Time Interval Meter (TIM) which was original started by the outgoing pulse feed to the detector thru the optical fiber. The TIM computed the time difference between the outgoing and incoming pulse thus determining the 2 way time-of-flight. The computer then calculates the range to the target records it on it internal memory and commands the emission of a new pulse and the entire process is repeated until the defined area of interest is scanned.

The block diagram shows additional subcomponents of the ILRIS unit. On-board 6-megapixel CMOS digital camera is used to provide the operator with a low scan rate video and high resolution stills of the scan area. The Camera is boresight calibrated with the LIDAR to provide red, green and blue channels to each laser point. The output from the camera is also projected with other control information to a 5.5 ” x 4 ” LCD viewfinder. On board data storage

is done on a conventional USB jump drive. The controlling and commanding of the ILRIS is performed thru proprietary software called “Controller” which runs from a computer or pocket pc. To provide connectivity to the PC the ILRIS has two network interfaces devices: a Ethernet interface card (IEEE 802.3) and a wireless network card (IEEE 802.11). Power to the ILRIS is provided from a 28 V DC battery pack or from a 120 VAC/28 VDC power adapter.

2.2.2 Vehicle

The vehicle selected for the M-TLS system is a Ford F250 4x4 crew cab long bed truck. The truck has undergone several modifications including the installation of a steel frame for mounting the telescopic lift and the installation of four electrical jacks which will enable automatic vehicle stabilization and leveling. The vehicle 4x4 capability allows the execution of off-road mapping projects, its 1600+ kg of cargo capacity allows the loading of the 374 kg lift with ample capacity for mapping, positioning and auxiliary equipment. Figure 2-3 shows the M-TLS truck with the lift deployed at half height.

Figure 2-3. Mobile Terrestrial Laser Scanning (M-TLS) system: truck, lift and ILRIS.

2.2.3 Lift

The lift is an AC powered JLG Push-Around Vertical Lift model AM 25. This lift has a stowed height of 1.97 m and once deployed it extends to 9.45 m. The truck was modified by bolting a steel frame directly to the back chassis, the lift then rests over the steel frame. An instrument aluminum frame was constructed to support the ILRIS, its power supply and an electronic tilt meter. The instrument frame is mounted on the top of the lift. With all these provision the ILRIS scanner can be lifted to a vantage point of up to 12 meters above ground level.

2.2.4 Power Subsystem

The M-TLS have components that require both AC and DC power. To supply the power requirements the M-TLS system has a Briggs & Stratton 6200 Watts electric start generator and a 12V DC battery bank. The electric generator is used when the lift needs to raised or lowered and to charge the battery bank. DC power is directly available from the battery bank and low power AC devices can be fed thru a DC to AC power inverter from the battery bank. Figure 2-4 shows the power plant installed on the truck bed.

Figure 2-4. M-TLS deployed in Georgia, showing the power generator and field computer on the truck bed.

2.2.5 Pan Tilt Base

Currently there are two pan & tilt bases available on the M-TLS system. The first one is an Optech manufactured base that is connected to the ILRIS 3D unit and controlled from the ILRIS control software. This base allows a complete 360° rotation in azimuth and 70° in elevation, with the 40°x40° ILRIS's field of view the tilt base permits a -20° to 90°or a -90° to -20° elevation coverage. The advantage of using this base is that the scan data can be automatically de-rotated and de-tilted in the Parsing process, yielding a complete coherent data set. The disadvantage is that when the ILRIS is powered up and it detects that is connected to a pan tilt base it will capture a 360° panoramic picture composed of 10 individual digital camera frames and this can be extremely time consuming if the user is just interested in scanning a narrow field. To overcome this disadvantage a second pan tilt base is available; the base was manufactured by QuickSet International and is designed for the operation of surveillance cameras. It has a loading capacity of 40 kg and a rotation range of ±217.5° in azimuth and ±90° in elevation. This pan tilt base can be controlled from a PC or from an analog joystick console. Figure 2-5 shows the two available pan tilt bases for the M-TLS.

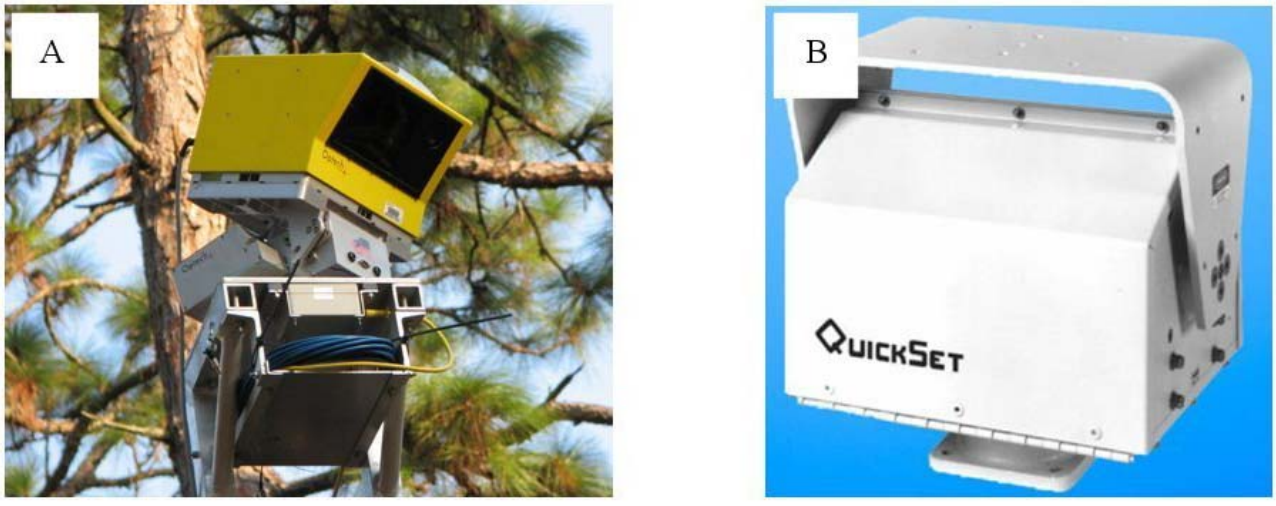

Figure 2-5. M-TLS pan tilt bases. A) Optech 360 base. B) Quickset QPT pan tilt base.

2.2.6 Video Camera

The MTLS is equipped with a Samsung SCC-C4201 high resolution color video camera. The camera has a built in X22 optical lens and an X10 digital zoom to provide an effective, enhanced focal length of 3.6 to 79.2mm. The 410,000 pixels CCD (811 x 508) outputs NTSC with 480 Horizontal Lines and 350 Vertical Lines. The video provides the operator with wide and narrow views of the scan project area. The output can be directly viewed on a TV screen or on the computer thru a video capture card. The video camera can also be used as a surveying and mapping tool during operation of the M-TLS dynamic mode. The video camera is mounted on top of the ILRIS unit by means of a special housing as shown in Figure 2-6.

2.2.7 On Board PC

Currently only data collection is done onboard. For this purpose a laptop containing the ILRIS controller software is used. The ILRIS to PC connection is done by the wireless peer to peer network. Data is stored in both the ILRIS USB disk and on the laptop hard drive. On a future a central computer that will control and record the data from the ILRIS, INS and cameras will be installed.

2.2.8 GPS

At this point in time the ILRIS unit can not do direct georeferencing. In the static mode, when a geo-referenced dataset is desired the use of GPS control points is required. This is usually done by surveying at least three control points well distributed both vertically and horizontally on the area to be scanned. An additional control point can be located by installing a GPS antenna on top of the ILRIS unit, by adding the proper XYZ offsets the GPS coordinates of that antenna reference point can be translated to the ILRIS coordinate origin. Figure 2-6 shows the provisions for the installation of a medium size L1/L2 marine antenna on the ILRIS unit. For the purpose of surveying the control points a set of geodetic grade GPS receiver are available

which include units from the ASHTECH models Z-Xtreme, Z-Surveyor and Z-12. Ashtech L1/L2 Choke Ring and marine L1/L2 model 700700 are used to collect the GPS signals. Figure 2-7 shows an array of GPS stations used for geo-referencing of M-TLS data set during the forestry experiment.

Figure 2-6. The ILRIS unit with on axis video camera and GPS antenna.

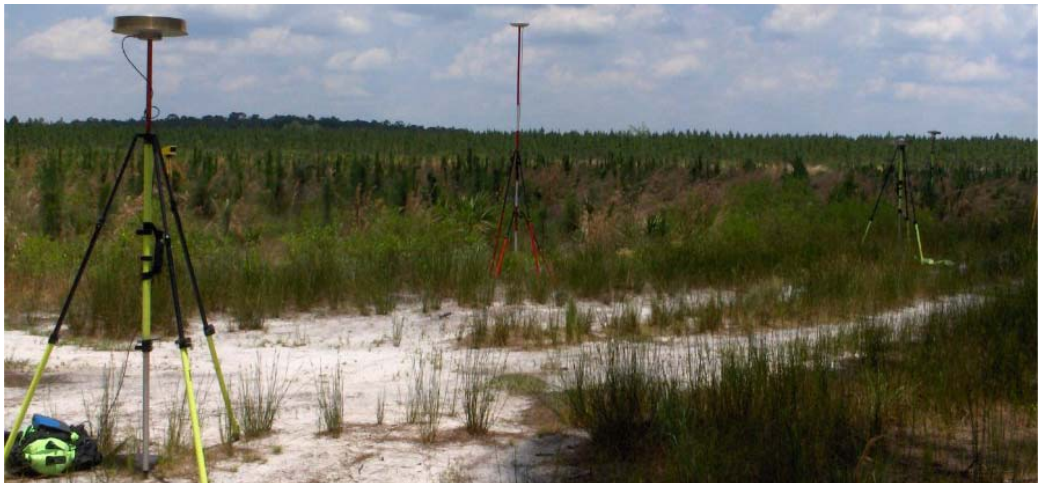
Figure 2-7. Array of geodetic quality GPS base stations used for geo-referencing.

2.2.9 Tiltmeter

An electronic tilt meter is installed under the instrument frame on the lift to measure the vibrations and motions to which the ILRIS is subjected and to ensure that during scanning operations the platform remains as steady as possible. The red ellipse on Figure 2-8 marks the installation position of the Tiltmeter unit.

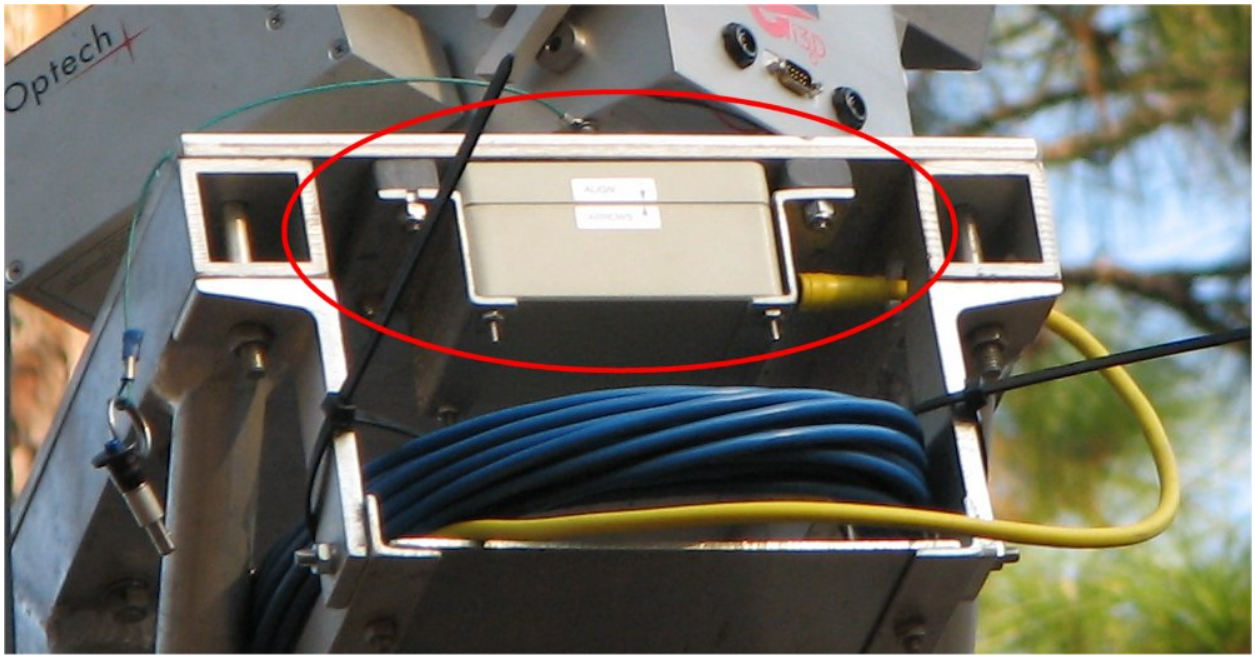

Figure 2-8. Installation of the tiltmeter unit on the instrument frame.

2.2.10 INS

When Optech releases the new generation of ILRIS with on the move scanning capability, the M-TLS will be capable of performing mapping operations in the dynamic mode. At this point the installation of an Integrated Navigation System must be performed. This can be in the form of a canned solution like the Applanix POS LV or with an in-house developed INS. The Applanix POS LV system includes a single frequency two antenna survey grade GPS array and an Inertial Measuring Unit. The IMU grade depends of the clearance obtained by the US Department of State regarding the International Traffic in Arms Regulations.

CHAPTER 3
WORKFLOW OF M-TLS OPERATIONS

3.1 Data Collection

Data collection design is the first step in M-TLS operations. There are no written rules on how to perform a data collection, it depends on very specific details of the project and the experience of the operator. Data collection design starts with an analysis of the requirements of area of interest; desired resolution or laser point spacing; laser return intensity or RGB texture; data set reference (sensor XYZ or geo-referenced to a particular datum) and accessibility to the scan area. With these inputs the operator defines the data set acquisition strategy that includes the selection of the scanning geometries (number and orientation of the scans) and the design of the GPS Control Points Network if the data set needs to be referenced to a particular datum rather than the natural XYZ sensor frame of reference.

Collection is performed with the Optech proprietary software “Controller”. The controller main screen displays a color image which covers the 40°x40° scannable field of view. The operator then selects a Region of Interest (ROI) to be scanned and based on a preliminary range acquisition, adjusts the spot spacing in angular or linear units. After setting the data storage directory the scan can be initiated. When using the Optech pan and tilt base the ILRIS will acquire a 360°x40° panorama consisting of 10 overlapping still frames. The complete panorama will be displayed in Controller window and the user can then set the ROI to be scanned. Figure 3-1 presents a screen capture of the Controller software.

For particular projects several setups are required. In some cases a combination of panoramic and frame scans have to be performed. The integrated M-TLS system provides up to 6 degrees of freedom (4 rotations and 2 translations) for performing scanning operations that guarantee that all possible facets of the object will be mapped under the most favorable

conditions. Figure 3-2 shows photographs of different configurations of the M-TLS used during data collections.

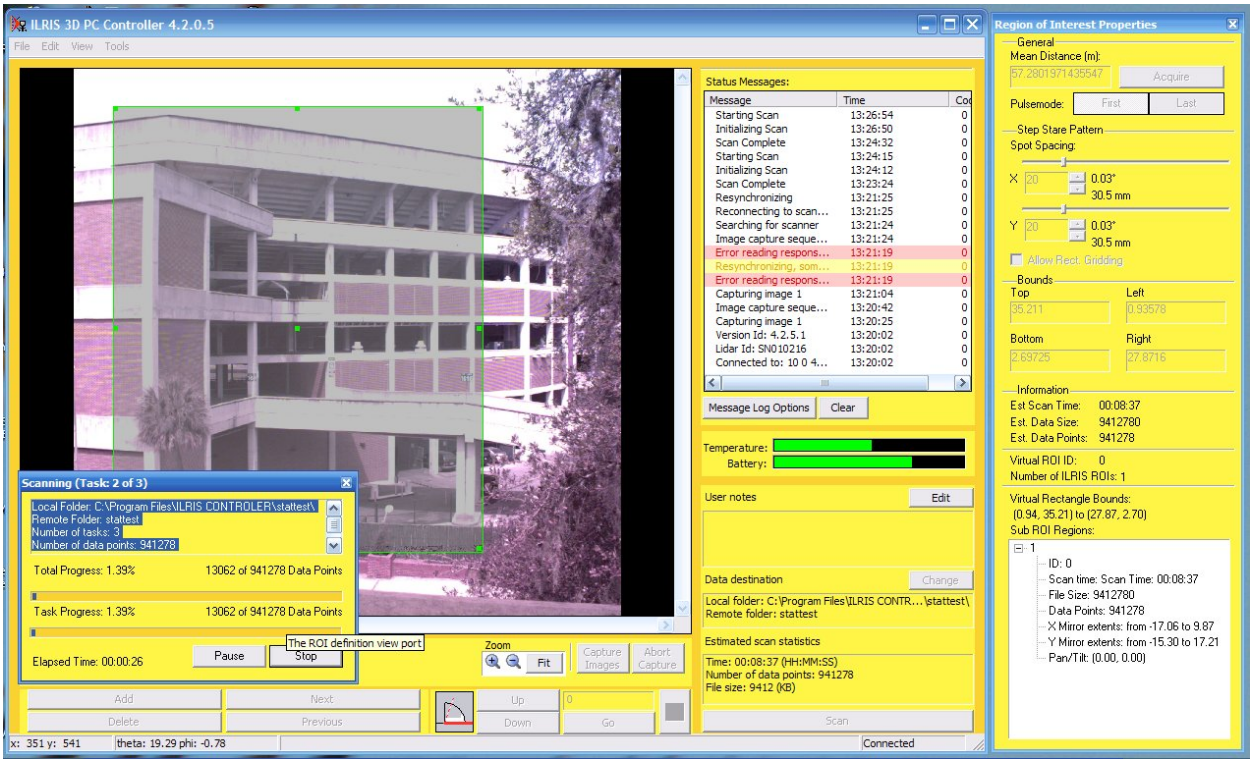

Figure 3-1. Screen capture of the ILRIS unit controller software during scanning operations.

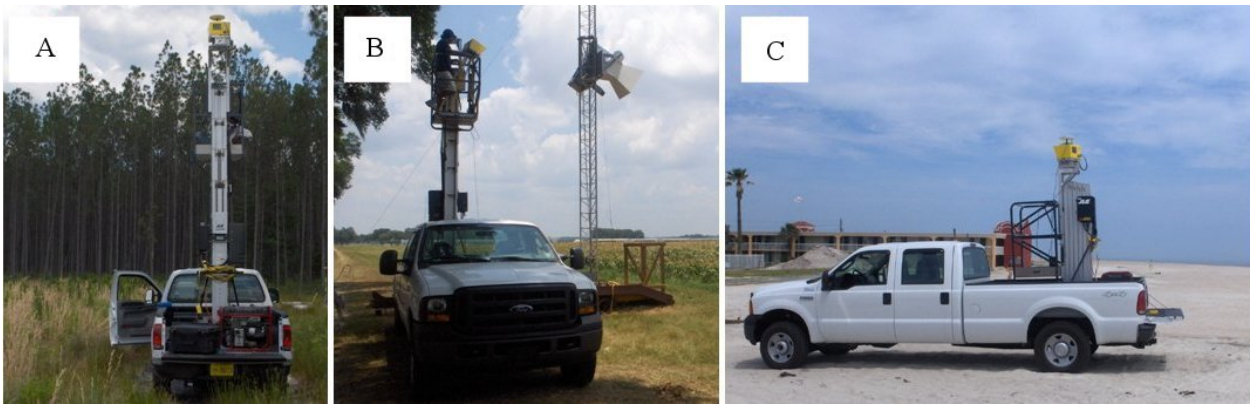

Figure 3-2. Different configurations of the M-TLS system during several data collection projects. A) Forest scanning B) Soil roughness experiment, a microwave radiometer can be seen behind the M-TLS. C) Beach erosion hot spot mapping in St. Augustine Fl.

3.2 Data Parsing

At collection the data is stored in a binary format and includes sensor orientation parameters and range for each measurements made. The raw data needs to be converted into a

position in a coherent 3D frame of reference. Additional information can be texture or color information from the intensity of the reflected laser signal or from a coregistered imaging sensor. This first step of processing is called Parsing and it is performed by the proprietary software "PARSER". With Parser the raw data is converted to any of the known point cloud formats that can be read by most LIDAR processing software for further manipulation and analysis.

Figure 3-3 shows a screen capture of the Parser software. The large screen shows the digital image of the scan surface, the red box encloses the selected region of interest. The Parser Settings tab allows the user to personalize the conversion process. There are options for the output file format, the choice of using the digital image to provide RGB color channels for each of the scanned points, smoothing of the range shots, corrections based on the Pan-Tilt orientation and an option for the positioning of the measurement origin.

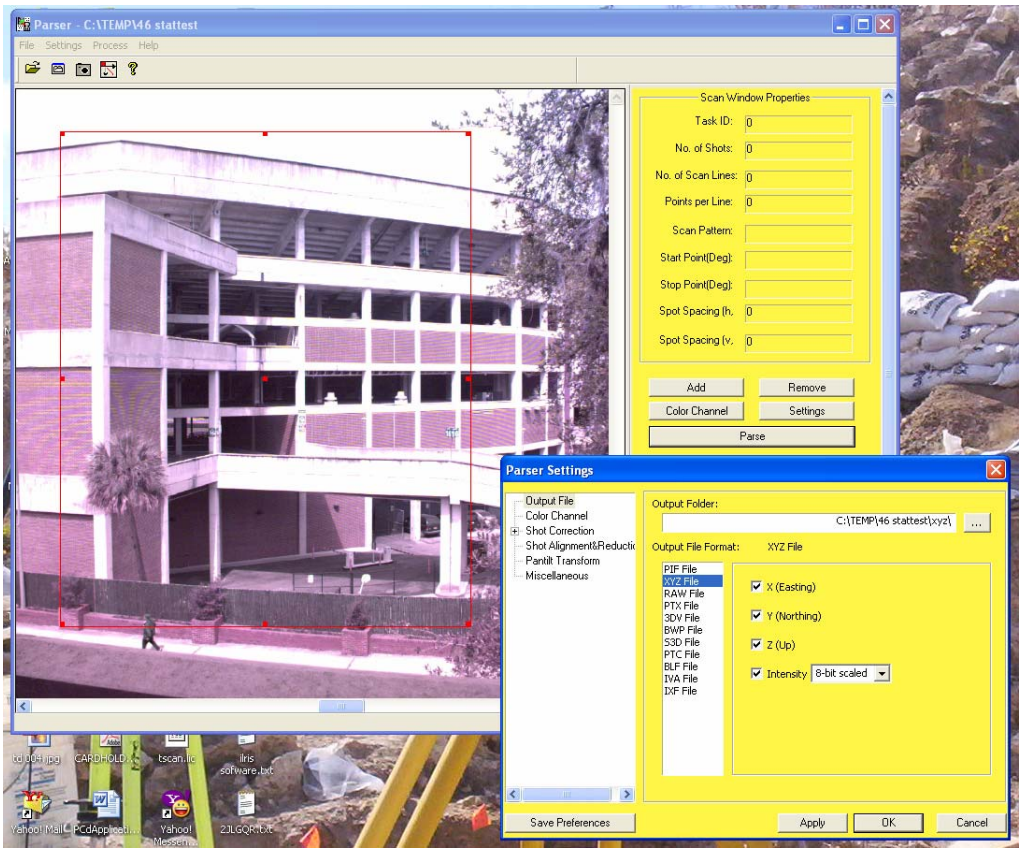

Figure 3-3. Screen capture of the Parser software during the setup of parsing settings.

The most common output selected is the ASCII XYZ File which converts the range, azimuth and elevation into a coordinate in a right hand Cartesian frame with the origin at the LIDAR reference point. Additional information can include a normalized 8 bit laser return intensity or RGB channels. This format is easily uploaded into point cloud processing software like QT Modeler, Terra Scan, Polyworks or Matlab for a customized analysis.

3.3 Data Manipulation and Information Extraction

Once the data is parsed is ready for uploading into specialized software that allow its manipulation, analysis and information extraction. The information extraction from a M-TLS is the final goal, it is a customized process for each application. Some of these specialized techniques are discussed on an application to application basis on chapters 4 to 7. However, there are several typical operations that can be performed on LIDAR point cloud data; these are visualization, transformations, segmentation, classification, filtering, gridding and specialized mathematical operations.

3.3.1 Visualization

The first thing that is done to a LIDAR data set is to look at it. Visualization is the most basic operation; however, a good visualization allows the analyst to asses the quality of the data set, it enables the planning and control of different processing schemes and finally will provide the presentation of the final product. Most LIDAR processing software will have a graphical interface that will render the numerical point cloud into an image, but there is a great range of options and functionalities that will vary among the different options. The simplest visualization will plot all the points with a single color and size, and the operations of Zoom, Rotate, and Navigate will be available. More advanced software will render each LIDAR point according to other characteristics, it can be brightness coded according to the laser return intensity, or RGB textured if the point cloud was coregistered with a digital image, it can also be color coded

according to elevation, range, class or any other attribute contained in the point cloud structure. Some software will allow the user to toggle between the rendering of the point cloud and the rendering of a Triangulated Irregular Network (TIN) or Digital Elevation Model generated from it, as shown in Figure 3-4.

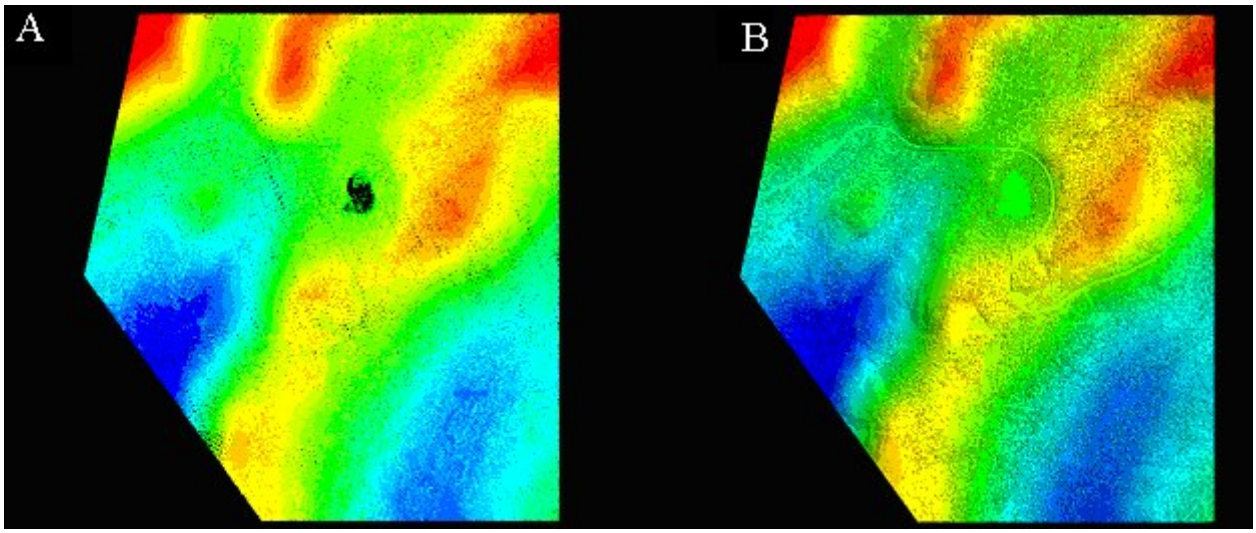

Figure 3-4. Visualization of LIDAR data. A) As a point cloud. B) As a DEM.

3.3.2 Single Point Selection

An important functionality of visualization software is the one that allows the user to manually do single point selection. This is to navigate through the point cloud using the zoom and rotate controls to pick out single points from the cloud.

3.3.3 Measurements

The ability to precisely select points from the clouds allows the analyst to make measurements such as distances between points, and angles between lines connecting the points.

3.3.4 Primitive Fitting

After selecting a series of points is possible to perform a primitive fitting operation. Primitive fitting is the application of the least square methodology to compute the spatial parameters that define simple geometric figures or volumes such as lines, circles, planes, spheres, cones. Primitive fitting allows computing the modeling accuracy of TLS. Imagine that

there is a sphere with a known radius. After the sphere is scanned a best fitting sphere is determined for the point cloud using least squares to minimize the residuals. The “fitted” or “modeled” sphere radius can then be compared to the known radius and the degree of agreement between both provides an estimate of the modeling accuracy. Figure 3-5 illustrate the entire process from point selection to the fitting of the sphere.

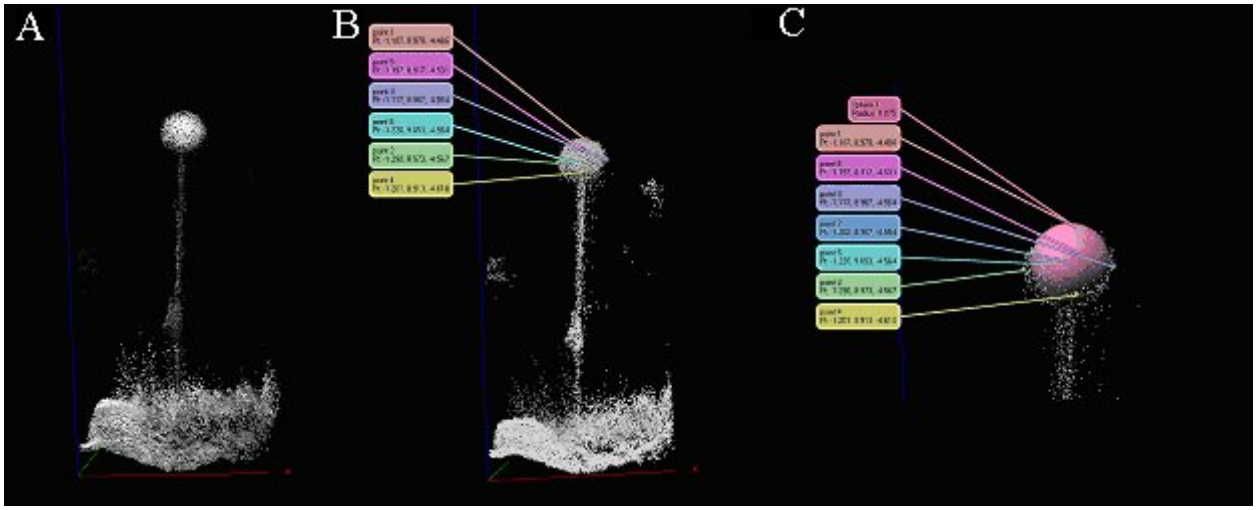

Figure 3-5. Primitive fitting process illustrated. A) Point cloud. B) Picking points from the sphere surface. C) Fitted sphere based on the picked points.

3.3.5 Generating Cross Sections

An important visualization tool is the selection of a particular baseline and the generation of a cross sectional view of the point cloud at that baseline.

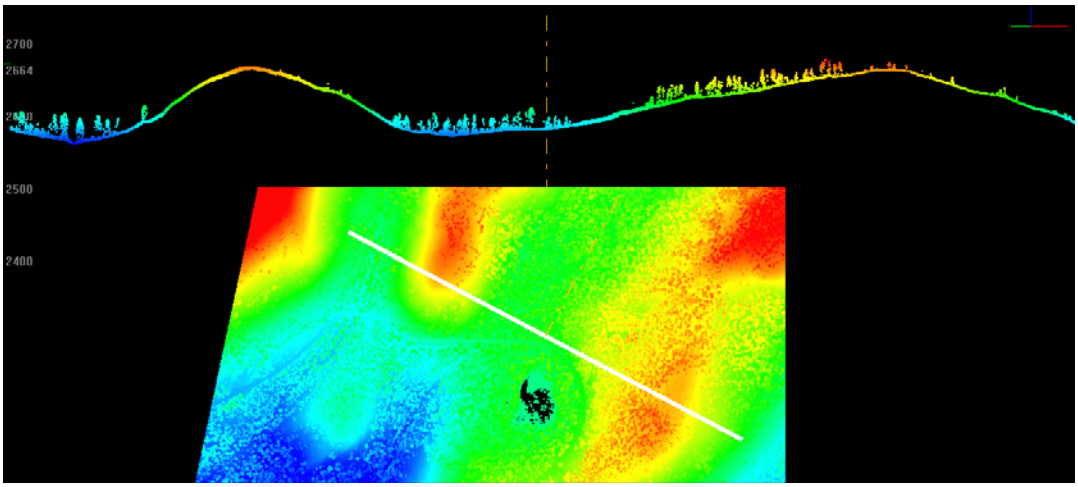

Figure 3-6. Cross section generation from the point cloud.

3.3.6 Transformations

There are countless transformations that can be applied to the point clouds, a few of the most frequent are described following:

3.3.6.1 Rotations and translations

Simple Transformation includes the translation or rotation of the entire point cloud on one or more of the coordinate axes.

3.3.6.2 Cropping

When an object is scanned there are always points that do not belong to the volume of interest. Cropping allows the creation of a point cloud with only the elements that falls within the 3D space of interest.

3.3.6.3 Merging

Point Cloud Merging is performed when several point clouds of the same object were collected from different angles or positions each having its own coordinate frame and there is the need to convert all of them into a single spatial coherent point cloud. Merging is performed by setting one point cloud as the base reference frame, and then common points or common primitives are identified between the base and the source point cloud. From the common points a 3D rotation and translation transformation is computed using least squares adjustment. Then the transformation is applied to the source point cloud to change its coordinate frame to the base reference frame. Figure 3-7 illustrates a merging operation between two point clouds color coded as white and pink that were obtained from different scan angles, using the common points method the pink point cloud was rotated to the white coordinate system to produce a single coherent data set.

With the Polyworks IMspect and IMAlign software the common points can be manually selected and then the transformation process is done automatically. Another option is to use

Polyworks IMspect to find the common point coordinates in both the source and the target frames create text files with those coordinates and then use TerraScan transformation modules to compute the parameters of the transformation and then manually apply it to the source point cloud. The advantage of this latter option is that TerraScan provides a residual analysis of the transformation based on the common points and this give the user an idea of the quality of the transformation.

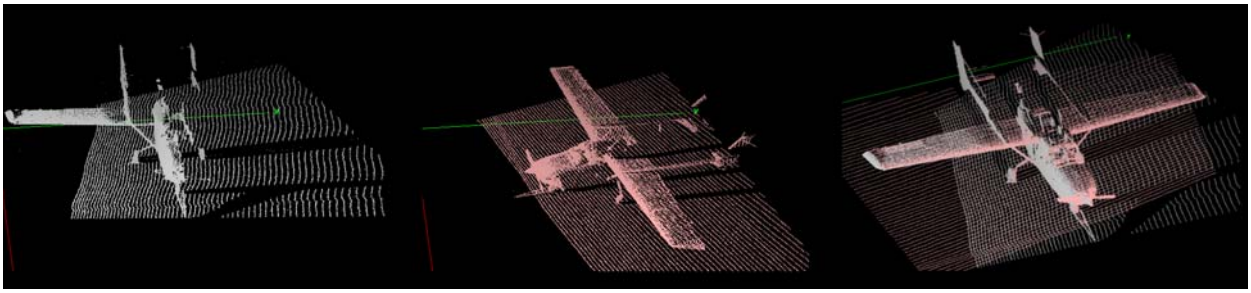

Figure 3-7. Point cloud merging example.

3.3.6.4 Geo-referencing

A transformation in which a point cloud with coordinates in arbitrary sensor space is converted into a geodetic coordinate frame is called geo-referencing. This operation has to be performed when absolute measurements have to be made or when the terrestrial data set will be merged or compared to an airborne data set. Similar to a merging operation, in geo-referencing there has to be a minimum of 3 non-collinear points for which coordinates on both sensor and geodetic frames are known. Based on that set of coordinates the parameters of a 3D rotation and translation transformation are computed. That transformation is then applied to the entire point cloud and as a result the data set is fixed to the specific geodetic frame. The accuracy of the geo-referencing depends primarily of the quality of the GPS observations, the vertical and horizontal strength of the control points network and the determination of the XYZ coordinates of the control points from the original point cloud. Geo-referencing can be performed using both Polyworks and TerraScan.

3.3.7 Segmentation, Classification and Filtering

Another important set of operations performed over the point clouds are the ones that allow performing segmentation, classification and filtering of the points.

3.3.7.1 Segmentation

Segmentation refers to the operation that will segment or segregate points into different groups based on characteristics without knowledge of what they really are. An example of segmentation could be the separation of points, based on intensity values, into low intensity, medium intensity and high intensity. Under this segmentation scheme points in each group will not necessarily share common spatial characteristics.

3.3.7.2 Classification

Classification implies the separation of points into different groups or classes defined by an intrinsic or natural characteristic. An example of classification is the separation of the points into vegetation, building or ground classes; each of these groups implies the knowledge of its nature.

3.3.7.3 Filtering

Filtering is the removal of a set of points from the clouds based on either a segmentation or classification scheme. An example of a segmentation scheme based filter could be the removal of points that are below a certain height value, without considering its nature (i.e. ground or low vegetation). A classification filter could be one that removes vegetation from an urban scene on which only brick and glass is wanted.

3.3.8 Gridding

A scanner point cloud by nature is an irregularly space data set. The process of converting the point cloud into a regularly spaced data set by means of interpolation is called gridding. Gridding allows the analyst to observe subtle features in the data set. There are many different gridding algorithms the more common are Nearest Neighbor, Inverse Distance Weighting,

Triangulation with Linear Interpolation, and Kriging. The regular nature of the grid allows the analyst to perform many mathematical operations such as areas and volumes computations, grid algebra, grid calculus, differentiation, gradients, grid comparison, as well as image processing operations. Gridding can be performed using specialized software such as Golden software "Surfer" or with built-in routines in Matlab. Figure 3-8 shows a regular grid surface model B) generated from the irregular spaced point cloud.

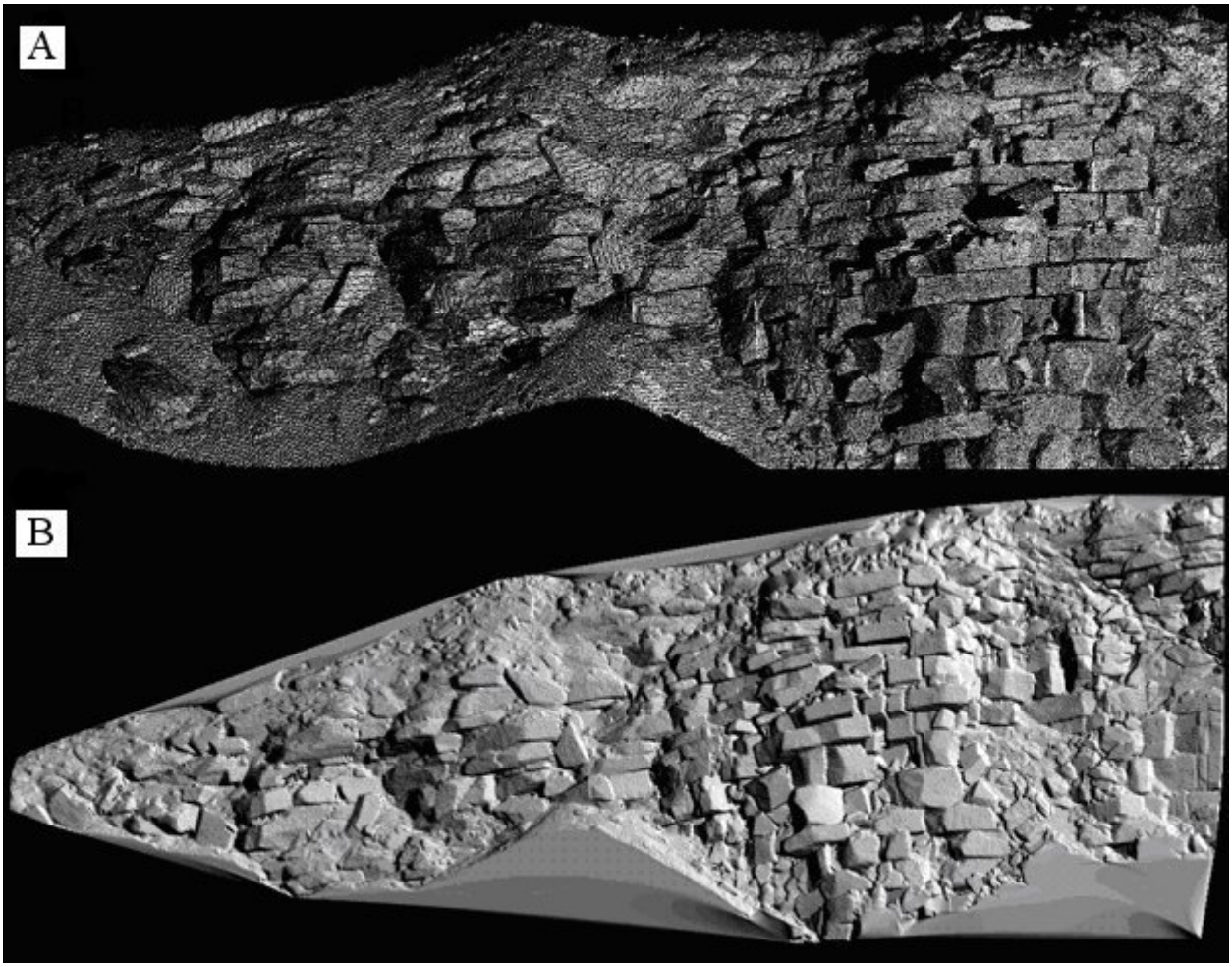

Figure 3-8. Gridding operations, from point cloud to grid. A) Point cloud to B) Surface Model

3.3.9 Advanced Mathematical Operations

The operations discussed so far are commonly performed by the LIDAR analyst using canned algorithms in commercial software packages. However, some applications require

advanced or specialized techniques that must be custom programmed in programming languages such as Visual C, Visual Basic or using higher level math tools such as Matlab or IDL. Examples of these advanced mathematical operations may include:

- Transformations from space to the frequency domain using the Discrete Fourier Transform or with the Discrete Wavelet Transform.
- The use of spin images to represent objects from a 3D dataset in a single 2D image.
- The application of advance image processing techniques and operations such as edge detection or morphological operations to a gridded dataset.

Figure 3-9 shows an example of and advanced mathematical operation. Were a discrete 2D Fast Fourier Transform was used to extract the stronger periodic components of the real terrain and then a 3D surface was generated from those components.

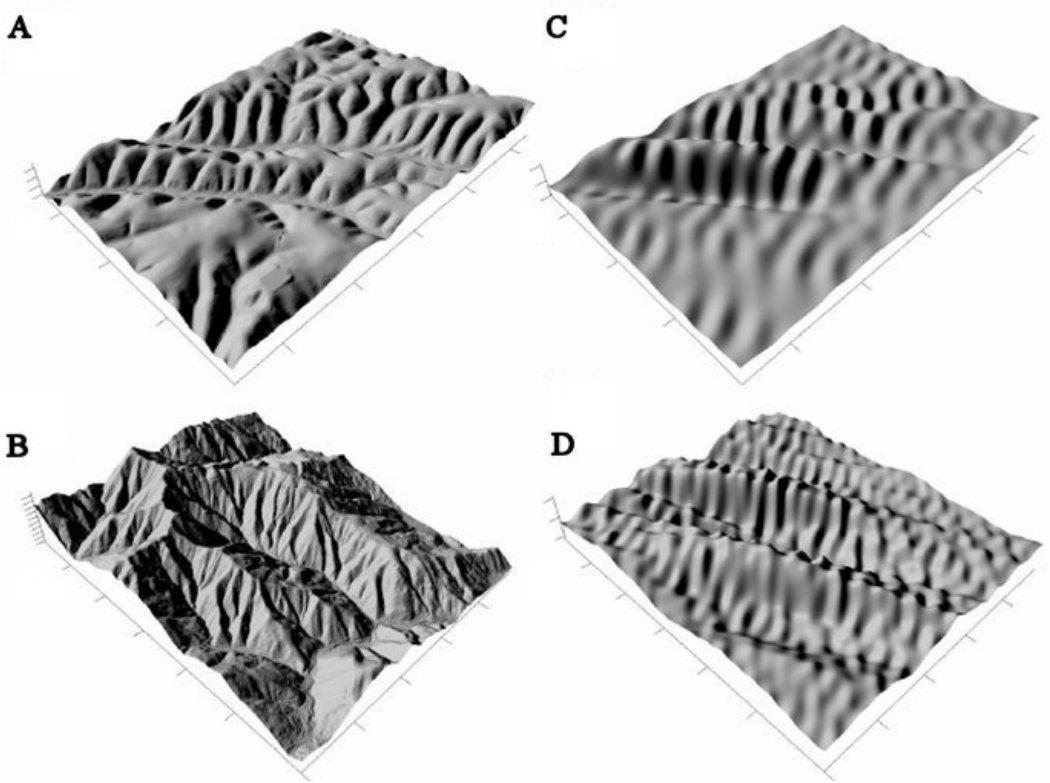

Figure 3-9. Examples of advanced mathematical operations in the processing of Airborne LIDAR data. Digital elevation models of A) Gabilan Mesa, Ca. and B) South Fork Eel river, Ca. C) and D) show visual representation of the most strongly periodic component of each landscape. (Perron, 2006)

CHAPTER 4
TESTED APPLICATIONS OF M-TLS

4.1 Common Applications of TLS

TLS units are marketed by the manufacturers mainly as surveying tools for engineering applications. These engineering applications include as-built-surveys, crime scene and traffic accident investigation, mine operations planning and supervision, transportation infrastructure mapping, bridge loading analysis, building damage assessment and urban modeling. The reason for this biased marketing is that TLS are expensive instruments that are often affordable only by companies that do large projects with huge capital investments, where the savings of time over classical mapping techniques are even greater than the cost of the TLS instrumentation. But even with that biased marketing over the last 5 years, some articles about scientific applications of TLS have been published in scientific journals or presented in professional meetings.

One of the first presentations reporting the application of TLS technology to scientific research was that of the University of Texas Bureau of Economic Geology “3-Dimensional Digital Outcrop Data Collection and Analysis Using Eye-safe Laser (LIDAR) Technology” presented on the 2002 convention of the American Association of Petroleum Geologists (Bellian et al., 2002). In 2003 a paper published in the International Society for Optical Engineering (SPIE) Optical Metrology for Arts and Multimedia journal entitled “High-resolution laser radar for 3D imaging in artwork cataloging, reproduction, and restoration” introduced the application of TLS for cultural heritage preservation. With respect to forestry one of the first articles published was “Using airborne and ground based ranging LIDAR to measure canopy structure in Australian forests” published on the Canadian Journal on Remote Sensing vol. 29, 2003 (Hopkinson et al., 2004).

These papers were the groundbreakers of the scientific applications of TLS. It is clear that TLS has a great potential to contribute to several fields of science that require precise spatial measurements. It is just a matter of making the technology available to researchers and providing them with technical support on the data processing and information extraction. Just as Airborne Laser Mapping proved to be a valuable tool, TLS will be accepted if it proves to be better that conventional data gathering techniques by providing higher quality and quantity of data faster and cheaper. Several applications were tested under this philosophy, a subset of which are briefly described in the following sections. These sections present a “Traditional” vs “Alternative” methods of collecting spatial field measurements. Subsequently, three of these applications will be thoroughly discussed in the next chapters, and include quantitative comparisons with the traditional field methods techniques.

4.2 Paleontology

Paleontology and archeology field techniques require extensive digging and constant measurements. Usually at a dig site, before digging operations begin, a regular grid is established. The positions of the fossils or artifacts that are discovered are carefully measured and recorded by photography. The current field methods are very time consuming can really slow the dig progress specially when a very important finds such as articulate skeletons or unique artifacts are discovered. TLS systems can be used in these type of cases to provide both photographic and 3D measurements. Figure 4.1 illustrate both the traditional and the alternative approach to obtain measurements at dig sites. Part A shows the traditional way were stakes and cordas are used to define the grid, while part B shows a TLS measuring and recording a dig site.Digital terrain models from TLS data can provide additional information for monitoring progress such as dig volume and cleared surface.

Figure 4-1. Traditional and alternative methods for measuring and recording spatial information in archeological and paleontological sites. A) Traditional grid. B) TLS mapping.

The paleontological application was tested at a Florida Museum of Natural History dig site located near Haile, Newberry; it is identified by Florida Museum as H7G. Figure 4-1b shows the ILRIS mounted on a tripod at that dig site. The site is a large sinkhole in a limestone quarry, containing fossil bones and teeth of about 40 different kinds of freshwater and land animals dated at about 2 million years old (Pliocene Epoch). Some fossils are preserved as intact skeletons but mainly isolated bones or teeth constitute the major finds. The study objectives were: 1) to establish a macro Geo-referenced 3D model of the dig site from several large scale ILRIS scans; 2) to obtain high density point clouds of small patches of the dig showing the fossils matched to the macro model and 3) if an interesting specimen was discovered the development of a multi angle high density point cloud model would be developed and embedded into the macro model.

Figure 4-2 shows a point cloud rendering of the macro model of the dig site. Figure 4-3 shows RGB textured renderings of high resolution point clouds obtained from a small patch of the dig site and Figure 4-4 presents before and after surface models generated from the point clouds. These were later used to determine the dig volume (~ 2.0 m^3) after one day of excavation.

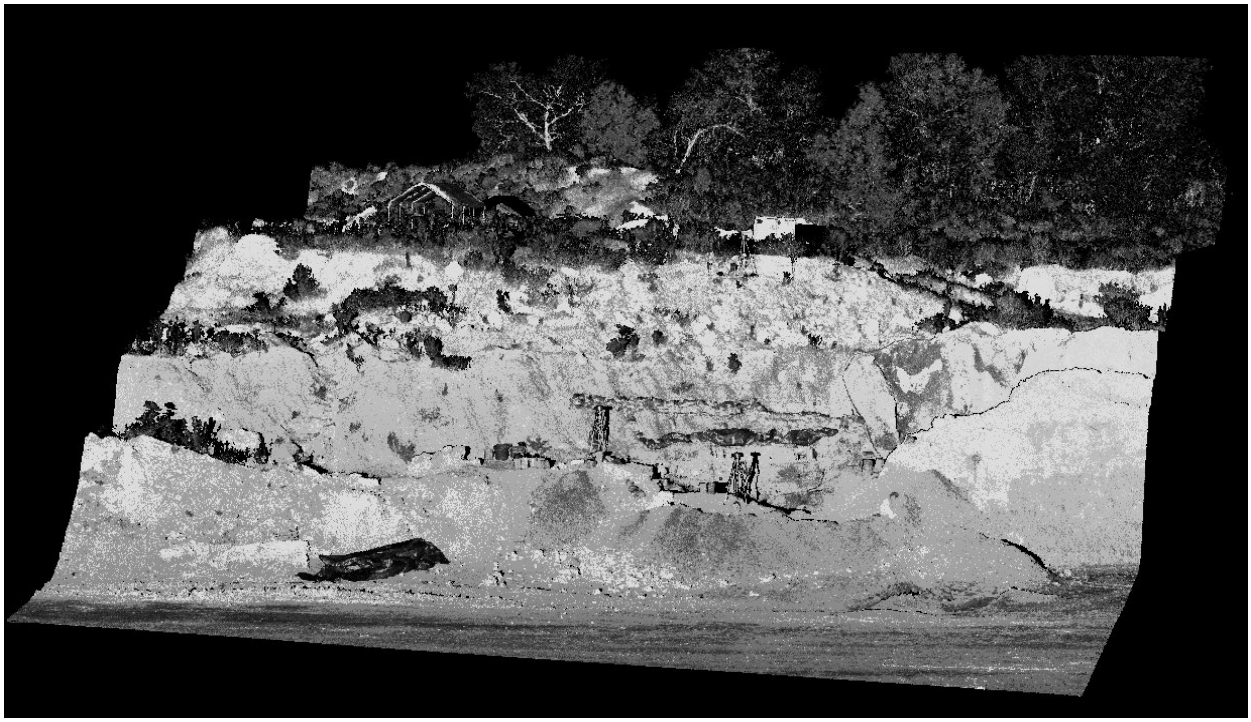

Figure 4-2. Rendering of the dig site point cloud macro model showing laser return intensity.

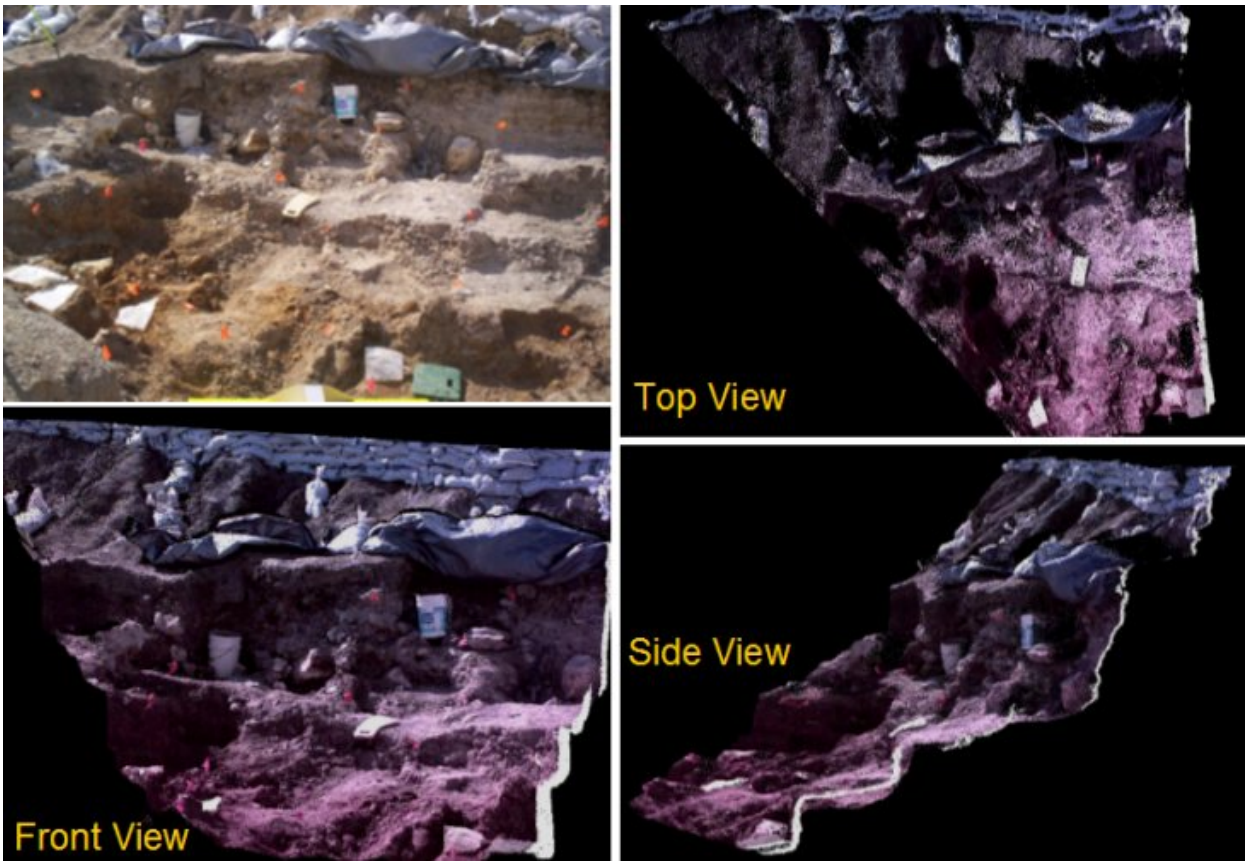

Figure 4-3. RGB textured renderings of high resolution point clouds.

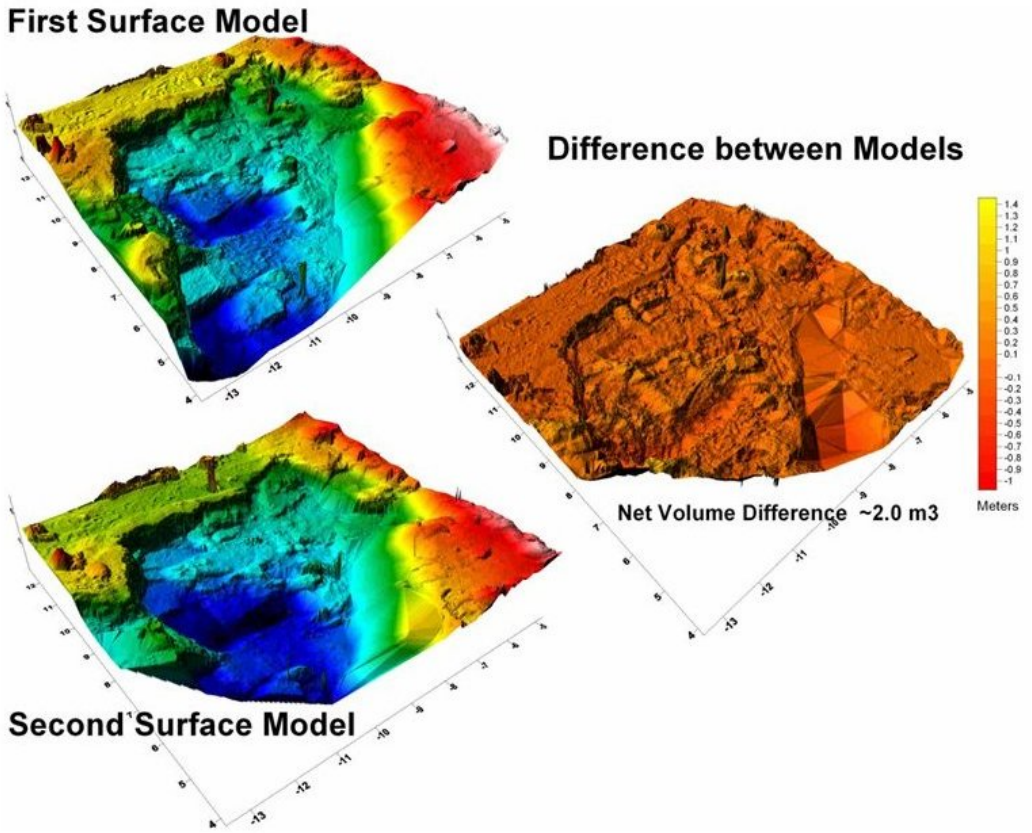

Figure 4-4. 3D surface grids used to compute the volume of dirt extracted in one day.

4.3 Structural Geology

Geology is a discipline that relies extensively on mapping for the spatial recording of topography, crustal elements like faults and folds, stratigraphy and many other features. Plane table mapping is a traditional geological mapping technique, on which simple tools (a flat leveled table, an angular measuring device and a scale) are used to create large scale (1:120) maps. Plane table was replaced by modern surveying equipment such as total stations and computer aided design (CAD) software. However, creating maps using the plane table or a total station are highly time consuming processes. Figure 4-5 shows the traditional table mapping technique and the alternative terrestrial laser scanning technique.

Figure 4-5. Traditional and alternative ways to perform geological field mapping. A) Traditional plane table mapping technique. B) Modern alternative mapping using TLS.

TLS are ideal for creating geological maps for the study of geomorphology, stratigraphy and structural geomechanics as described by University of Texas Bureau of Economic Geology (Bellian et al., 2002). The tested application of TLS to structural Geology was in support of NCALM PI Stephen Martel of the Department of Geology and Geophysics, University of Hawai'i at Manoa. Dr Martel has been developing theoretical models on the effect of topographic curvature on near-surface stresses and the creation of sheeting joints. Sheeting joints are opening mode rock fractures that form subparallel to the topographic surface, develop to depths of at least 100 m and they occur mainly on regions where the topography is convex (Martel, 2006). The geology of Yosemite National Park in California exhibits vast areas with exposed sheeting joints; TLS mapping was performed on the Tuolumne quarry located along the Tioga road. The objectives of the project were 1) to map the sheeting joints on the exposed wall of the quarry on a 3D geodetic space and, 2) to the sheeting joints orientation to the topographic curvature of the area obtained from ALSM and the mechanical stress to which the formation is subjected.

Data was collected on September 22 and 23, 2006. The dataset consisted of 7 overlapping scans and vector observations for 6 reference GPS base stations that were used for the geo-referencing of the data sets. The binary scan files were parsed to generate the XYZ & Laser

Intensity and XYZ & RGB ASCII text files. Using Innovmetric Polyworks IMInspect module common points were identified in the overlapping scans to perform the merging operations. The coordinates of common points were input to Terrasolid Terrascan to compute the solid 3D translation and rotation transformation parameters. After the transformation parameters were computed, the six sets of point clouds were transformed to the central scan coordinate system and a single point cloud was generated.

Using Polyworks IMInspect module, the GPS control points were identified in the merged point cloud and their sensor XYZ coordinates were determined. The GPS observation files were processed using the NGS Online Positioning User Service (OPUS) (http://www.ngs.noaa.gov/OPUS/) and the GPS coordinates for the control points were determined. The standard deviation of the coordinate components varied between 0.014 to 0.789 meters, with a mean of 0.219 meters. With the sensor and UTM coordinates of the GPS control points; Terrascan was used to compute the solid 3D translation and rotation transformation parameters for the data set. The RMS of the residuals of the transformation on the control points were 0.253919157, 0.156471707, 0.423406924 meters for the Easting, Northing and Elevation components. The merged data set was geo-referenced and transformed to a UTM zone 11 (NAD_83) point cloud.

Using Applied Imagery QT Modeler, intensity and RGB textured images were generated from the point cloud. In Figure 4-6 renderings of the point clouds from top and front view are presented. Using Terrascan, the point cloud was broken into tiles that later were imported to Golden Software Surfer to produce regular 2cm grids of the vertical walls. The triangulation with linear interpolation algorithm was selected for the grid creation. From the grids, shaded relief images were produced; Figure 4-7 shows one of such images where the layered sheeting joints

are clearly seen. The images rendered from the grids allows to determine the 3D spatial orientation of the joints with respect to the surrounding topographic landscape.

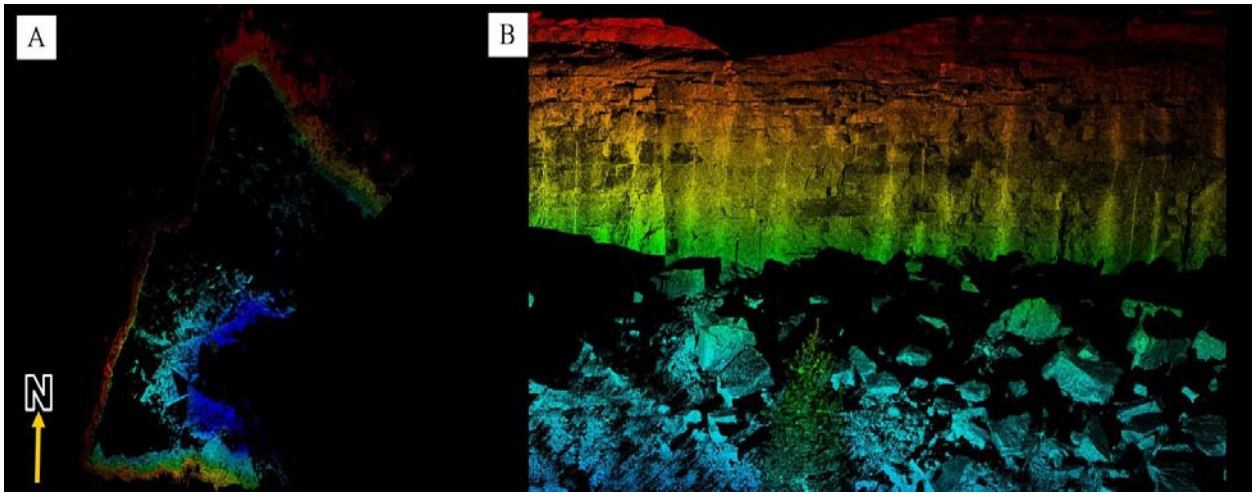

Figure 4-6. Geo-referenced point cloud rendering of the Tuolumne quarry. A) Top view. B) Front view.

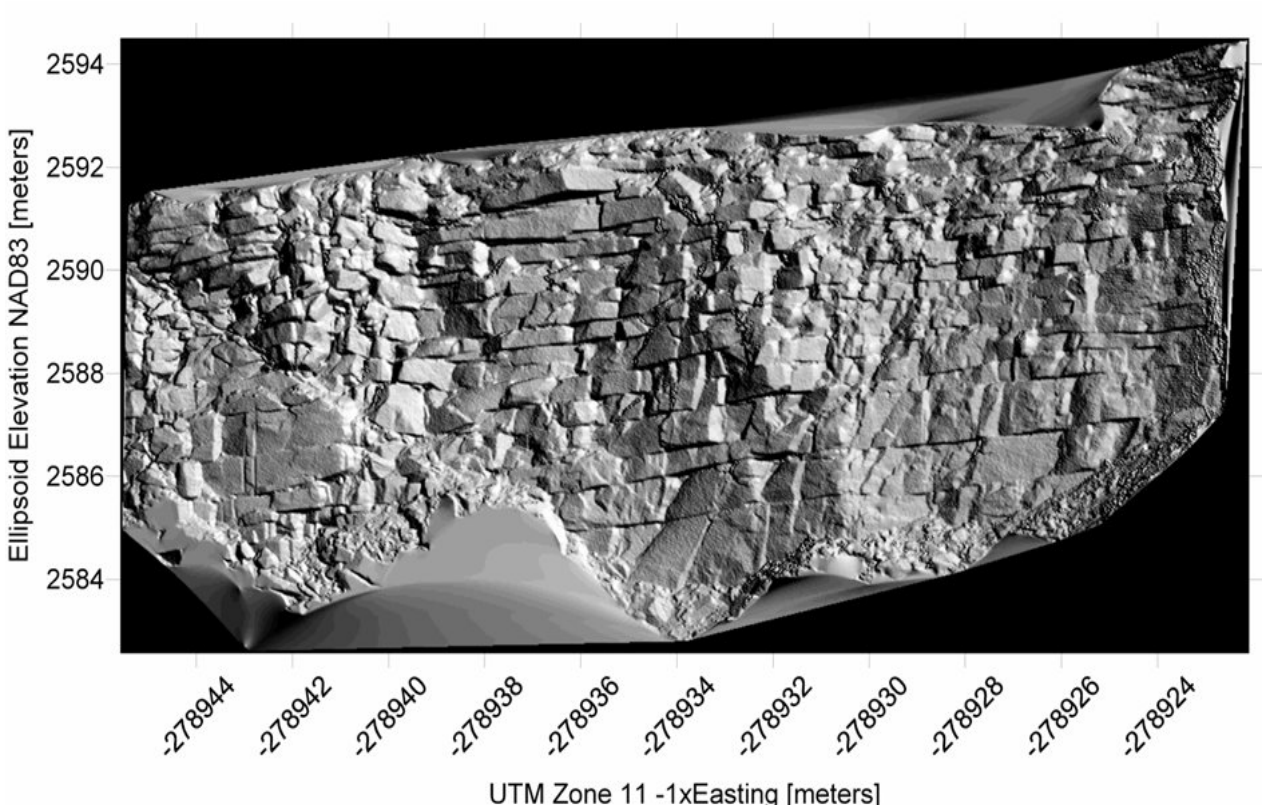

Figure 4-7. Shaded relief image from a gridded model of the south wall of the quarry.

4.4 Wildlife Management Conservation

Typical wildlife management and conservation activities include the catch and release of specimens for measuring, weighing and biological sample collection. Under certain circumstances where there is a high risk of injury to wildlife personnel, when it is desired that the specimen not undergo the stress of capture or when just spatial measurements are needed a TLS may be an efficient alternative to the capture, measure and release method. In this experiment an alligator was scanned from a safe distance of twenty meters without perturbing the specimen. The results prove that is feasible to obtain accurate measurements of several dimensions such as length and thorax diameter. Volumetric models can also be created from the data, which provide a wealth of information for time series analysis. Figure 4-8 shows the traditional way of measuring alligators or crocodiles, it also shows the rendering of a point cloud obtained by TLS of an alligator. From the point cloud the alligator length was measured.

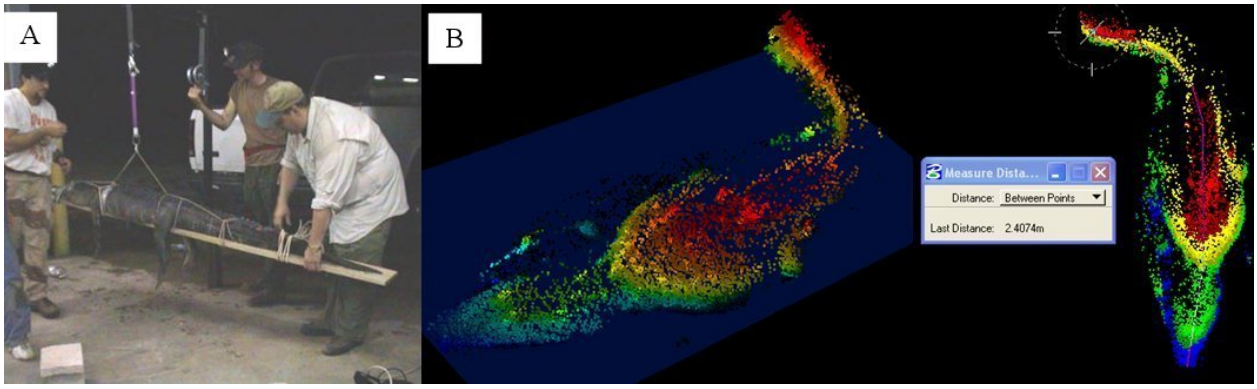

Figure 4-8. Methods of measuring alligators and crocodiles. A) Traditional method. B) Alternative method from TLS point clouds.

4.5 Coastal Morphology

The state of Florida has over 32000 kilometers of tidal shoreline of which more that 960 kilometers are beaches. The activities that are generated around these beaches, such as tourism, constitute a great source of income for the state. A large portion of the low-lying sandy beaches and dunes along the Atlantic coast are subject to modification by high surf generated by

northeasterly winds or by catastrophic phenomena as tropical storms and hurricanes. Traditional methods of data collection and map generation for beach profile change studies include differential leveling, traversing, static and kinematic GPS and aerial photogrammetry. These techniques are not only costly, time-consuming, and labor-intensive but also have poor spatial resolution (Shrestha, et al. 2005). Current Florida Department of Environmental Protection (FDEP) standards for beach profile topographic surveying require cross shore transects at Bureau of Beaches and Coastal Systems (BBCS) reference points, which are approximately 1,000 feet apart along shore, with a collection interval not to exceed 25 feet. and at all grade breaks and attributed items along the profile sufficient to accurately describe the topography at the profile locations (BBCC, 2004). These techniques do not have the spatial or temporal resolution required to precisely quantify and study the processes of beach erosion, especially on erosion hotspots. Part A OF Figure 4-9 illustrate the use of RTK GPS to generate beach transects and part B shows the UF M-TLS system used to generate beach surface maps.

Figure 4-9. Methods for generating beach profiles. A) Using Real Time Kinematic (RTK) GPS. B) Alternative method using the M-TLS.

The M-TLS was used to monitor an erosion hot spot located near the St. Augustine pier, Fl. at high spatial (cm level) and temporal (biweekly) resolution. The methodology employed for data collection and analysis as well as the results are presented in Chapter 5.

4.6 Soil Science

In soil science; active and passive microwave remote sensing techniques are applied to the derivation of soil parameters such as temperature and moisture. In order to derive soil moisture from radar sensors it is necessary to have a priori knowledge of the soil surface roughness. Traditionally soil roughness has been characterized as a single scale process obtained from 2D profiles and parameterized by the root mean square (RMS) of the height (s), the correlation length (ℓ) and autocorrelation function ($\ell(h)$).

The traditional methods of obtaining the soil profiles are the Needle-like Profiler and the Mesh Board. A complete description of these mechanical profilers and the data collection procedures is provided by Mattia et al. (2003). The main disadvantage of these mechanical methods is that they tend to disturb the surface that is under study. Mesh Boards have to be hammered into the soil, while Needle-like Profilers tend to penetrate into the surface yielding noisy measurements of the heights. Modern methods are aimed to not disturb the surface; they are non-contact instruments. These instruments include laser profilers, optical imagers and acoustic backscatter instruments (Mattia et al., 2003; Zribi et al., 2000; Oelze et al., 2003). Figure 4.10 illustrate the meshboard and alternate method for deriving soil roughness metrics.

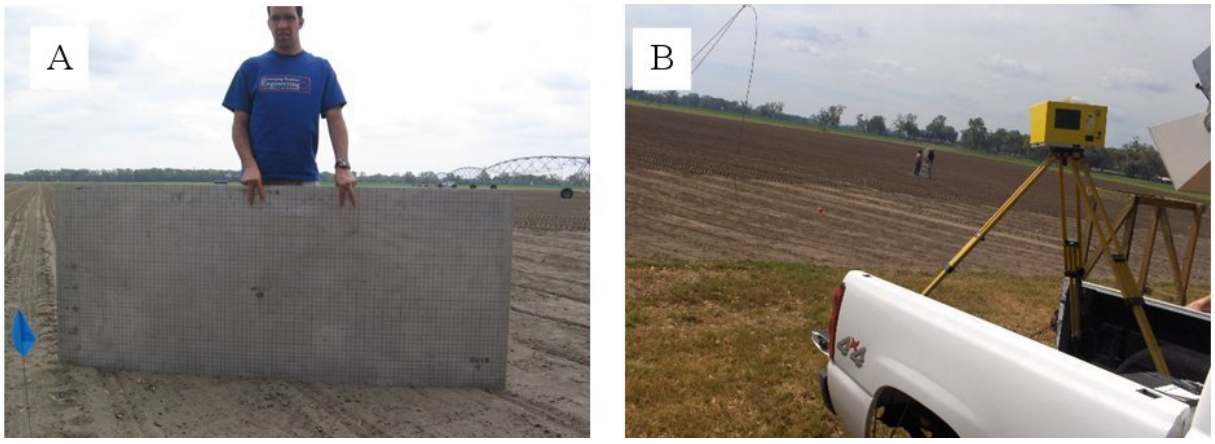

Figure 4-10. Methods for deriving soil roughness metrics. A) Traditional way using the mesh board. B) Alternative method using TLS to create 3D maps of the soil surface.

The M-TLS is an excellent tool for soil roughness measurements because it has the capability of producing terrain models at sub-centimeter scales with the additional advantage over traditional instruments and methods that it provides a complete surface digitizing, rather than digitized line profiles. The M-TLS was used to collect data in an experimental plot at the University of Florida Plant Science Research and Education Center at Citra, Florida and at a commercial plantation plot near Hastings, Fl. A detailed description of the data reduction, analysis and result is presented in Chapter 6.

4.7 Forestry

The estimation of forest structure and volume has for a long time been of great interest to the scientific community because of its ecological and economic importance. Traditional methods of performing these measurements and estimations even over a small plot of forest require a great amount of man power and many hours of field work. These methods require the manual measurement of tree height, stem diameter at breast height (dbh), stem location and stem density. Figure 4-11 part A shows the traditional way of measuring dbh, part B illustrate the use of a Biltmore stick to estimate tree height, part C show the alternative method of using TLS to generate point clouds from which dbh and tree height can be derived.

Figure 4-11. Methods for estimating forestry metrics. A) Traditional method for measuring dbh. B) Traditional method for estimating tree height. C) Alternative method using the M-TLS to create 3D maps of the forest.

Since the early 1990s Airborne Laser Mapping (ALM) has been used to determine forest metrics. ALM provides a large spatial coverage with very detailed 3D information of the forest upper canopy; however it provides very limited information of the forest understory structure and mass. Some experiments have proven that TLS can be used to provide high detail information on the understory with a limited spatial coverage due to the line-of-sight obstruction caused by the same trees. An opportunity was identified for which dataset from both airborne and terrestrial platforms could be merged. The tested approach consisted of developing techniques for geo-referencing TLS data set to achieve a seamless fusion with ALM data to generate high density point cloud of forest plots from which forestry metrics can be derived. This application is fully described in Chapter 7.

CHAPTER 5
ST. AUGUSTINE BEACH EROSION HOT SPOT MAPPING

5.1 Motivation

Costal engineers and scientists have known that beaches are subject to both natural or artificially induced sediment transport. With the execution of large beach fills projects along the coasts of America in the 1980's and early 1990's, valuable experience was gained in long-term maintenance and beach-monitoring programs. That experience led to the recognition, systematic monitoring and study of Erosion Hot Spots or EHS. An EHS is an area that erodes more rapidly than the adjacent beaches or more rapidly than anticipated during beach fill design. Today knowledge of coastal processes is capable of explaining what causes most types of EHSs and to formulate appropriate correction actions. EHSs can be classified and defined by several metrics such as loss of beach width (recession rate), loss of sediment volume (erosion rate), percentage of fill remaining of the amount placed, and perception of how a fill should perform relative to adjacent beaches or to historic rate (Kraus & Galgano, 2001).

Airborne Laser Mapping technology has been extensively used to study large scale beach erosion. ALSM data covers a long stretch of beach with a moderate sample density of approximately 1 laser return per square meter (however, most current ALSM systems such as the Optech Gemini are capable of high pulse rates >100 kHz, with these type of systems 8 to 10 laser returns per square meter can be achieved). This sampling capability enables the detection of submeter-scale changes in shoreline position and dune heights over periods of a few months. However, it might not be as effective for mapping short term, small scale variations that are characteristic of some localized erosion hot spots. The M-TLSS, on the other hand, can provide high density point clouds (centimeter scale point spacing) of smaller areas known to be highly

prone to erosion. This chapter will discuss the application of M-TLSS as a complement to ALSM in the study of beach morphology in the St. Augustine, Florida area.

5.2 Use of LIDAR Technology

Airborne LIDAR has been used since 1996 to study beach erosion. Early projects included the Airborne LIDAR Assessment of Coastal Erosion (ALACE) that was a partnership between NOAA, NASA, and the USGS and the Laser Swath-mapping Evaluation and Resurvey (LASER) undertaken by the University of Florida, the Florida Department of Environmental Protection and the Florida Department of Transportation. Numerous papers have been published on the subject proving the success of this application.

At the time of this writing, a literature search for the application of terrestrial laser scanners to study erosion hot spots yielded no results. The only reference was to a poster presentation at the 2005 meeting of The Geological Society of America (GSA). The abstract describes the use of a Terrestrial Laser Scanner to map a beach re-nourishment plan covering 8.59 km of shoreline at Folly Beach, South Carolina (Kaufman et al. 2005).

5.3 Data Collection

A known erosion hot spot (EHS) along the St. Augustine Beach, Fl. area was selected for this study. The EHS is located on the beach in front of the St. Augustine Beach Front Resort (300 A1a Beach Blvd, St. Augustine, Fl.). Figure 5-1 shows a map and a near infrared aerial photo of the study site, the orange polygon defines the mapped area. Data were collected on 4 dates, one prior the beginning of the Hurricane season on May 23, and 3 takes at two week intervals on October 28, November 10 and November 25, 2006. GPS data for the geo-referencing of the data set were also collected on the first three takes using Astech Z-Extreme and Astech Z-Surveyor geodetic grade receivers.

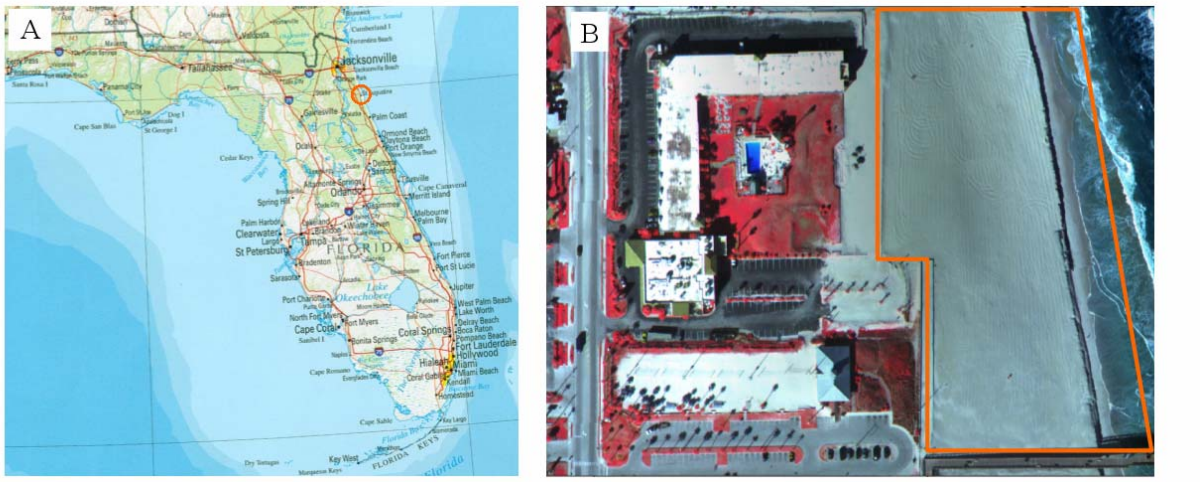

Figure 5-1. Beach erosion hot spot study site location. A) Florida map, orange circle marks the location of St. Augustine. B) Aerial infrared photograph of the study site, orange polygon marks the specific mapped area.

5.4 Data Processing

The first step in the preliminary processing was the merging of individual scans taken for each day into a single point cloud in the sensor based coordinate system (XYZ). Polywork's Inspect N-pair common point method was used for merging the scans. The next step was the geo-referencing of the point clouds; on the first take 7 GPS control stations were deployed, for these stations both XYZ and Easting, Northing, and Height coordinates are available which allows for the computation of a 3D solid rotation and translation transformation. Figure 5-2 shows a rendering of the March 23rd geo-referenced point cloud, NAD83 was used as horizontal datum and NAVD88 as vertical datum. In Table 5-1 the control points coordinates used for the geo-referencing transformation and the transformation residuals for the first data set are presented. To achieve comparable datasets the geo-referencing of the last 3 point clouds were performed using 12 common points to the first geo-referenced point cloud. The RMS from the process of coregistration of the point clouds based on the twelve common points are presented in Table 5-2.

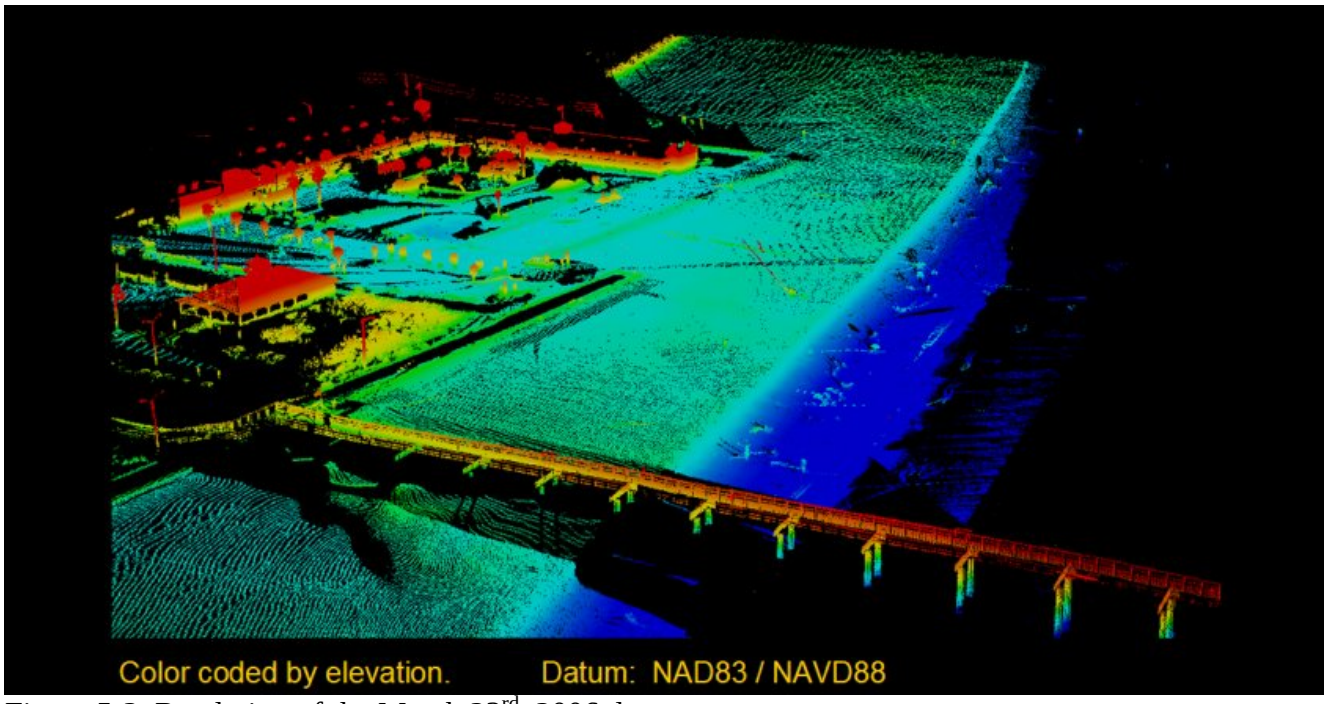

Figure 5-2. Rendering of the March 23rd, 2006 dataset.

A set of control features that were used to visually verify the coregistration of the point clouds are presented in Figure 5-3. Different colors are used to identify point clouds collected on different days. From this figure it can be verified the relatively good agreement in coregistration among the scans as described by the RMS values of Table 5-2.

Table 5-1. Control points used for the geo-referencing of the March 23, 2006 dataset.

P	Sensor Coordinates [m]			Geodetic Coordinates [m]			Transformation Residuals		
	X	Y	Z	Easting	Northing	E Hgt	Est	Nrth	Hgt
P1	-27.497	-46.728	-0.623	474315.01	3303135.38	-23.59	-0.083	0.034	0.007
P2	-78.630	-32.978	-1.623	474346.58	3303177.83	-24.24	0.053	-0.002	-0.022
P3	5.096	63.037	-2.603	474404.80	3303064.44	-24.42	0.054	0.064	0.077
P4	58.391	108.561	1.111	474427.29	3302998.09	-20.61	0.088	0.067	0.366
P5	-166.835	-38.306	-1.419	474374.32	3303261.80	-23.89	-0.001	-0.066	0.039
P6	0.000	0.000	0.000	474348.44	3303092.52	-22.23	-0.284	0.050	-0.249
P7	32.780	171.860	0.959	474495.48	3302998.67	-19.34	0.174	-0.148	-0.218
				RMS of Transformation Residuals [m]			0.137	0.074	0.190

Table 5-2. Point clouds coregistration RMS values.

Point Clouds	Coregistration RMS [m]		
	Easting	Northing	Height
1-2	0.108	0.237	0.135
1-3	0.090	0.211	0.116
1-4	0.086	0.133	0.098

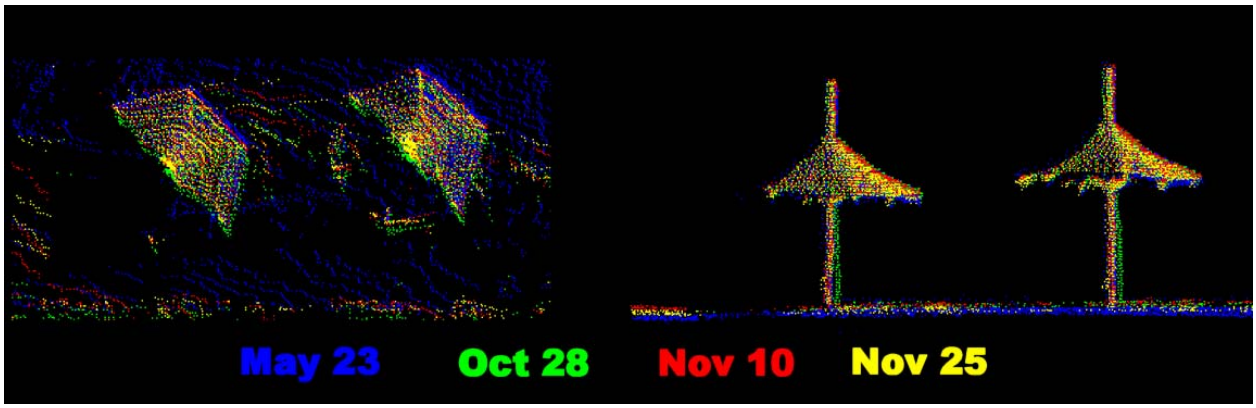

Figure 5-3. Features used to check the co registration of the point clouds.

The third step consisted of cropping the point clouds to the specific area of interest as defined by the orange polygon on Figure 5-1 B and filtering to remove all the non-surface objects (people, beach chairs, etc.). The fourth and final step was the creation of 10 cm spacing regular grids by the method of triangulation with linear interpolation using Surfer & Matlab software packages. Figure 5-4 present image maps created from the 10 cm elevation grids.

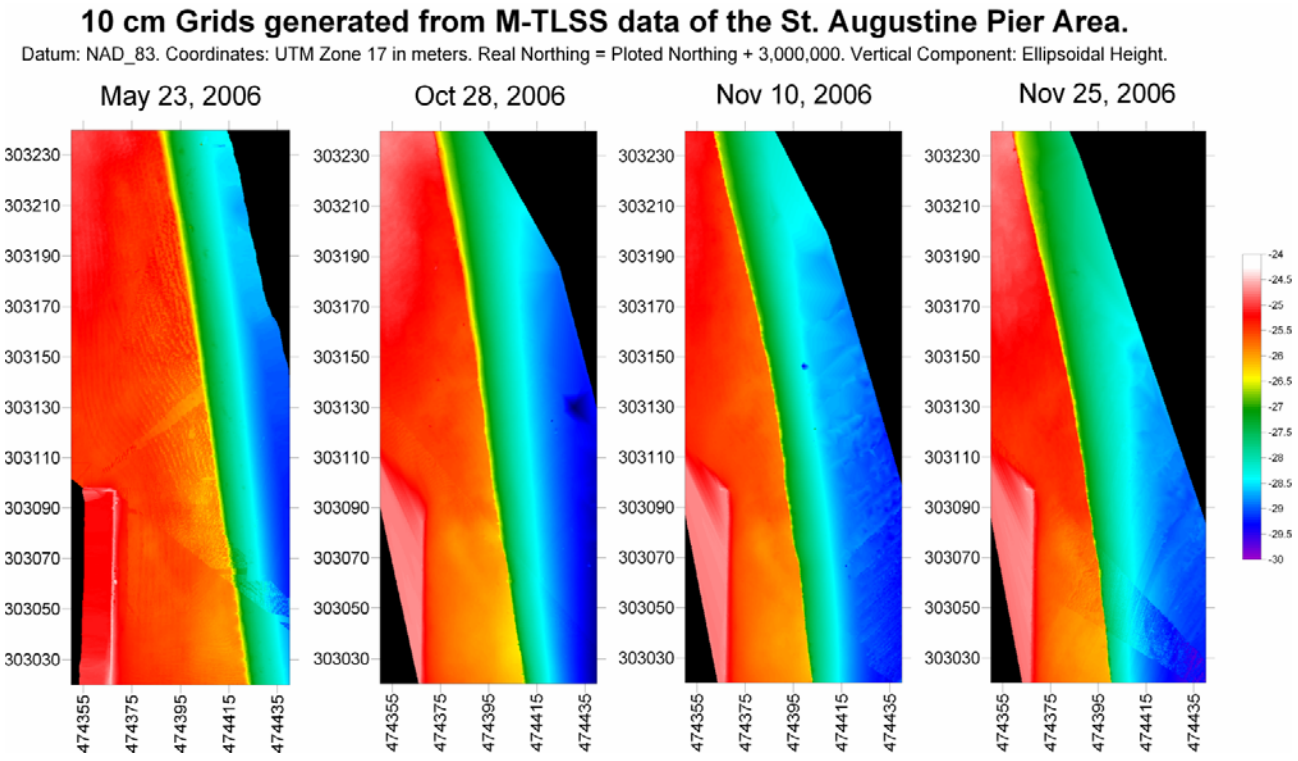

Figure 5-4. Image maps from the 10 cm elevation grids.

5.5 Results

5.5.1 Elevation Changes

Elevation changes were computed for both short and long term periods. Using Surfer the elevation grids were differenced two at a time. Two comparisons were performed for long term change (May 23 to October 28 and May 23 to November 25) and two for short term change (October 28 to November 10 and November 10 to November 25). The results of the elevation change detection are presented as difference grids on Figure 5-5. The long term change grids reflect an average of 20 cm of reduction in the berm elevation and a 1.4 to 2 m difference in elevation between the berm and the surf zone. The short term change grids show a general preservation of the berm elevation and an average difference of 1m in the berm to surf zone elevation.

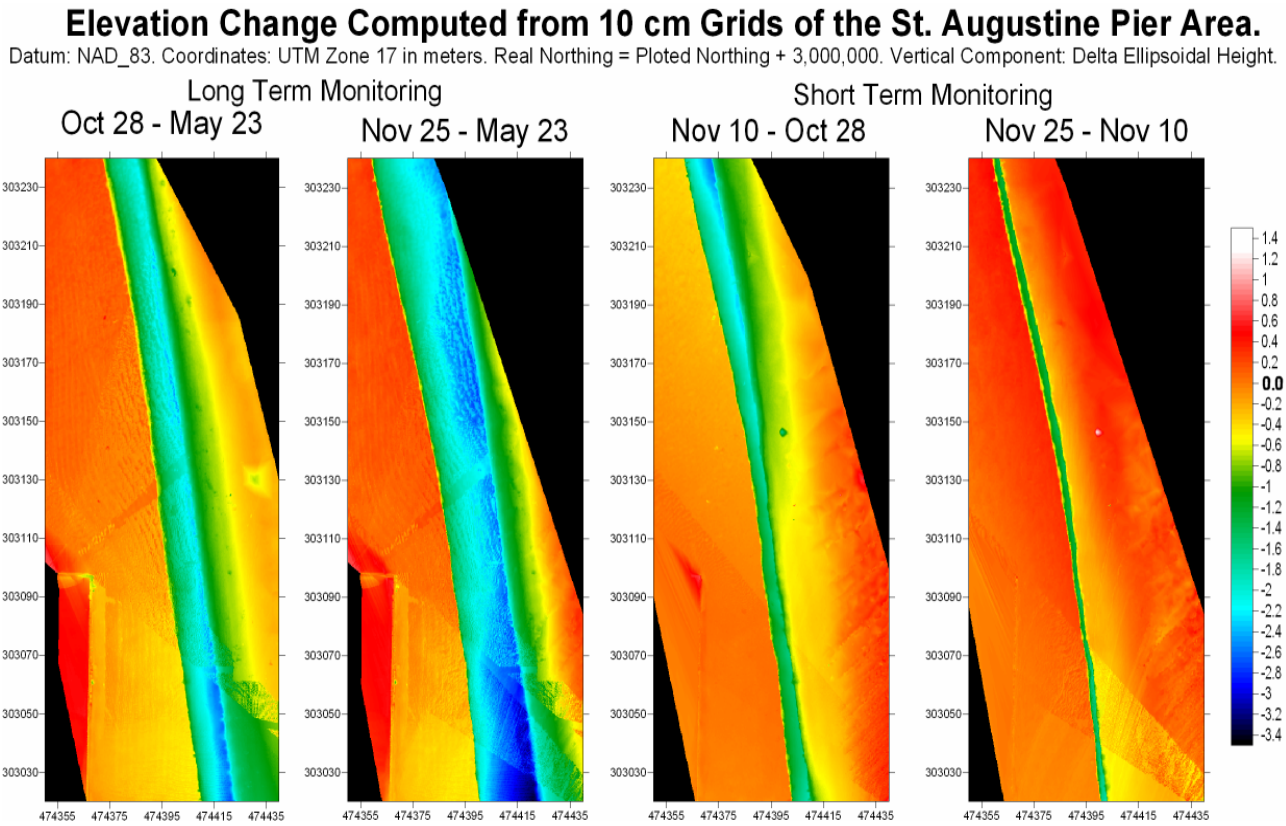

Figure 5-5. Image maps from the elevation change grids.

5.5.2 Volume Changes

Total volume differences were computed and normalized to obtain lost volumes per unit beach length and rates of lost volume per unit beach length. For planners and engineers the total volume lost is important because that translates directly to the renourishment costs, however absolute measurements are difficult to use for comparisons; lost volumes per unit beach length and rates of lost volume per unit beach length to provide a better understanding of the magnitude of the change. Table 5-3 summarizes some of the volume computations performed from the elevation grids.

Table 5-3. Summary of volume change computations.

From	To	Days	Lost volume [m^3]	Volume loss rate [m^3/day]	Volume loss/beach unit length [m^3/m]	Volume loss/beach unit length rate [m^3/m day]
5/23/2006	11/25/2006	186	13168.245	70.79702	59.31642	0.318905
5/23/2006	10/28/2006	158	9166.72	58.01722	41.29153	0.261339
10/28/2006	11/25/2006	28	4945.707	176.6324	22.27796	0.795641
10/28/2006	11/10/2006	13	5535.53	425.81	24.93482	1.918063

5.5.3 Beach Line and Crest of Berm Extraction From the Grids

The recession of the beach line is an important phenomenon to record and quantify. The beach line is defined by the mean higher high water (MHHW) line; which is an average of the higher high water height of each tidal day over nearly 19 years. For the study area the mean higher high water line is determined at 0.6 meters for the NAVD88 vertical datum. Because the elevation grids were created using ellipsoids heights a conversion from orthometric height to ellipsoidal height was performed. The average Geoid separation was found to be 28.612 meters so the beach line was extracted from the -28.012 meters ellipsoidal height contour. Similarly the crest of berm was extracted from the -26.5 meters contour, Figure 5-6 contains plots with the beach and crest of berm lines.

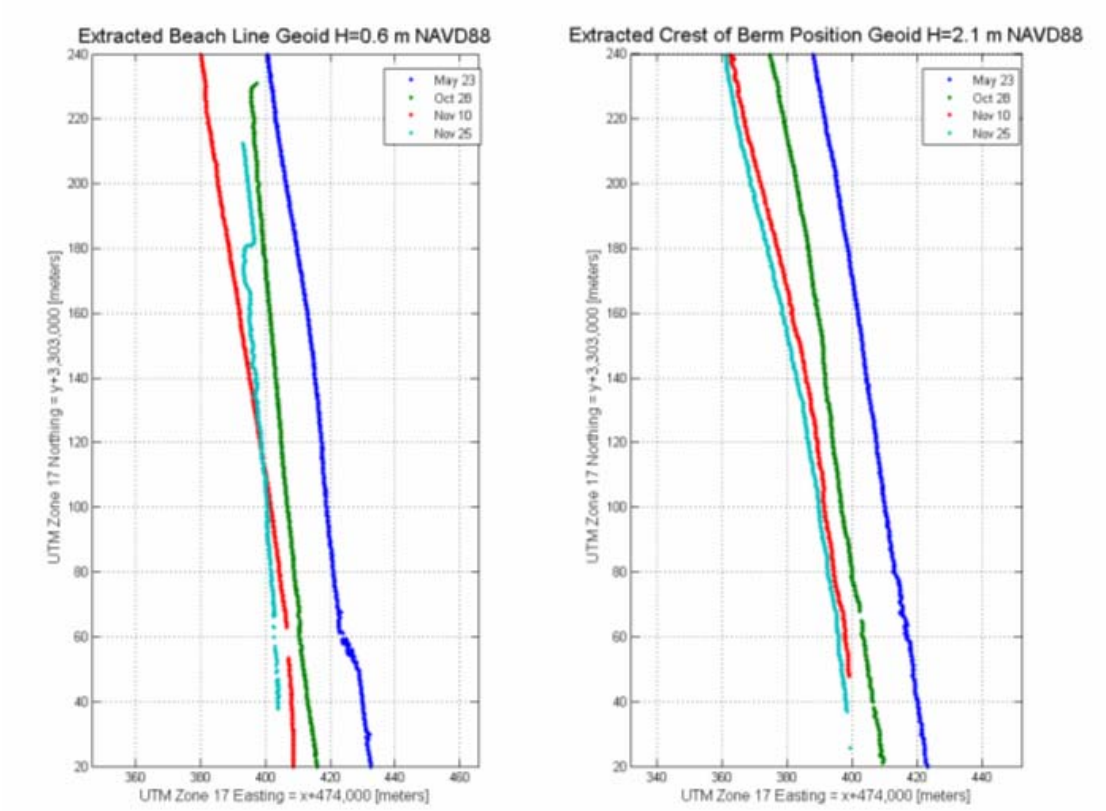

Figure 5-6. Beach line and crest of berm position plots for each of the data collection dates.

5.5.4 Across Beach Profile Extraction

The traditional data collection method for studying beach erosion is transect sampling. FDEP standard require cross shore transects at every 1,000 feet apart along shore; with a collection interval not to exceed 25 feet and at all grade breaks. From the M-TLS dataset generated grids, transects can be obtained automatically at higher resolutions such as presented in Figure 5-7. To do any kind of interpretation with this transects is necessary to specify a tolerance in the horizontal and vertical components due to the accuracy of the coregistration procedure. This tolerance is in the same order of the highest residual of the coregistration control points. These residuals were in the order of 11cm in the East-West direction, 24 cm in the North-South direction and 13 cm in the vertical dimension. From these transects it can be seen that the beach line and the berm line receded twenty meters on average. However, the most interesting

result is that half of that recession occurred in the last four week period of the complete 27 week observation program. This accelerated erosion can be related to the appearance of the North Eastern winds which are recognized as the main sediment transport mechanism of that area. The berm maintained a constant height of roughly 3 meters above the beach line.

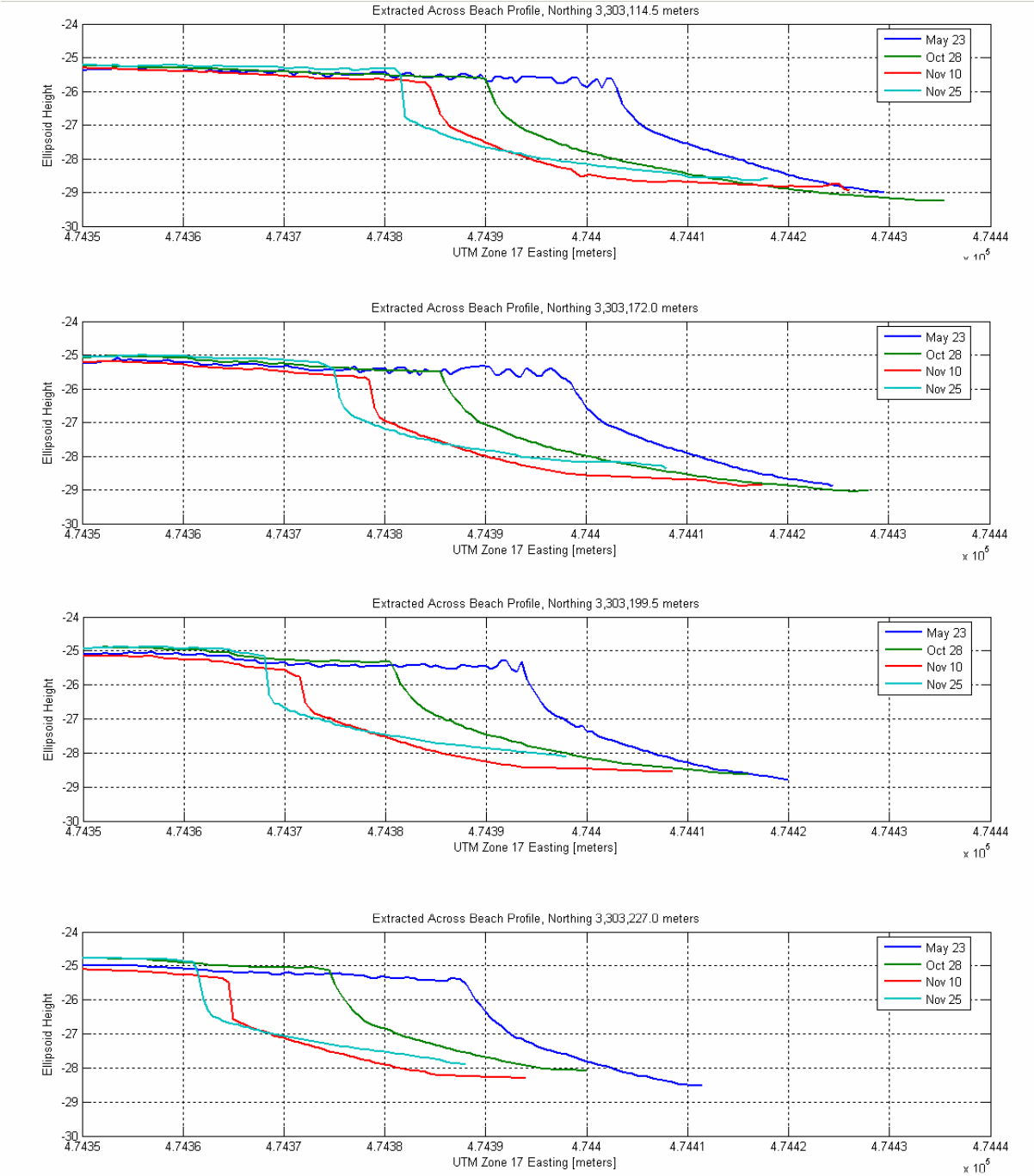

Figure 5-7. Beach profiles extracted from the grids showing the recession of the berm.

5.6 Comparison Between Traditional Methods and M-TLS

Based on the resolution established by FDEP standards for beach profile topographic surveying, simulated GPS or leveling profiles were generated to illustrate the difference in resolution between traditional surveying methods and these achieved by the M-TLS. The results are presented in Figure 5-8, these show that the traditional methods do not capture the small scale details of the beach and berm surface. It can also be seen that the traditional method can over estimate beach erosion as they do not sample properly the berm crest.

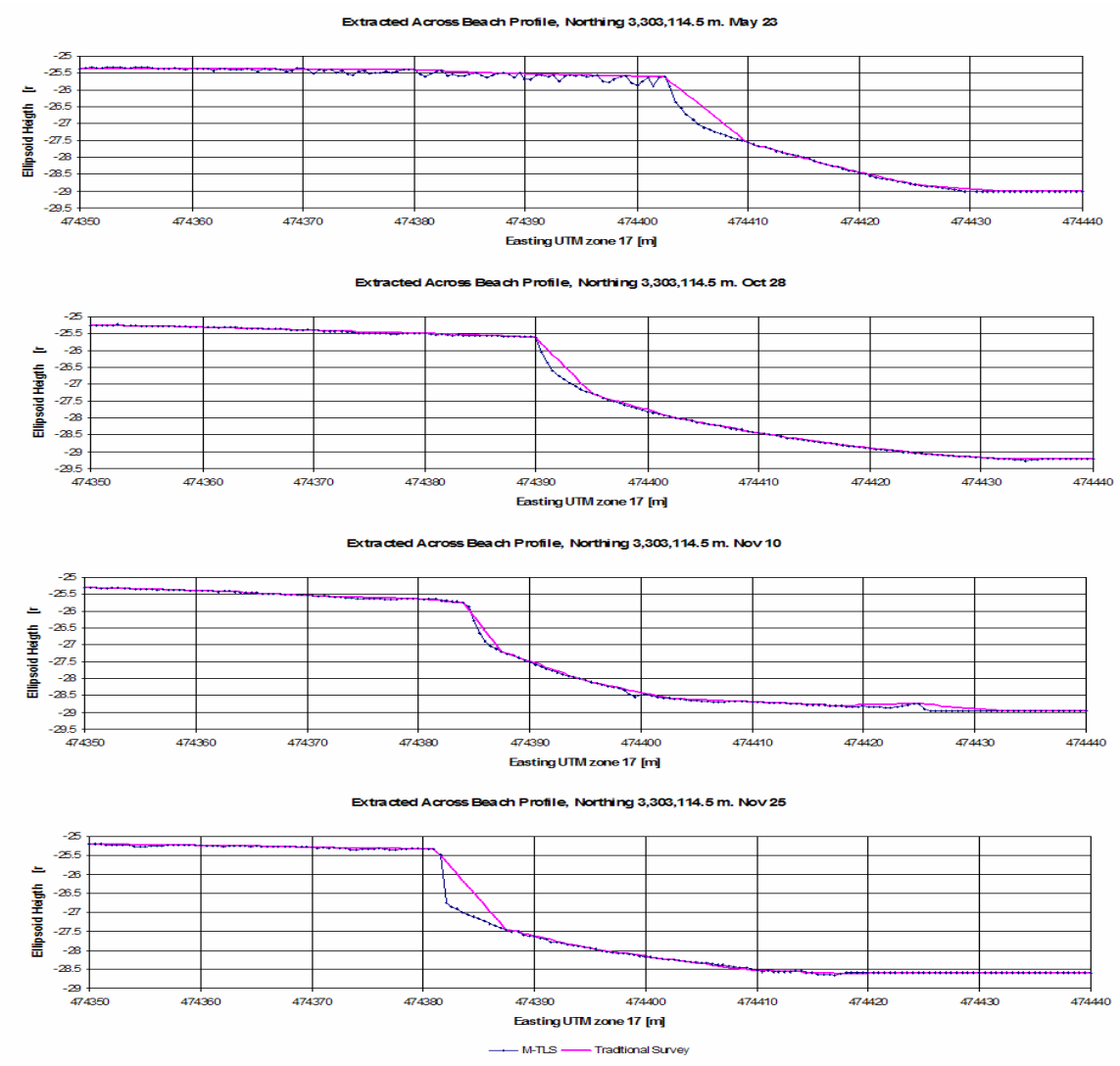

Figure 5-8. Comparison of profile resolution generated from traditional methods and M-TLS.

CHAPTER 6
SOIL ROUGHNESS METRICS DETERMINATION

6.1 Motivation

The application of active and passive microwave remote sensing is increasing in the field of soil science as a tool to map soil properties. It is possible to use microwave backscattering to extract geophysical surface parameters such as soil moisture content and soil surface roughness. The scattering of microwave energy is determined by the sensor parameters such as wavelength, polarization and observation geometry; it also depends on the surface dielectric properties and roughness. In theory it is a simple computation to solve for one of the parameters (moisture or roughness) having prior knowledge of the other and of the microwave energy backscattering. However many practical problem arise when trying to parameterize the soil surface roughness. (Callens et al.; 2006 & Zribi et al.; 2000) Traditionally soil roughness has been characterized as a single scale process obtained from 2D profiles and parameterized by the root mean square (RMS) height (s), the correlation length (ℓ) and autocorrelation function ($p(\ell)$). The main limitations of this modeling as reported in the literature are:

- The soil surface and its roughness are multiscale in nature, simplifying them to single scale parameters implies a loss of information.
- Theoretical and field data have shown that different values of the roughness parameters, especially on "s" and "ℓ", can be obtained from the same surface as a function of the profile length, discretization interval, the instrument resolution, and the overall shape of the profile.
- The surfaces are assumed to follow Exponential or Gaussian distributions without having the ability to check these assumptions.

To overcome these limitations and the inadequacy of the single scale models in describing complex soil surfaces, several alternative multiscale roughness description models have been proposed. They include the mixture of small and large single scale features, the use of random fractals and fractal dimensions to describe the surface (Davidson et al., 2000), and the use of

plane facets and 3D statistical analysis (Zribi et al., 2000). However, the universally accepted theoretical microwave backscattering models such as the Small Perturbation Model (SPM), Kirchoff Approximation (KA) and the Integral Equation Model (IEM) continue to require only the single scale parameters as inputs.

A novel approach using the M-TLS to scan scattering surfaces to generate 3D terrain models was explored. From the 3D models the distribution function of the single scale parameters can be obtained, which is expected to fully describe the surface roughness, thus overcoming the limitation of under representation produced by the profiling sampling methods.

6.2 Use of LIDAR Technology

The traditional methods of obtaining the soil profiles to compute the roughness parameters by mechanical means are the Needle-like Profiler and the Mesh Board. A complete description of these mechanical profilers and the data collection procedures is provided by Mattia et al. (2003). The main disadvantage of these mechanical methods is that they tend to disturb the surface that is under study. Mesh Boards have to be hammered into the soil, while Needle-like Profilers tend to penetrate into the surface yielding noisy measurements of the heights. Modern methods are aimed at not disturbing the surface; these methods use non-contact instruments such as laser profilers , optical imagers and acoustic backscatter instruments (Mattia et al., 2003; Zribi et al., 2000; Oelze et al., 2003).

Laser profilers have been used intensely for soil roughness digitizing; most of them are commercial systems capable of high spatial resolutions of the order of 1 mm or less but limited to relatively short profile lengths, usually no more than a few meters. Special laser profilers have been develop to allow the measurement of longer profiles, such as the CESBIO-ESA laser profiler, which is capable of acquiring roughness profiles up to 25 m long (Davidson et al., 2000).

Whether using mechanical or non-contact techniques, there are sources of error that are common when characterizing the soil roughness. These are the truncation Error, which arises from measuring relatively short profiles; and profiler error, which is due to the intrinsic limitations of a measurement method (Mattia et al., 2003). It is expected that by full surface digitizing, using the M-TLS, the errors from these sources will be drastically reduced. A search of the literature found no journal papers on the use of terrestrial laser scanner to digitize a surface and later compute its roughness parameters.

6.3 Data Collection

Data was collected using the ILRIS in an experimental plot at the University of Florida Plant Science Research and Education Center at Citra, Florida. The collected data contains the soil surface of the footprints of two passive microwave radiometers operating in the L and C bands. Three different time samples were collected, the first just after soil tilling, the second after corn planting and the third after the crop was harvested. An additional data set that contains a larger horizontal variation was collected on a commercial plantation near Hastings, Florida. A description of the collected data is provided in Table 6-1.

Table 6-1. Soil roughness collected datasets

Dataset ID	Collection Date	Conditions	Radiometer Footprint
Field1	March 08, 2006	After Tilling	-
Field3			Mesh Board Test
Citra01	March 10, 2006	After Planting	L
Citra02			C
Citra03			Mesh Board Test
Citra04			Mesh Board Test
Citra05			L
Citra06			C
CitraCBand	May 30, 2006	After Harvesting	C
CitraLBand			L
Hastings	October 28, 2006	Plowed and Planted	N/A

Two traditional meshboard measurements were made near the L Band and C Band radiometer footprints with the soil tilled. For the present analysis only two data sets will be considered: Citra 02 and Hastings.

6.4 Data Processing

The first step in the process was to prepare the point clouds for analysis. For each test area this consisted of converting the existing tilted point cloud terrain into that of a flat level terrain. The angles required to perform the transformation were determined by fitting a plane to selected ground points, finding the normal vector and computing the rotation angles about the X and Y axes. The rotation was performed using TerraScan transformation module. Once leveled the point cloud was rotated about the Z axis to align the radiometer footprint axes to the point cloud X and Y axes. Finally the point cloud was cropped to a 4 x 6 meter plot corresponding to the radiometer footprint. Figure 6-1 shows renderings of the raw and a rectified and point cloud.

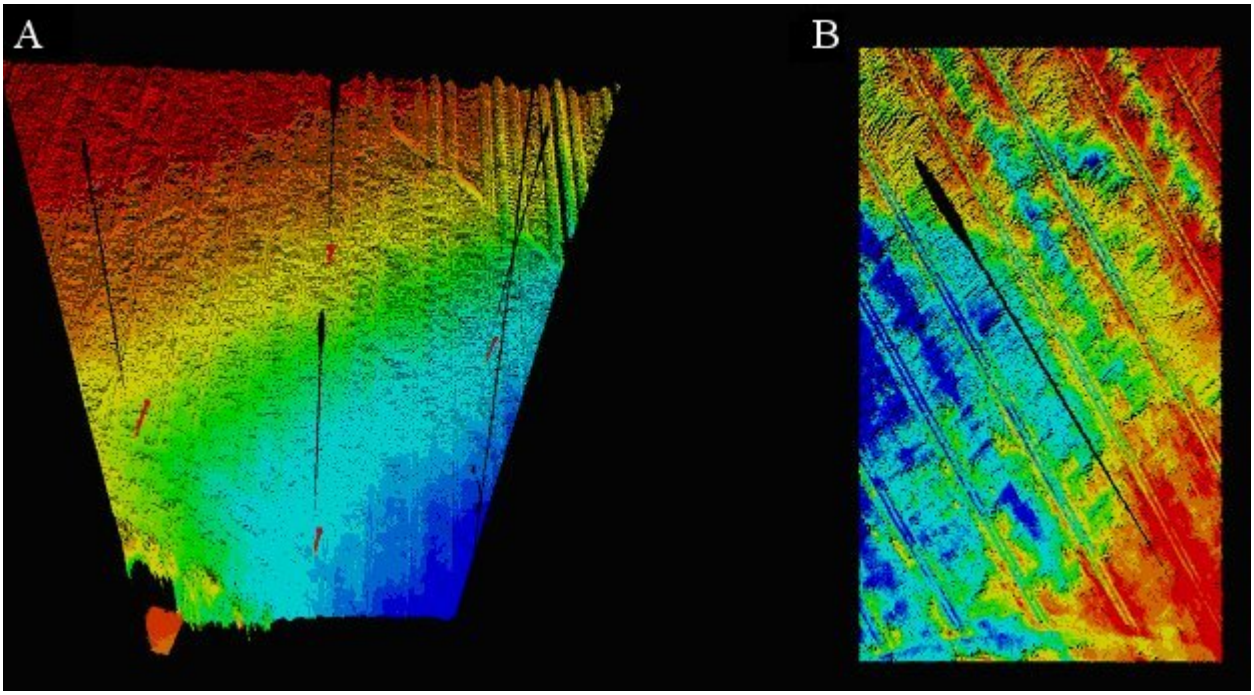

Figure 6-1. Dataset preprocessing steps. Rendering of A) raw point clouds and B) rectified point cloud from the Citra 02.

From the cropped and rectified point clouds regular grids with one cm cell spacing were created using a triangulation with linear interpolation gridding function in Matlab. Figure 6-2 shows image maps of the elevation grids for two of the analyzed dataset.

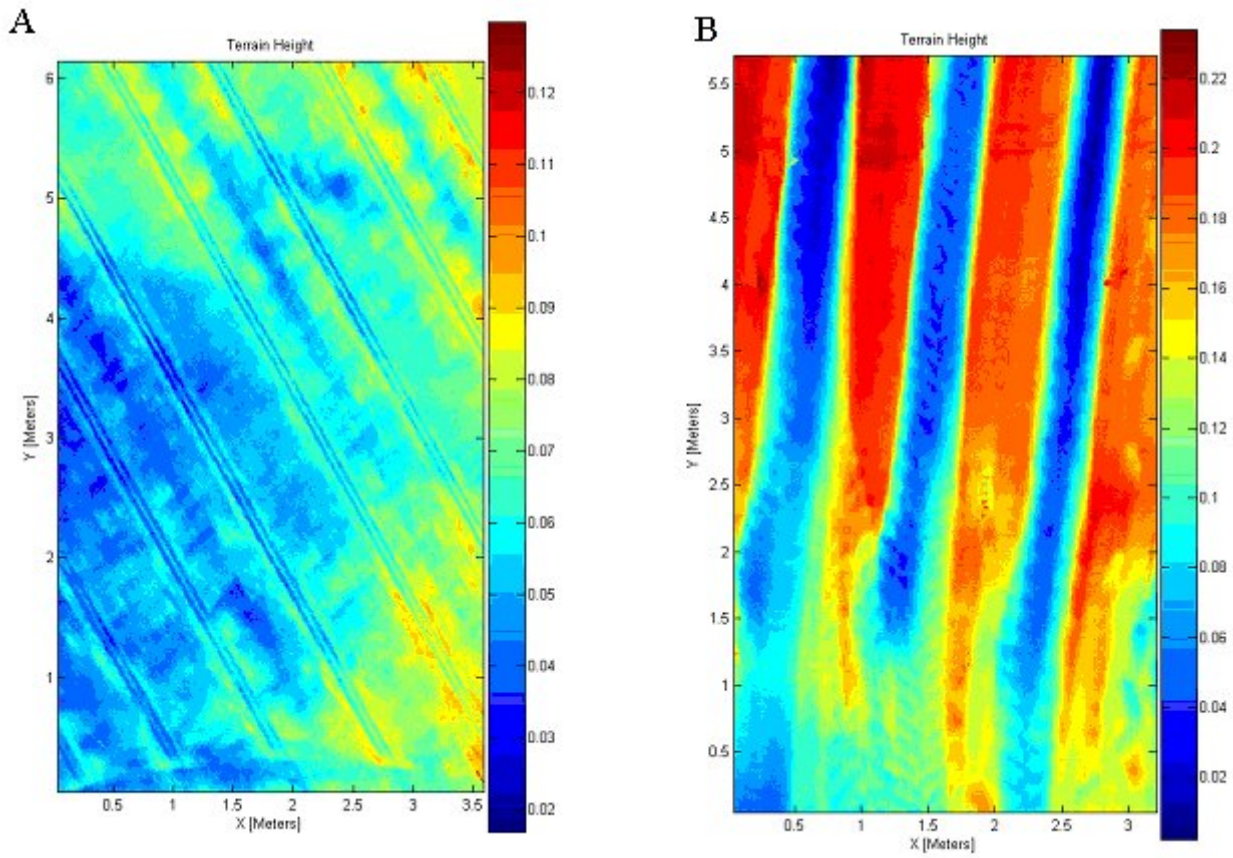

Figure 6-2. Renderings of the 1 cm elevation grids. A) Citra 02. B) Hastings.

The cropped point clouds and the grids were used to derive the roughness metrics. The expressions for the height RMS, correlation length and autocorrelation function for 2D profiles are given in Table 6-2. Several tests were performed to prove the advantages of using MTLS datasets to extract the single scale metrics over the traditional profiling methods. These tests are:

- From the regular grid a set of random 2D profiles was extracted parallel to the X and Y axes. The root mean square height (s) and the correlation length (l) for each profile were computed using the traditional formulas. Mean and standard deviations of the roughness parameters of the profiles of the same plot were computed.
- The formulas used to compute root mean square height (s) and correlation length (l) from the 2D transects were extended to 3D surfaces and are used to compute the roughness metrics for

the two plots. The correlation was also extended from 1D to 2D, so the correlation length could be found for either X and Y, or a combination of both directions. The 2D correlation length was converted into a 1D length and distribution functions of correlation lengths were obtained.

- Comparisons were made between the averaged roughness parameters values from the random profiles with the ones obtained from the 3D models.

- Test were performed to verify the assumption that the autocorrelation functions follow Exponential or Gaussian forms.

Table 6-2 Definition of soil roughness parameters.

	Callens et al.	Thoma et al.
Height mean	$\bar{z} = \frac{1}{N}\sum_{i=1}^{N} z_i$	
Height RMS	$s = \sqrt{\frac{1}{N-1}\left[\left(\sum_{i=1}^{N} z_i^2\right) - N \times \bar{z}^2\right]}$	$s = \sqrt{\frac{1}{N}\sum_{i=1}^{N}\left(z_i - \bar{z}\right)^2}$
Normalized correlation function	$\rho(h) = \rho(j\Delta x) = \frac{\sum_{i=1}^{N-j}\left(z_i \times z_{i+j}\right)}{\sum_{i=1}^{N} z_i^2}$	$\rho(h) = \rho(j\Delta x) = \frac{\sum_{i=1}^{N-j}\left[\left(z_i - \bar{z}\right)\left(z_{i+j} - \bar{z}\right)\right]}{\sum_{i=1}^{N}\left(z_i - \bar{z}\right)^2}$
Correlation length	$l \; such \; that : \rho(l) = \frac{1}{e}$	
Exponential autocorrelation function	$\rho(h) = e^{\left(-\frac{\lvert h \rvert}{l}\right)}$	-
Gaussian autocorrelation function	$\rho(h) = e^{\left(-\frac{h^2}{l^2}\right)}$	-

6.5 Results

6.5.1 Simulated Profiling Results

From the elevation grids random transects were extracted parallel to the X & Y axes to simulate traditional soil roughness profiling techniques. Using the 2D formulas the roughness metrics were computed to verify the variability of the metrics with the profile selection. Figures 6-4 to 6-7 show the extracted profiles and their respective normalized autocorrelation plot from the Citra 02 and Hasting datasets. The red line in the autocorrelation plots represents the 1/e value used to determine the correlation length.

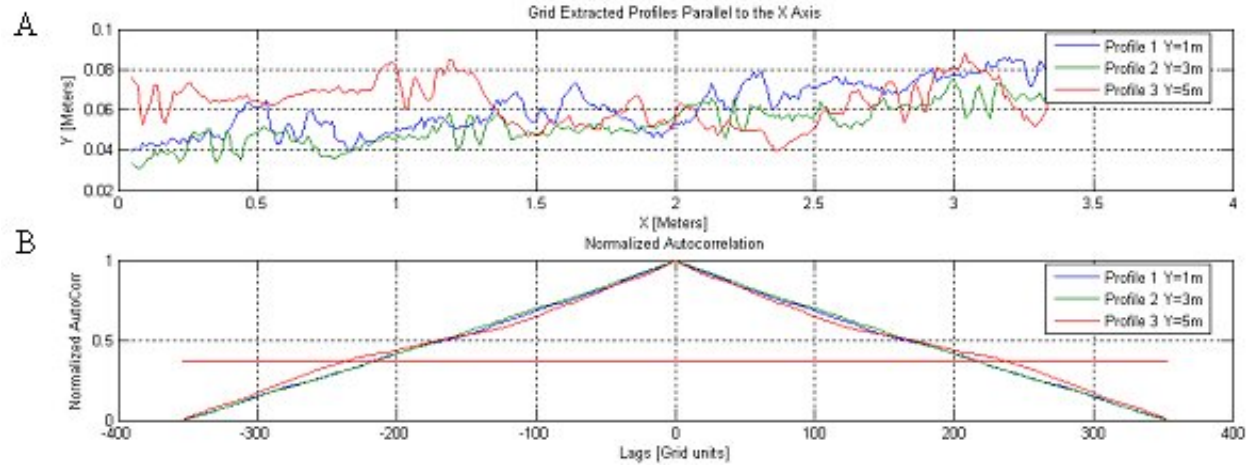

Figure 6-4. Roughness parameter plots for the Citra 02 dataset parallel to the X axis. A) Extracted profiles. B) Normalized autocorrelation plot.

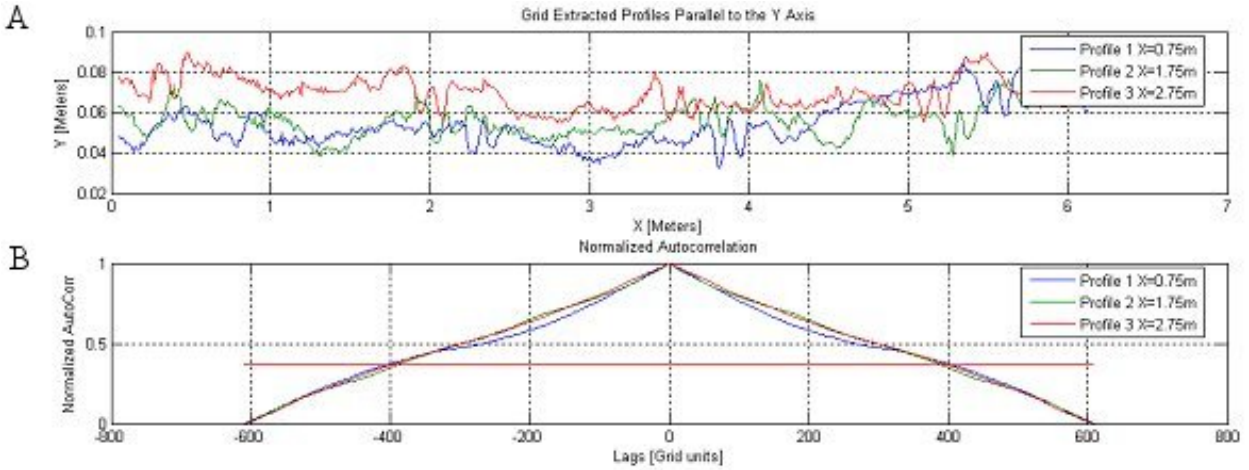

Figure 6-5. Roughness parameter plots for the Citra 02 dataset parallel to the Y axis. A) Extracted profiles. B) Normalized autocorrelation plot.

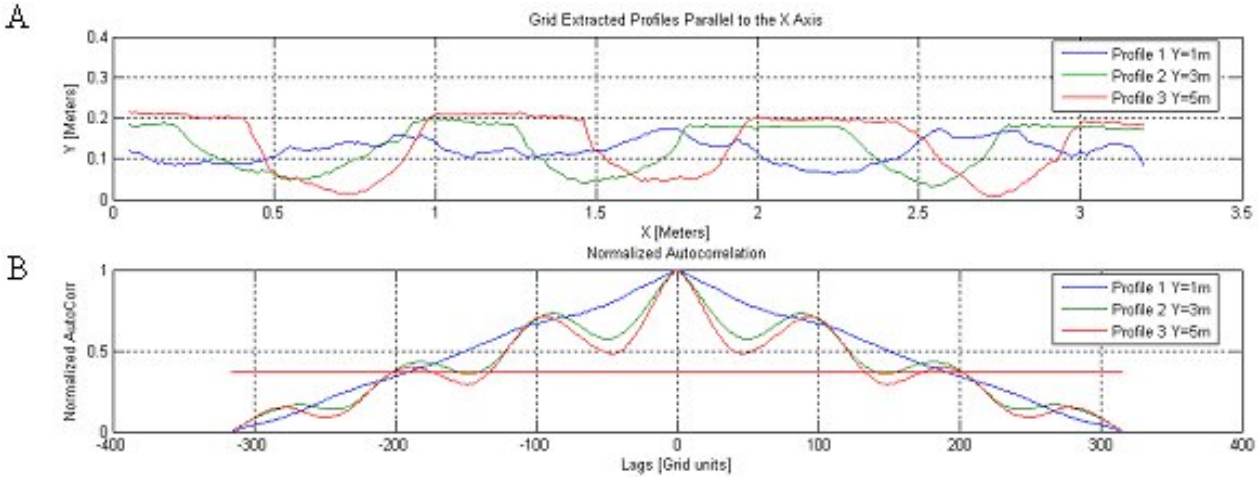

Figure 6-6. Roughness parameter plots for the Hastings dataset parallel to the X axis. A) Extracted profiles. B) Normalized autocorrelation plot.

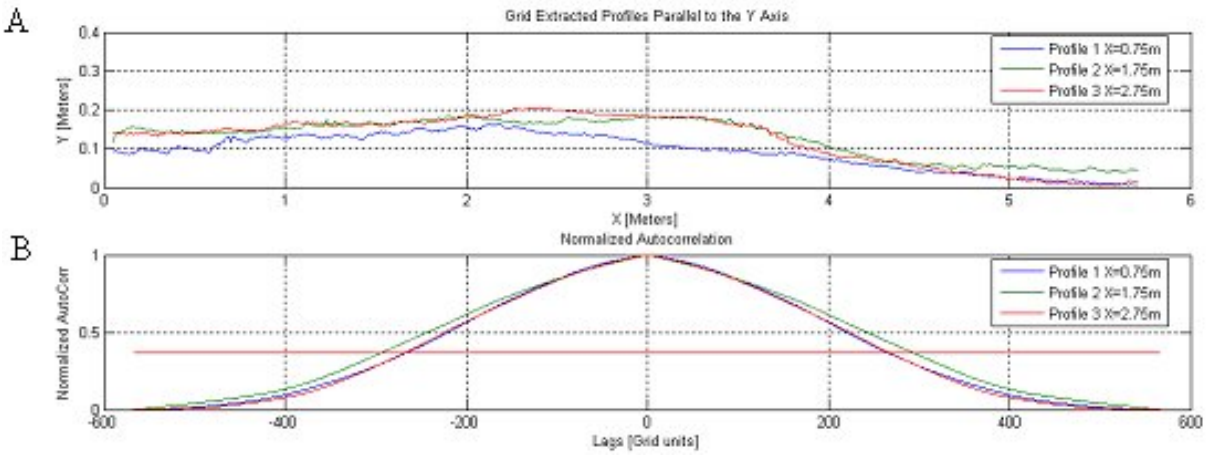

Figure 6-7. Roughness parameter plots for the Hastings dataset parallel to the Y axis. A) Extracted profiles. B) Normalized autocorrelation plot.

The results of the roughness metrics are summarized in Table 6-3 for the Citra 02 data set and in Table 6-4 for Hastings. It can be observed from the tables that the mean height RMS from profiles in both directions (parallel to Y axis and parallel to X axis) are relatively close (3 to 25% variation), however the correlation length can vary greatly between directions (39-77%).

Table 6-3. Soil roughness parameters results from random profiles for the Citra 02 grid.

Data set	RMS regular spacing [m]	1/e correlation length [m]
Citra 02 Y=1 m	0.0133	2.1718
Citra 02 Y=3 m	0.0100	2.1657
Citra 02 Y=5 m	0.0108	2.3727
Citra 02 X=0.75 m	0.0115	4.0464
Citra 02 X=1.75 m	0.0079	3.8960
Citra 02 X=2.75 m	0.0077	3.9844
Mean parallel to X	0.0114	2.2367
Mean parallel to Y	0.0090	3.9756
Overall mean	0.0102	3.1062
Overall σ	0.0022	0.9565

Table 6-4. Soil roughness parameters results from random profiles for the Hastings grid.

Data Set	RMS Regular Spacing [m]	1/e Correlation Length [m]
Hastings Y=1 m	0.0277	1.9087
Hastings Y=3 m	0.0543	2.0181
Hastings Y=5 m	0.0715	2.0127
Hastings X=1 m	0.0458	2.6581
Hastings X=3 m	0.0497	2.9350
Hastings X=5 m	0.0633	2.6739
Mean parallel to X	0.051	1.980
Mean parallel to Y	0.053	2.756
Overall Mean	0.052	2.368

6.5.2 Extension of the 2D Formulas for a 3D Surface.

The height RMS formula provided for 2D profiles in Table 6-2 is valid without modification for the 3D soil surface. For 2D profiles the correlation length is defined as the distance for which the value of the normalized 1D autocorrelation is 1/e. The concept can be extended for a 3D surface by computing a 2D autocorrelation with two parameters (x lag and y lag) which results in a 3D surface. The 1/e contour can be located on that surface, and the correlation length can be defined as the scaled distance (considering grid element size) from the origin to a particular point on the contour. The advantage of this method over the traditional profiling method is that from this a complete distribution function of the correlation length is obtained rather than a single value.

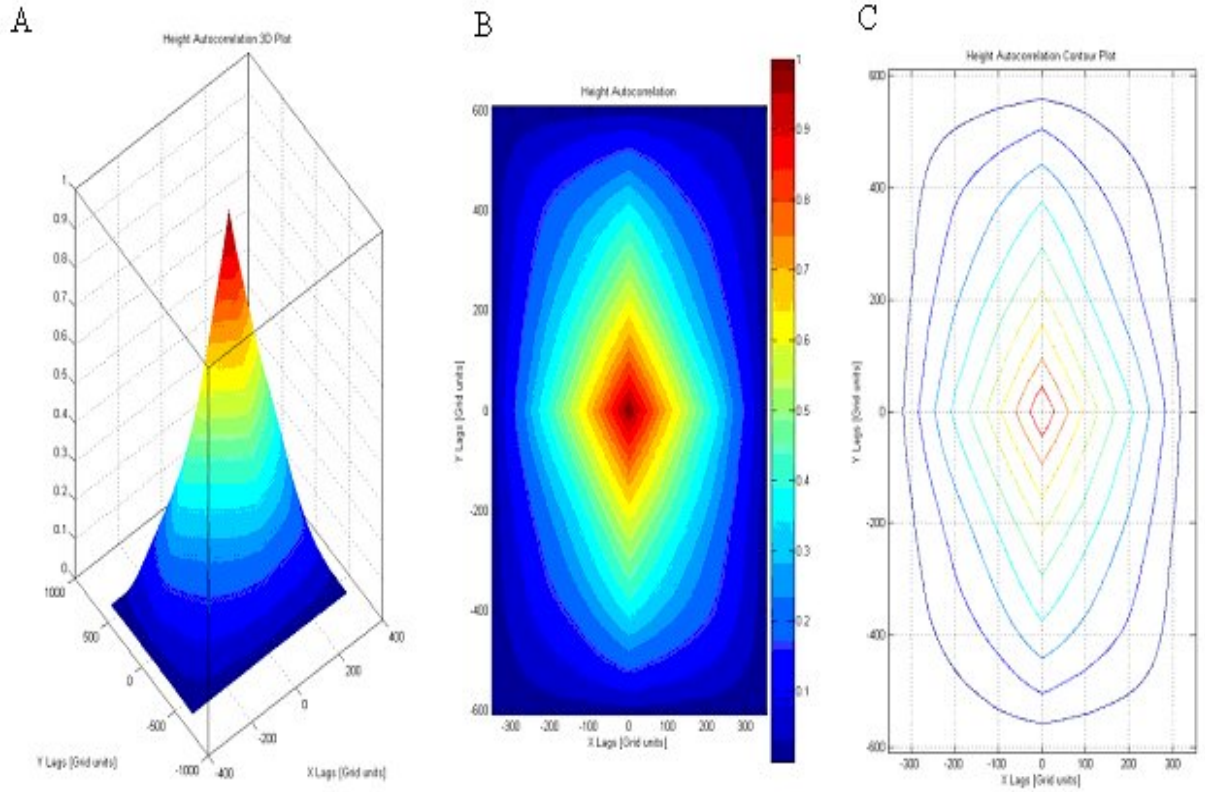

Figure 6-8. Citra normalized height autocorrelation. A) 3D plot. B) Color map. C) Contour plot.

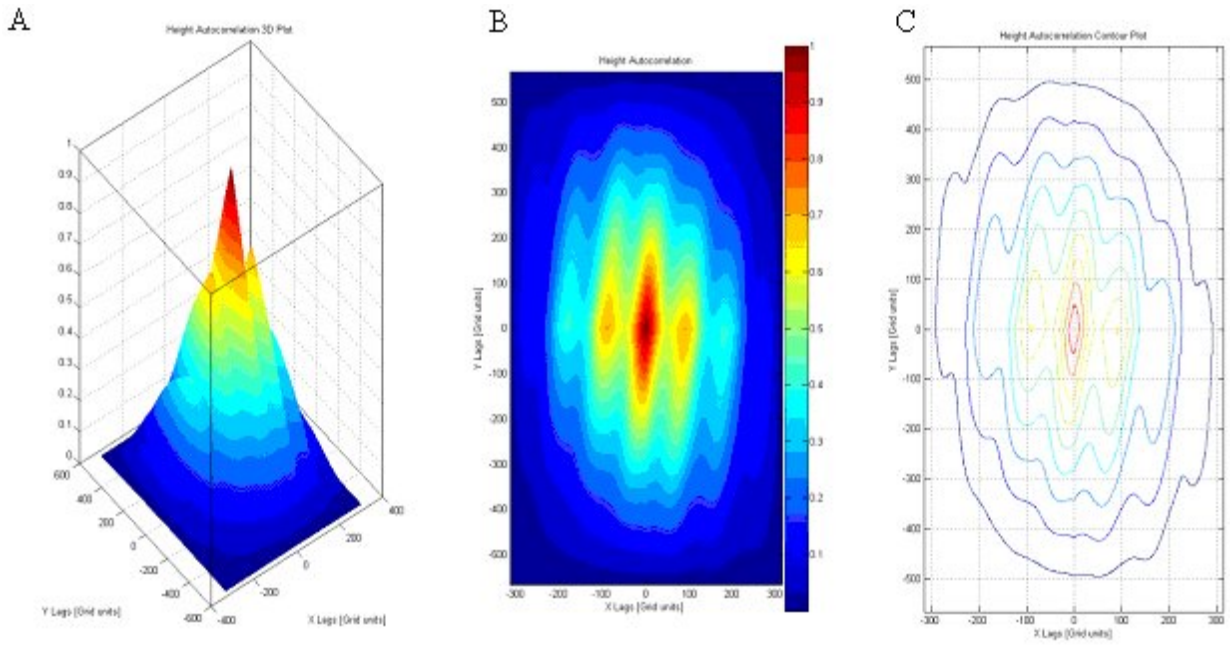

Figure 6-9. Hastings height autocorrelation. A) 3D plot. B) Color map. C) Contour plot.

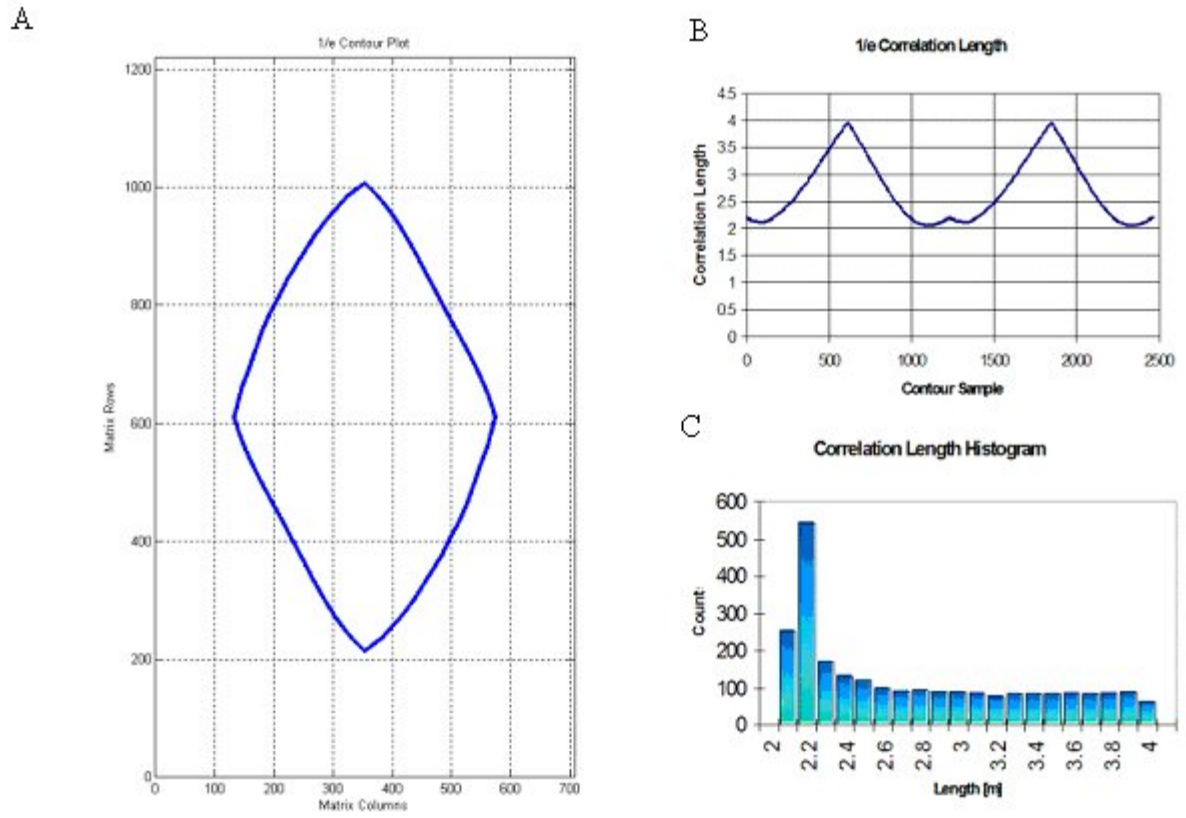

Figure 6-10. Correlation lengths extraction for the Citra 02 dataset. A) 1/e contour plot of the 2D autocorrelation function. B) Unfolded correlation length plot. C) Distribution function of correlation lengths.

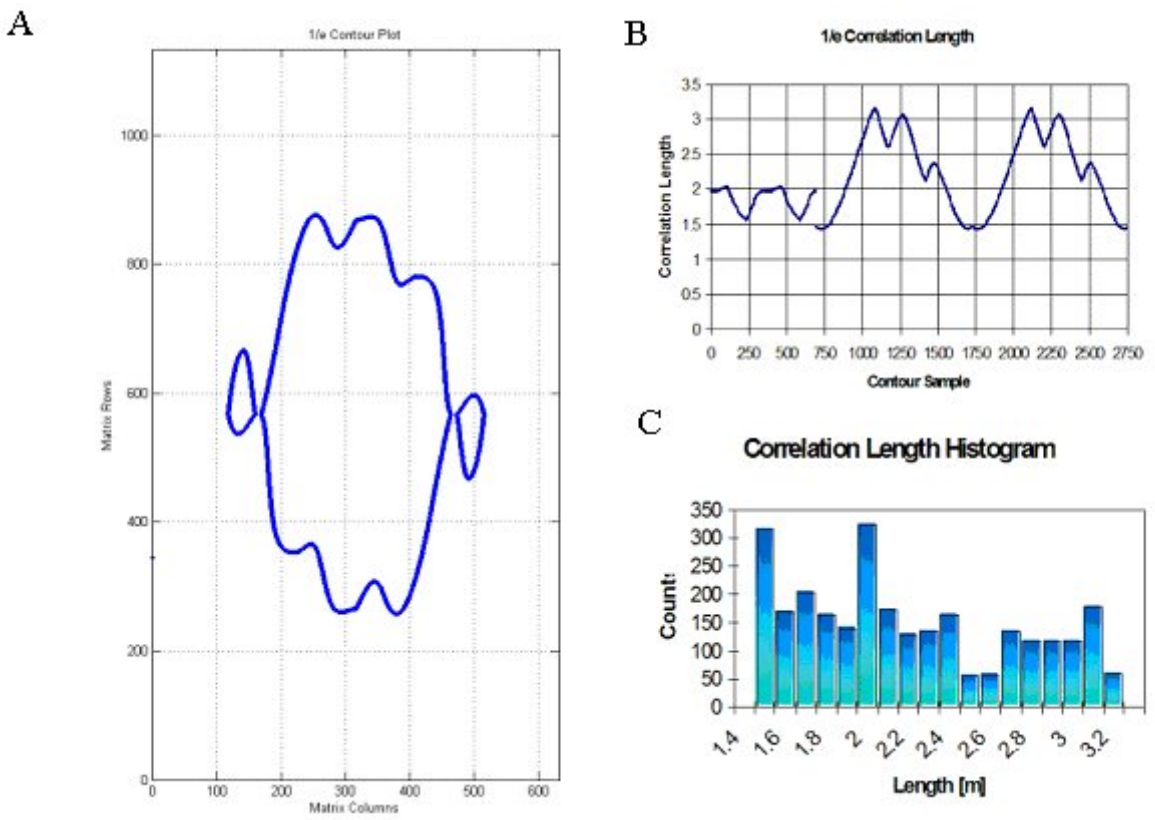

Figure 6-11. Correlation lengths extraction for the Hastings dataset. A) 1/e contour plot of the 2D autocorrelation function. B) Unfolded correlation length plot. C) Distribution function of correlation lengths.

Graphs of the 2D autocorrelation are presented in figures 6.8 and 6.9, part A of the figures are 3D plots that show the normalized autocorrelation function as a function of the X and Y lag units. Part B is an image map of the same normalized autocorrelation values and part C is a contour plot of the correlation values. From the normalized autocorrelation the 1/e contour can be extracted as shown in figures 6.10 and 6.11 part A. From each point in the contour its direction and correlation length can be computed. In part B of figures 6.10 and 6.11 the contour is unfolded and the correlation length for each point is computed and plotted without taking into consideration the direction. The obtained correlation length are then grouped and binned to create the histograms on part C of the figures. Table 6-5 provides a summary of the roughness parameters values extracted from the 3D surface models. From this table and figures 6.10C and

6.11C it can be seen that the mean correlation length is not necessarily a good descriptor of the distribution.

Table 6-5. Soil roughness parameters from 3D surface models

Roughness Parameter	Citra 02	Hastings
(s) RMS height from point cloud [m]	0.013546	0.05013
(s) RMS height from grid model [m]	0.012674	0.0547
(ℓ) Mean correlation length [grid units]	271.78	215.25
(ℓ) Mean correlation length [m]	2.7178	2.1525
Standard deviation of correlation length [grid units]	60.42	52.23
Standard deviation of correlation length [m]	0.6042	0.5223

6.5.3 Comparisons of Roughness Metrics From Profiles vs. Full Surface

The values of the roughness parameters obtained from the random profiles and the 3D surface are tabulated for comparison in tables 6.6 and 6.7.

Table 6-6. Comparison of soil roughness parameters for Citra 02 from 3D surface models and random generated profiles.

Roughness Parameter	3D Surface	Transects // to X	Transects // to Y	All transects
(s) RMS height [m]	0.012674	0.0114	0.0090	0.0102
(ℓ) mean correlation length [m]	2.7178	2.2367	3.9756	3.1062
Min correlation length [m]	2.0597	-	-	-
Max correlation length [m]	3.9651	-	-	-
Mode correlation length [m]	2.2	-	-	-
σ of correlation length [m]	0.6042	0.1178	0.0756	0.9565

Table 6-7. Comparison of soil roughness parameters for Hastings 02 from 3D surface models and random generated profiles.

Roughness Parameter	3D Surface	Transects // to X	Transects // to Y	All transects
(s) RMS height [m]	0.0547	0.051	0.053	0.052
(ℓ) mean correlation length [m]	2.1525	1.980	2.756	2.368
Min correlation length [m]	1.4200	-	-	-
Max correlation length [m]	3.1620	-	-	-
Mode correlation length [m]	2.1	-	-	-
σ of correlation length [m]	0.5223	0.062	0.156	0.438

6.5.4 Distribution Functions of the 3D Correlations Lengths.

From Table 6-2 it can be seen that the distributions of the correlation lengths are assumed to follow either and exponential autocorrelation function (ACF) or a Gaussian autocorrelation function form. One of the advantages of the full surface digitizing is that the complete

distribution function of the correlation lengths can be obtained. Figure 6-12 shows the distribution and compares it with a normal Gaussian distribution. It can be clearly seen that the distribution is not close to either an exponential or Gaussian distributions.

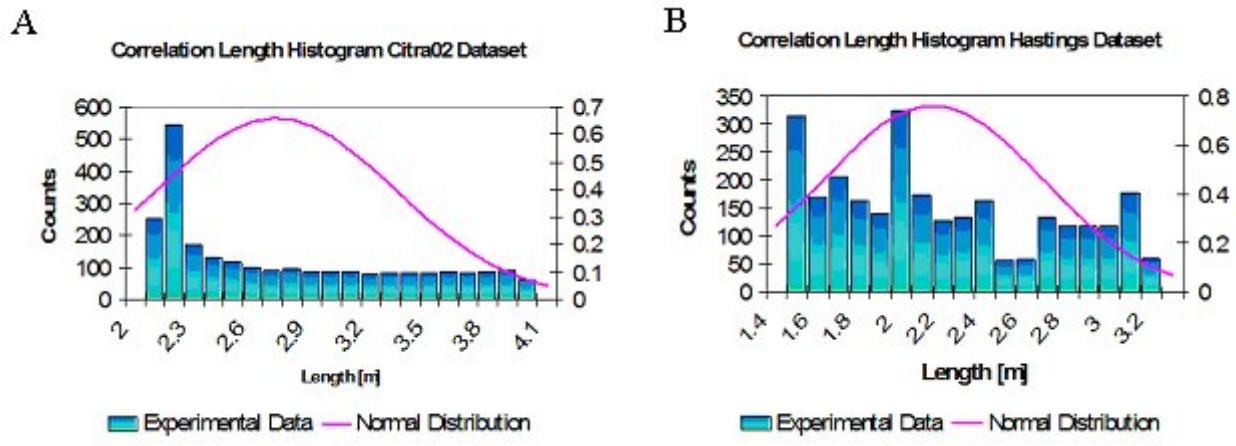

Figure 6-12. Comparison of experimental correlation length distributions with respect to the assumed normal distribution. A) for the Citra 02 dataset B) for the Hastings dataset.

6.6 Comparison with the Traditional Meshboard Method.

On March 10, 2006 meshboard measurements were made near the footprints of the radiometers. Figure 6-13 illustrate the meshboard technique, a picture is taken of the interface between the soil and the board. Image processing software is used to digitize the coordinates of the soil surface based on the mesh printed on the board.

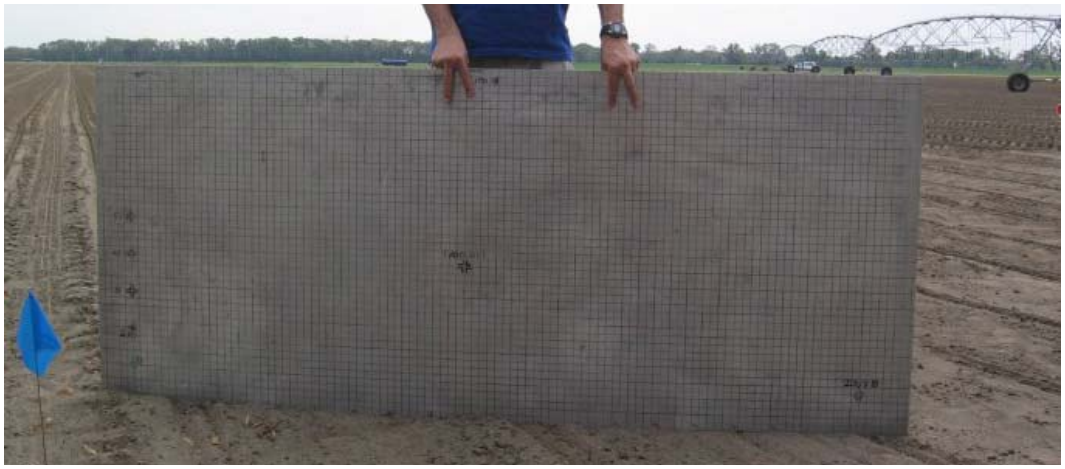

Figure 6-13. Meshboard used to digitize the soil surface transect.

Figure 6-14 show the digitized soil surface transect from one of the footprint areas based on the meshboard method. On part A the irregular spaced points are plotted, part B plots a regular spacing (1 cm) sampling interpolation. Part C is a plot of the normalized 1D autocorrelation.

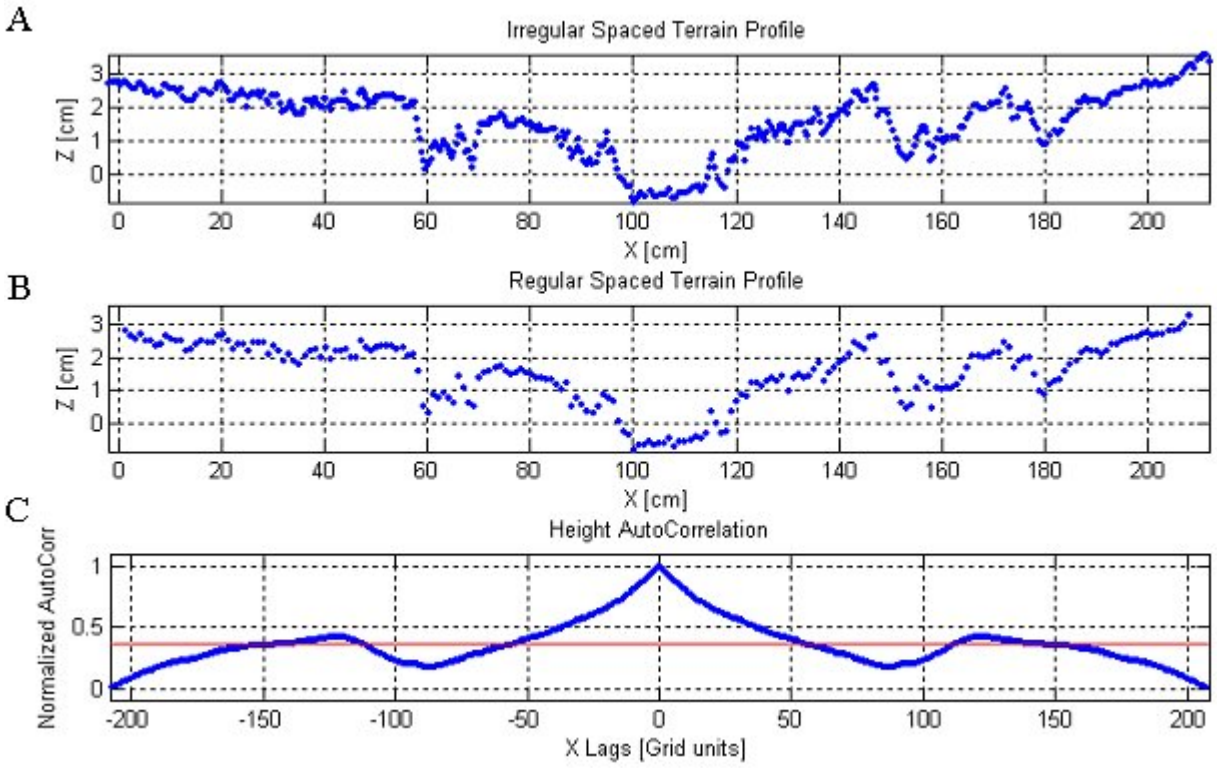

Figure 6-14. Plots of meshboard derived data. A) irregular sampled profile B) regular spacing profile C) normalized height autocorrelation.

The results obtained from the traditional meshboard method are compared with the results obtained thru the 3D datasets in Table 6-8. There is a disagreement in the values obtained from the different methods, being the greatest difference the autocorrelation length on the C-band radiometer footprint.

Table 6-8 Comparison of soil roughness metrics obtained from the traditional and alternative method.

Data Set	RMS all points	RMS regular spacing	1/e correlation length
MB Near L Band FPT	0.009158 m	0.009291 m	1.427 m
3D L Band FTP	0.02179 m	0.022513 m	2.2512 m
2. Near C Band FPT	0.013117 m	0.012122 m	0.284 m
3D C Band FTP	0.013546 m	0.012674 m	2.7244 m

6.7 Conclusions

Having a 3D data set of a scattering surface allowed us to demonstrate the common sense knowledge that the values of the derived soil roughness parameters are highly variable depending on the profile selection. It was also possible to derive the traditional 2D profile metrics from an entire 3D surface, having not a single value for correlation length but a range of values that fully describe the scattering surface. This proved the advantage of a full surface modeling over the traditional profiling methods.

CHAPTER 7
FORESTRY METRICS APPLICATIONS

7.1 Motivation

The estimation of forest structure and volume has for decades been of great interest to the scientific community because of its ecological and economical importance. Traditional methods of performing these measurements and estimations, even over a small plot of forest, are labor intensive and require many hours of field work. Several non-invasive remote sensing technologies have been tried to simplify these tasks and collect more accurate measurements in less time.

Over the past several years a great amount of experience has been obtained in the application of Airborne Laser Mapping (ALM) to study forest structure and estimating its biomass. ALM provides a large spatial coverage with very detailed 3D information of the forest upper canopy; however, it provides very limited information of the forest understory structure and mass. On the other hand, Ground-Based Scanning Laser or Terrestrial Laser Mapping (TLM) can provide very detailed 3D information on the understory structure with limited spatial coverage due to the line-of-sight obstruction caused by the trees. In contrast to ALM, which is a relatively mature technology with commonly accepted data collecting techniques and procedures, there are no guidelines or uniformly accepted procedures on how to set up a TLM system to obtain data for forestry applications.

Bibliographical research indicates that very few efforts have been made to use TLM to investigate Forest Metrics and structure. Previous work has been limited to assess the potential of TLM for replacing traditional field techniques to determine basic tree & plot metrics such as tree height, stem diameter at breast height (DBH), stem location and stem density; or as ground validation for airborne remote sensing technologies.

The long term goal of this project is to develop techniques for a seamless merging of ALM and TLS observations to generate high density point clouds of forest plots. The final goal is to develop high resolution laser tomography through a multi-platform and multi-imaging-geometry data integration to generate a virtual “Forest Cube” for which all metrics can be derived with high levels of accuracy and precision. With the derived metrics of several of these “Forrest Cubes” of statistically sampled plots combined with the large spatial coverage of ALM, forest-wide metrics can be estimated with a high degree of confidence. The first step and shorter term goal is to develop the required field techniques and procedures for TLM forestry data acquisition and geo-referencing for a typical small size test plot.

7.2 Use of LIDAR Technology

In the early 1980s LIDAR scanners were developed to obtain high accurate measurements of surface elevations from airborne and spaceborne platforms. These first systems are classified as large footprint LIDARs because the intersection of the laser beam with the surface is a circular or elliptical spot of several meters in extent. The first LIDAR systems suitable for vegetation and forestry studies had a footprint of less than a meter and were designed to record only the first received return (Lefsky et al. 1998). Those systems evolved to present day airborne laser scanners that generally have small footprint and the capability of recording multiple returns, as well as their intensities. Detailed descriptions of LIDAR technologies instrumentation and operation can be found in Wehr & Lohr (1999) and Baltsavias (1999).

Ground-Based Laser Scanning or Terrestrial Laser Scanning (TLS), is a relatively new technology compared with their flying counterparts. They evolved from the Electronic Distance Measurement (EDM) devices used in traditional surveying. Terrestrial laser mapping systems produce very accurate 3D data sets of large surfaces rapidly. Other surveying or photogrammetric techniques require much longer acquisition times and yield much fewer 3D

points. A ground-based laser scanner provides 4 quantities for each sampled point, three are positional information in a Cartesian reference frame: the (x,y,z) coordinates, and the fourth quantity is the magnitude or intensity of the return signal. The sampling resolution is measured in angular units because linear spacing between points depends on the range. For a 2 milliradian angular resolution the linear spacing between samples is 1 cm at 10m or 10 cm at 100 meters. The key features of a ground-based laser scanning system are: a) range accuracy: which is dependent on the pulse duration, b) maximum range: which depends on the laser output power and the receiver sensitivity, c) scan rate: depends on how fast are the laser and receiving electronics, d) the angular resolution, e) field of view: the last two depend on the mechanics of the scanning mirror system, and the last but most important is the f) laser, which is characterized by its wavelength and beam divergence. More detailed information on TLS can be found in Lichti et al. (2002).

7.3 Previous Works

Over the last two decades multiple papers on Airborne LIDAR applications to vegetation and forest studies have been published, discussing the capabilities and limitations of the different systems and applications. Some of the most complete and interesting papers are: Lefsky, et al. (1998); Lefsky et al. (2002) and Næsset & Gobakken (2005). The overall conclusion is that airborne LIDAR mapping is a very powerful tool for deriving and modeling forest metrics; however, it has the limitation of the low sampling of the understory canopy.

Previous works on the application of TLS to forestry have aimed to compare tree & plot metrics such as tree height, stem diameter at breast height (dbh), stem location and stem density derived from TLS with the same metrics derived with traditional ground techniques. These works have had different approaches with respect to scanning geometry and the shape of the defined plot. Watt & Donoghue defined circular plots of 0.02 hectare (ha) and obtained a quasi-

complete scan of the area with only two scans from opposite points. Hopkinson et al. defined 35 m x 35m (0.12 ha) square plots and performed 5 scans per plot. Both studies concluded that TLS was a powerful tool in determining forest variables; however it is limited by obstructions of the line of sight that determines the useful range of this type of instrument.

The above papers prove the usefulness of both airborne and terrestrial based systems in the estimation of forest metrics. The work presented here is aimed at developing data acquisition and processing techniques that will enable the combination of data from multiple platforms (i.e. Airborne & Terrestrial) and geometries that will produce a complete well sampled data set over the complete structure of a small plot of the forest.

7.4 Data Collection

The test site for the experiment was at the Intensive Management Practice Assessment Center (IMPAC) operated by the Forest Biology Research Cooperative (FBRC), and located 10 km north of Gainesville, Florida USA. The center is a research plantation of the southern pine species loblolly (Pinus taeda L.) and slash (Pinus elliottii var. elliottii). The Airborne Laser data was collected on October, 2005 using the UF Optech Inc. ALTM 1233 laser mapping system flown on a Cessna 337. The airborne system, when operating at a flight height of 600 m AGL, at a flight speed of 60 m/s and a LASER pulse repetition frequency of 33 kHz yields a point density of roughly 1 laser return per square meter. Two sets of terrestrial Laser Data were collected, the first in November 2005 and the second in June of 2006 using the UF Mobile Terrestrial Laser Scanner (M-TLS) system based on the Optech ILRIS-3D terrestrial imaging LIDAR. Figure 7-1 presents an aerial photo of the test site, and Figure 7-2 presents a shaded relief model rendered from the airborne laser scanner data.

Figure 7-1. Aerial photographs of the test site. Downloaded from the Florida Department of Environmental Protection, Land Boundary Information System. http://data.labins.org/2003/MappingData/DOQQ/doqq.cfm

The terrestrial laser mapping data consisted of five independent scans taken from different angles and elevations. The total number of return points in the terrestrial clouds was 3,765,084. The TLM instrument provides a set of points (x,y,z,I). The first three points provide the spatial information of the scanned surface point. These x,y,z coordinates are distances referred on an orthogonal frame of reference whose origin is the scanner sensor head. Geo-referencing was accomplished by setting GPS control points that were included in the scans, and later determining the geodetic coordinates of these control points. Data was collected using ASHTECH Z-XTREME receivers, and ASHTECH Choke Ring Antennas Model 700936 Rev D. A total of 8 stations were surveyed, 6 corresponding to the GPS control points and 2 for the scanning locations.

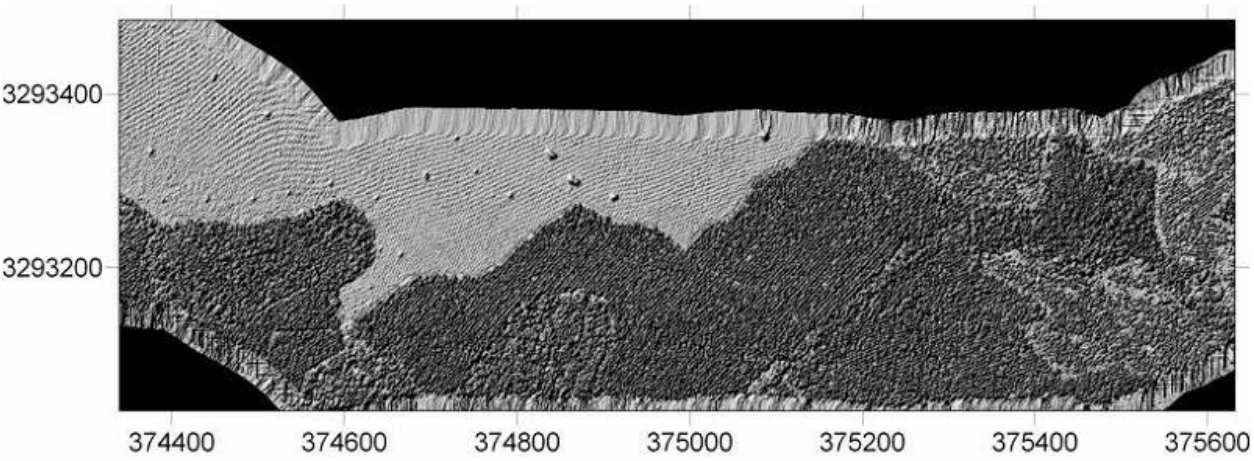

Figure 7-2. Shaded relief digital elevation model rendered from the airborne laser scanner data of the test site. The edge effects are caused by the method used to interpolate the LIDAR observed data to obtain a uniform spaced (gridded) surface model.

7.5 Data Processing

The five individual point clouds were merged into a single data set in a single sensor coordinate frame using the Innovmetric (http://www.innovmetric.com/Manufacturing/home.aspx) Polyworks Inspect software employing the n common point alignment procedure. The GPS reference point (ARP) were used as the reference points for the alignment. For georeferencing the dataset into a NAD83 Datum expressed in UTM Zone 17 coordinates, 8 control points were surveyed. Their coordinates in both geodetic and sensor spaces are listed in the Table 7-1.

Table 7-1. M-TLS data set geo-referencing control network.

Station	Geodetic space coordinates UTM zone 17			Sensor space coordinates		
	Easting (X)	Northing (Y)	Ellipsoid Height (Z)	x	y	z
GPS1	374997.280	3293231.190	26.067	1.156	21.033	-2.505
GPS2	375004.345	3293235.345	24.982	-6.77	19.81	-4.403
GPS3	375014.622	3293203.487	35.906	-4.275	54.339	-2.766
GPS4	374994.418	3293223.649	25.736	7.06	26.576	-3.955
GPS5	375011.541	3293247.681	25.621	-18.4871	11.63806	-3.71564
GPS6	375011.129	3293242.494	23.451	-15.7089	16.51747	-5.505
IL01	374989.820	3293251.056	23.701	0	0	0
IL0_	375015.927	3293268.460	24.739	-30.9398	-5.44228	-2.60267

Following, a 3D translate and rotate conformal transformation was applied using the Terrasolid (http://www.terrasolid.fi/) Terrascan software. The inputs for the computation of the 9 parameters were the sensor space and geodetic space coordinates of the GPS antennas reference point (ARP). In Table 7-2 the residuals of the control points based on the geo-referencing transformation are presented.

Table 7-2. Geo-referencing residuals analysis.

Station	Adjustment Residuals			Square of the Residuals		
	Easting (X)	Northing (Y)	Ellipsoid Height (Z)	x	y	z
GPS1	-0.0736	0.0591	0.3474	0.005417	0.003493	0.120687
GPS2	-0.0198	0.0011	0.4919	0.000392	1.21E-06	0.241966
GPS3	0.0459	0.2654	-0.3605	0.002107	0.070437	0.12996
GPS4	-0.0541	-0.0475	-0.2618	0.002927	0.002256	0.068539
GPS5	0.0493	-0.0022	0.1346	0.00243	4.84E-06	0.018117
GPS6	This control point was eliminated after a preliminary adjustment					
IL01	-0.055	-0.1356	-0.1181	0.003025	0.018387	0.013948
IL0_	0.1073	-0.1404	-0.2336	0.011513	0.019712	0.054569
Root Mean Square of the Residuals (Meters)				0.063032	0.127779	0.304205

Once the Terrestrial Point cloud was geo-referenced in the same datum and coordinate system as the airborne data, both datasets were merged into a single file and were viewed and rendered. Figure 7-3 is a rendering of the fused point cloud color coded by elevation; the yellow ellipse indicates the overlaying of the high density terrestrial point cloud. It can be observed the adequate mapping of the undercanopy structure by the high density of the blue and green color coded points. Figure 7-4 is a rendering of a 3.0 m wide transect depicting the match between the airborne and the terrestrial point clouds in the along flightline direction, red dots represent the low density points obtained from the airborne scanner and the white dots represents the high density terrestrial point cloud. Figure 7-5 illustrate the match between the airborne and the terrestrial point clouds in the across flightline direction.

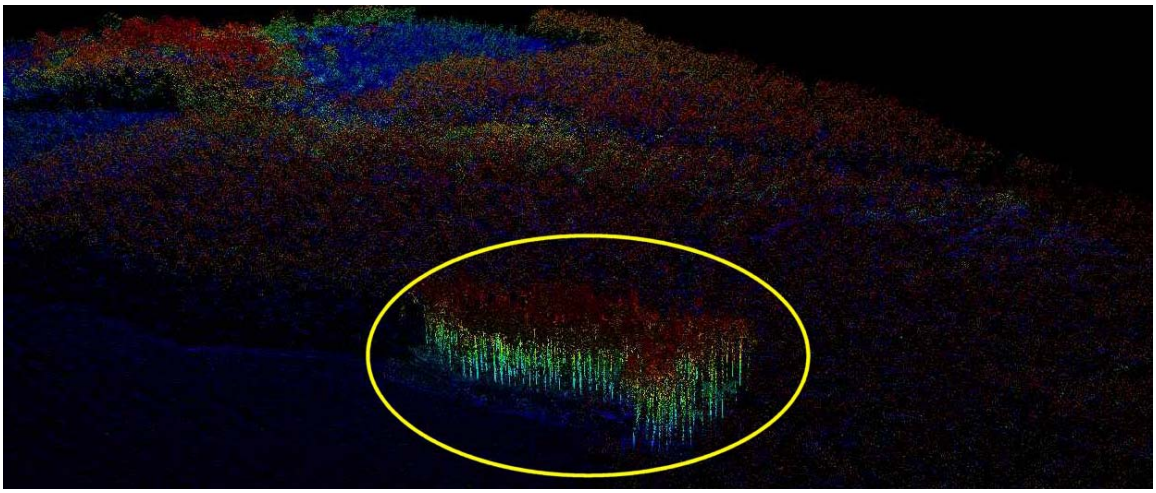

Figure 7-3. Rendering of the fused point cloud, color coded by elevation.

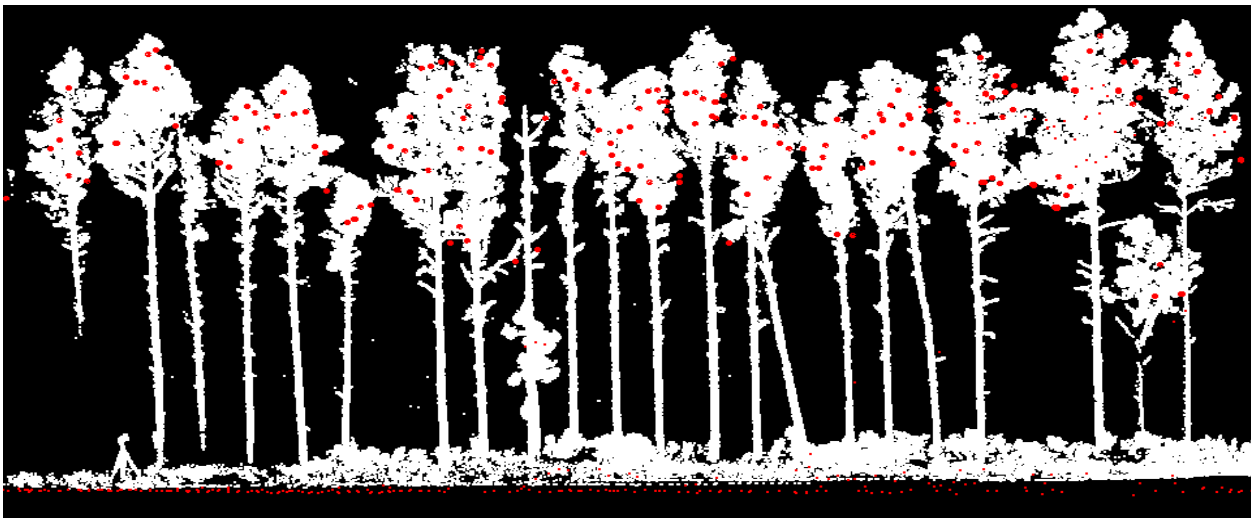

Figure 7-4. Rendering of fused point cloud cross section in the along the flightline direction.

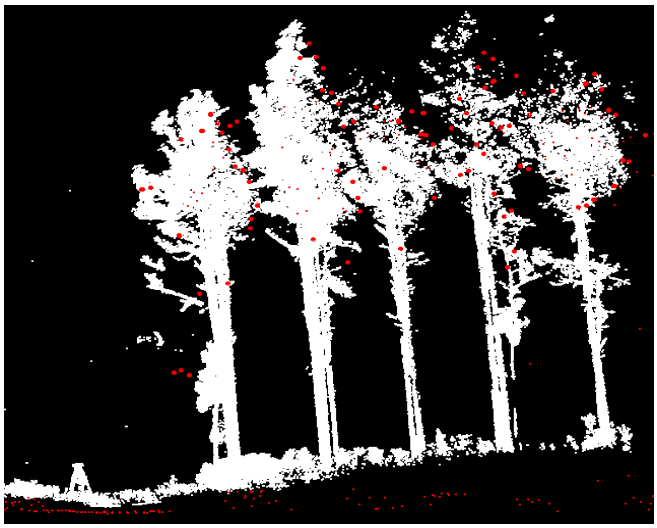

Figure 7-5. Rendering of fused point cloud cross section in the cross flightline direction

Figures 7.6 to 7.8 are renderings of the fused airborne and M-TLS point cloud, some of the GPS tripods and Antennas that were used as control points can be observed in the renderings.

Figure 7-6. Rendering of the fused point cloud, grey scale from the laser return intensity.

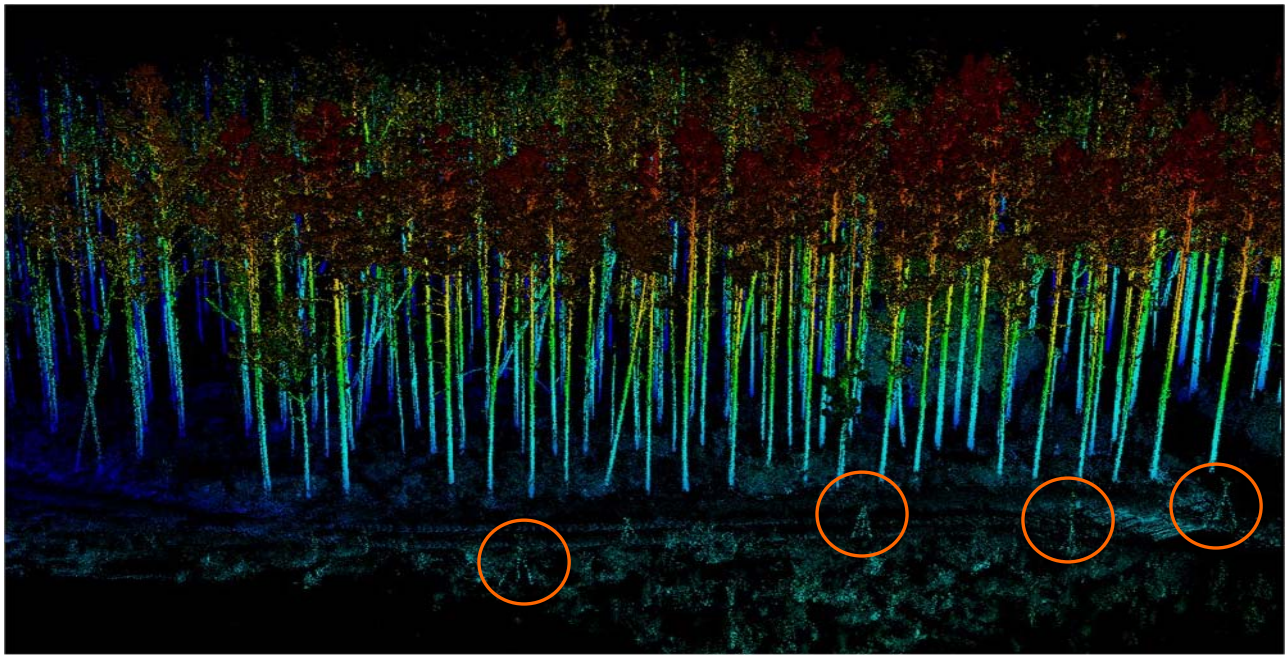

Figure 7-7. Rendering of the fused point cloud, color coded by elevation + laser return intensity.

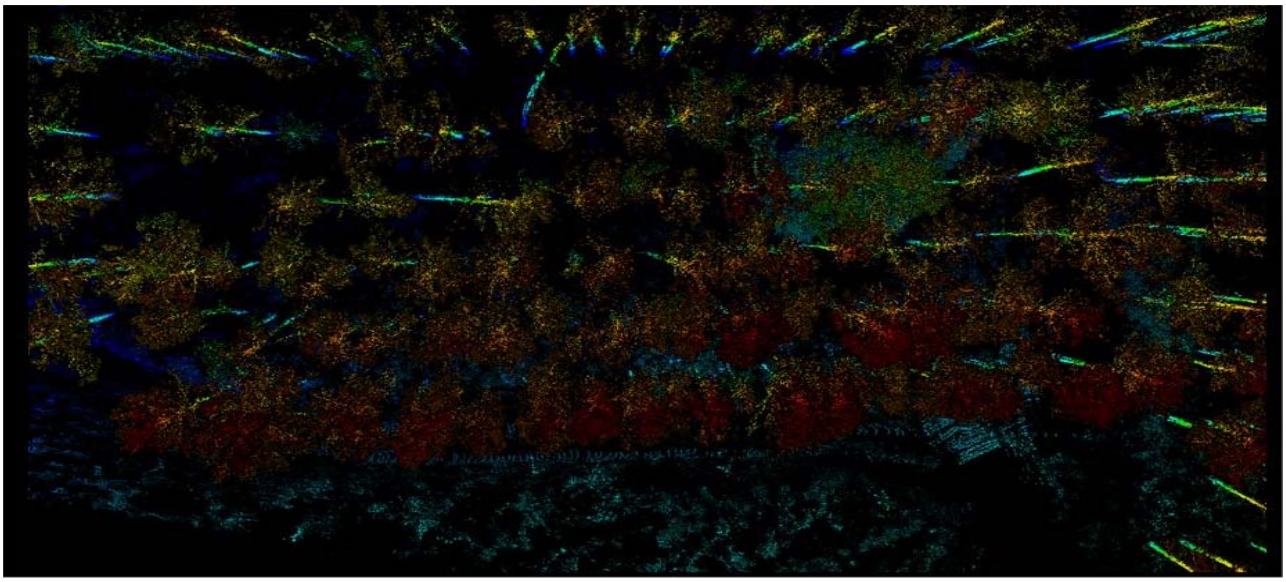

Figure 7-8. Rendering of the top view of fused point cloud, color coded by elevation + laser return intensity

7.6 Results

The objective of merging the airborne and terrestrial point clouds was to synergize the vantage points of both geometries to develop a dataset that could permit the extraction of the Tree & Plot Metrics (Tree Height, Stem Diameter at Breast Height DBH, Stem location and Stem Density) with higher levels of precision and accuracy than those using a single geometry. From the fused point cloud a "Forest Cube" was extracted, its ground dimensions are 40.4m x 19.16m with an area of 774.15 m². From this virtual "Cube" all the metrics will be derived. Figure 7-9 shows renderings of the "Forest Cube".

7.6.1 Stem Density

For stem density determination, a manual count of the standing stems was performed. To facilitate the count the "cube" was skimmed to 1/20th of its point density, was filtered so that only points that had heights between 2.3 and 6.3 m above ground level were displayed and was visualized in an oblique view. Figure 7-10 shows the stem count by row, a total of 96 standing stems were counted, which yield a stem density of 1 stem per 8.06 m² or 1240 stems/hectare.

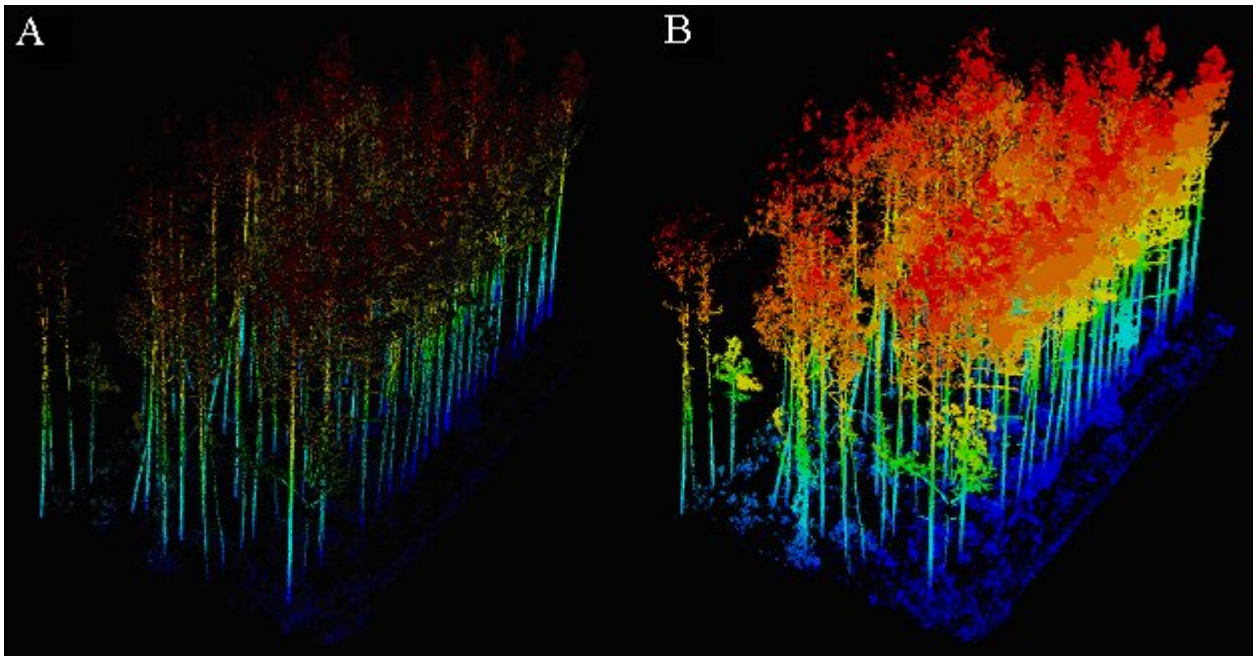

Figure 7-9. Rendering of the “Forest Cube”. A) Color coded by elevation and intensity. B) Color coded only by elevation.

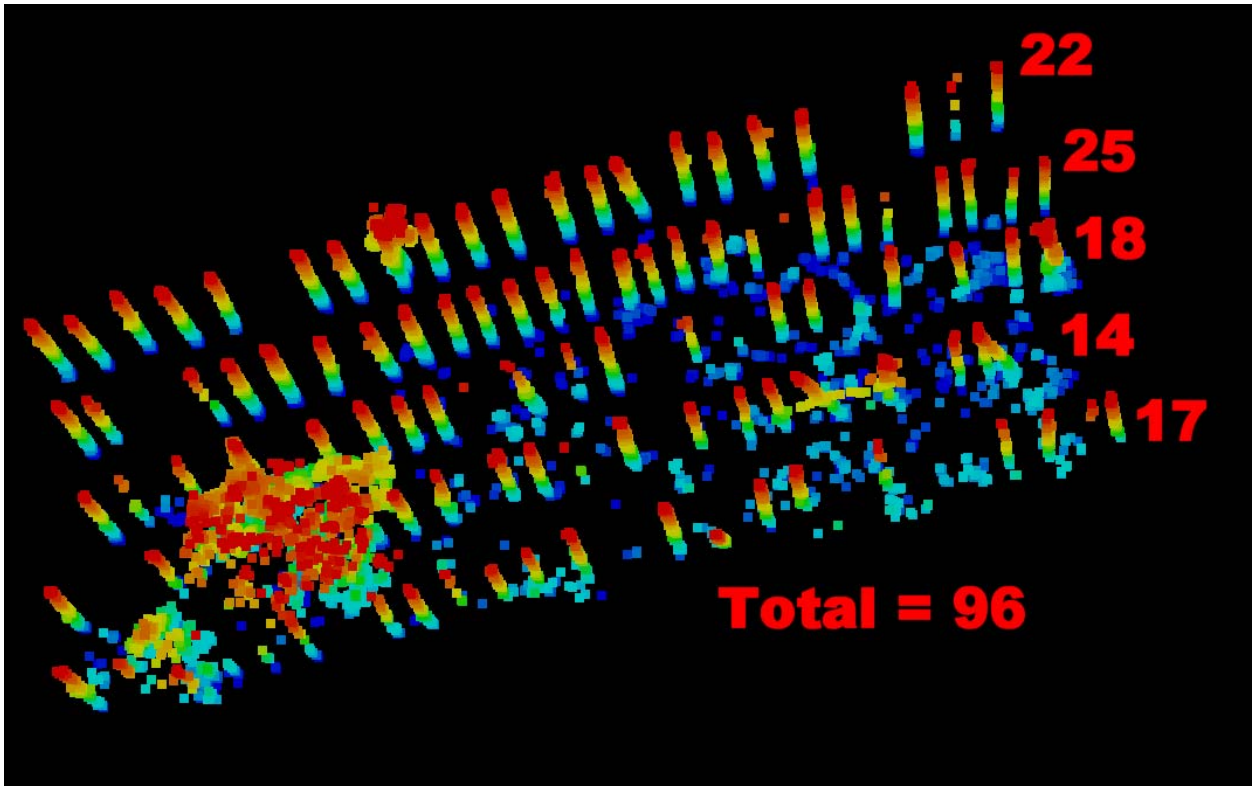

Figure 7-10. Rendering of point cloud used for stem counts.

7.6.2 Stem Location

Previous published works have also performed stem location measurements, however they were referred to arbitrary sensor coordinates. In this work, the dataset was referenced to geodetic coordinates, providing absolute coordinates of the stem location. The ideal approach is to fit a circle to a low cross section of the tree and determine the coordinates of the circle origin and the circle radius. Polyworks INspect or TerraScan can be used for this purpose.

7.6.3 Stem Diameter at Breast Height DBH

Stem diameter at breast height is defined as the stem diameter at a height of 1.4 m (4.5 ft). The stem diameter can be determined in conjunction of the stem location. Figure 7-11 illustrates the fitting of a circle from a section of a point cloud at breast height, from which the stem locations and DBH were determined.

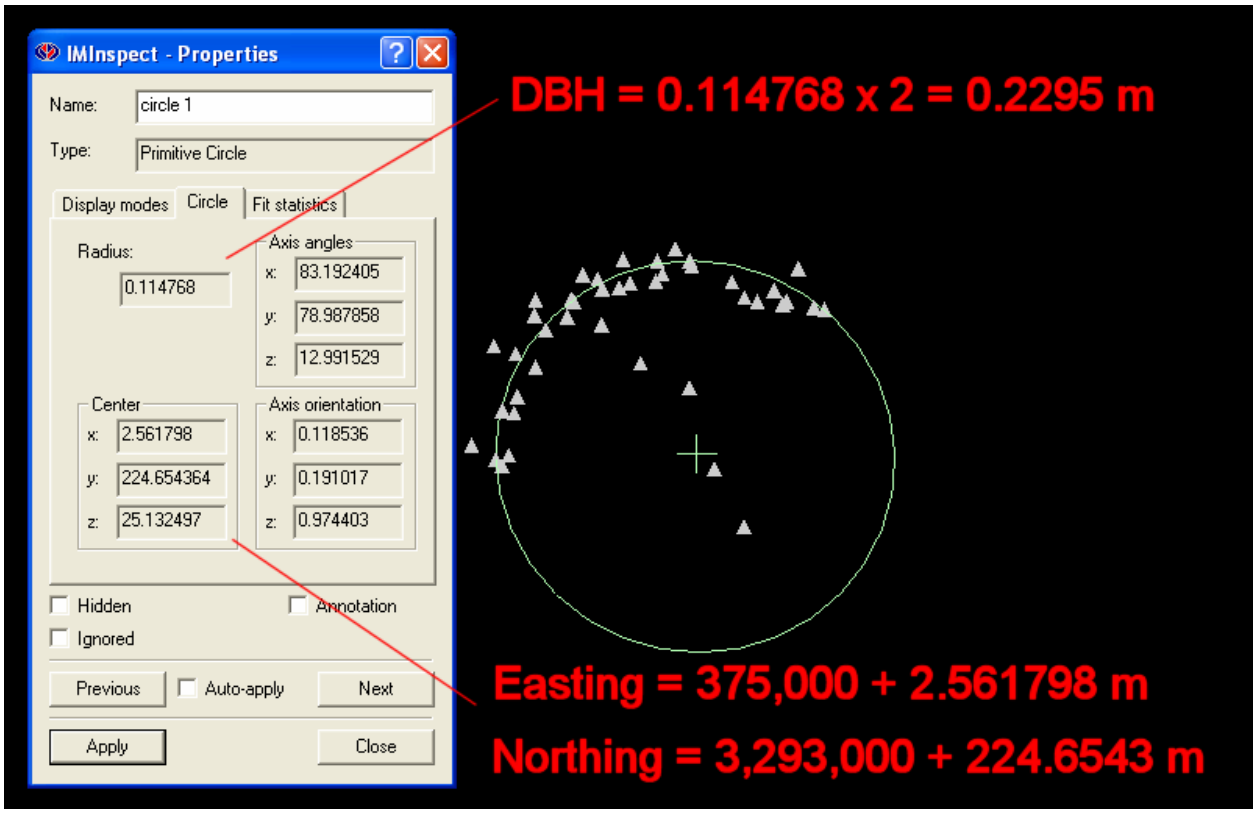

Figure 7-11. Fitting of a circle at breast height for determining DBH and stem location.

7.6.4 Tree Height

Using Terrascan, points contained in a cylindrical volume centered at the stem location coordinates were extracted from the "Forest Cube"; the maximum and minimum height points were obtained and the difference between them was computed yielding the tree height. Figure 7-12 shows a rendering of the points extracted for a single tree with a height histogram used for the determination of the tree height.

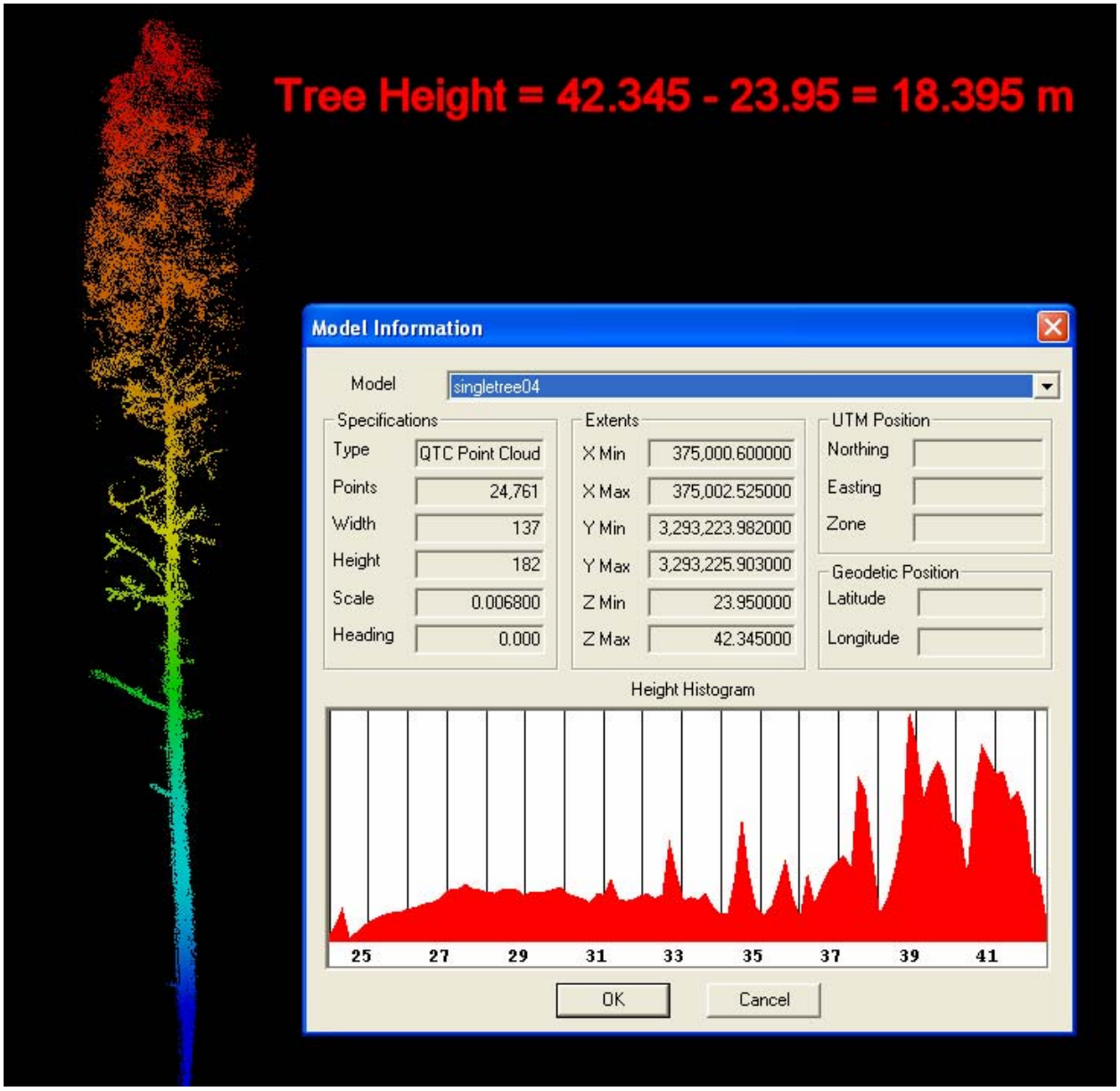

Figure 7-12. Single tree height determination.

7.6.5 Stem Volume

Tree stem volume may be a vague concept; it may be used to refer to the total stem volume or to the “Merchantable Volume”, which is defined for a particular length of at trunk up to which a particular product may be obtained. There are many ways that foresters estimate the stem volume, and they vary greatly from place to place, based on the purpose and tree species. Usually foresters have tables that require tree species, diameter at breast height and the merchantable height (or total tree height) as inputs. The tables are based on allometric equations which are empirical regressions that relate stem volume and biomass of species to diameter at breast height and/or to tree height. For this particular dataset it is impossible to determine the stem merchantable volume because the trees on the plantation are relatively young and have not reached the diameter and height at which they are considerable exploitable. However the point cloud can be used to estimate the total stem volume (including bark) from the ground to the crown. TerraScan was employed to obtain the tree diameter at different heights as shown in Figure 7-13.

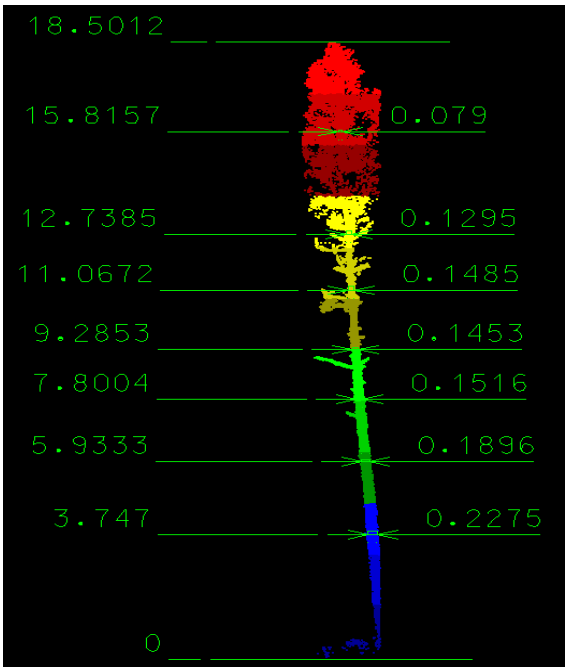

Figure 7-13. Diameters at different heights for volume computations

Each section between diameter measurements can be approximated as a truncated cone from which the total stem volume was computed. Table 7-3 summarizes the diameter and height measurements that were used for the stem volume computation.

Table 7-3. Diameter and heights measurements for stem volume estimation

Height above ground [m]	Diameter [m]	Area [m²]	Segment height	Segment volume
0	0.2295	0.041367	1.4	0.057914
1.4	0.2295	0.041367		
3.747	0.2275	0.040649	2.347	0.096245
5.933	0.1896	0.028234	2.186	0.074878
7.8004	0.1516	0.01805	1.8674	0.042862
9.2853	0.1453	0.016581	1.4849	0.025705
11.0672	0.1485	0.01732	1.7819	0.030202
12.7385	0.1295	0.013171	1.6713	0.025401
15.8157	0.079	0.004902	3.0772	0.02678
18.395	0	0	2.5793	0.004214
Total stem volume [m³]				0.384201
Total stem volume modeled as cone regressed from data [m³]				0.394114637

7.6.6 Tree Biomass Estimation

There are multiple formulas that provide estimates of the total aboveground biomass for all hardwood and conifer species in the U.S. One formula, presented by Jenkins et al. (2003) is:

$$bm = e^{(\beta_0 + \beta_1 \ln(dbh))}$$

where:

bm = total aboveground biomass (kg) for trees 2.5-cm dbh and larger

dbh. = diameter at breast height (cm)

β_0 and β_1 are fit parameters for each species

For the tree sample that has been worked throughout this chapter the result of the biomass estimate is:

$$bm = e^{(\beta_0 + \beta_1 \ln(dbh))} = e^{(-2.5356 + 2.4349 \ln(22.95))} = 162.99\,[kg]$$

7.7 Comparison with Traditional Methods

Several of the individual tree metrics were obtained or derived from the traditional forestry techniques and methods as depicted in Figure 7-14.

Figure 7-14. Individual tree metric measurement. A) Circumference at diameter height to determine DBH. B) Estimation of tree height.

For the tree that was used to derive its metrics from the LIDAR point cloud, 6 measurements of its circumference were measured (62.5, 60.5, 61.2, 61.5, 61.0, 61.8 cm) which yielded and average DBH of 19.55 cm. Also three estimates of its height were obtained using the traditional Biltmore Stick (19.28, 17.36, 18.2 m) which yields an average tree height of 18.28 m. From these measured metrics several others can be derived, a summary of the comparison of the directly measured and derived metrics obtained from the point cloud and traditional metrics are presented on Table 7-4.

Table 7-4. Comparison of the metrics derived from traditional methods and from the TLS point cloud.

Metric	Traditional Method	From M-TLS point cloud	% Difference
DBH	0.1955 m	0.2295 m	17.39 %
Tree Height	18.28 m	18.395 m	0.63 %
Stem Volume	-	0.3842 m^3	-
Stem Volume approximated to Cone	0.1829 m^3	0.2536 m^3	7.07%
Biomass	110.31 kg	162.99 kg	47.8 %

7.8 Conclusions

It was possible to extract plot and individual tree metrics from the fused data set combining both airborne and terrestrial scanners. However there is more work to be done in the areas of merging and geo-referencing of the terrestrial point clouds, such that a more coherent data set

will be available for data extraction. All the work presented here was done in a manual fashion. However, all of the activities can be written into algorithms that will automate the data extraction process. The synergy of airborne and terrestrial laser scanning technologies can prove highly valuable to Forest Science, providing vast amounts of information that can enable the improvement of the allometric models.

CHAPTER 8
SUMMARY

8.1 Conclusions

Terrestrial Laser Scanners (TLS) are very versatile measuring and mapping tools, but as with any other tool, to become the "method of choice" they have to prove to be efficient in their application. This means that they have to be better, faster and cheaper than the alternate equipment and techniques. Better, faster and cheaper implies both qualitative and quantitative improvements; such as more measurements with greater accuracy at significant savings in time, labor and capital investments. In their short lifetime TLS units have proven their advantage over traditional surveying equipment and methods in many engineering applications such as As-Built documentation and transportation infrastructure management. With respect to the application of TLS to scientific mapping, measurement and documentation; it is clear that they are faster and better than the traditional techniques. What is left is to prove is that they can also be more economic.

For the tested applications in the fields of geology, paleontology, forestry and coastal morphology the ILRIS unit and/or the M-TLS system proved to collect data more accurately at higher resolutions and faster than the conventional techniques. The resulting dataset that can easily exceed several hundreds of megabytes is both the TLS greatest strength and weakness. On the positive side the dataset contains a wealth of spatial and spectral information from which an infinite amount of measurements can be derived, and the researcher can revisit the "virtual site" over and over again without leaving the office. On the negative side, more data is not necessarily better. In some cases more data can overwhelm the researcher. It can burry the phenomenon of interest under millions of unnecessary data points. In some extreme cases the analytical models used to describe the phenomenon simply can not handle the extreme resolution of a TLS dataset.

Finally, many researchers are interested in obtaining their metrics and can be careless about performing all the preprocessing (point cloud cropping, merging and geo-referencing) required to have a usable dataset. However, these disadvantages or weakness can be capitalized into an opportunity to help develop strong relationships between scientists and geosensing engineers thru collaborative research projects.

A result of all the tested application was the investment of hundred of hours in data analysis which yielded a wealth of experience in the operation of LIDAR processing software. From that experience it can be concluded that there is no single software package that provides all possible tools required for the application of TLS dataset for scientific purposes. For most of the projects operations were performed in at least 3 software packages: Polyworks, Terrascan and QT Modeler; in some cases Surfer was employed to create grids and Matlab was used to code special customized codes for the extraction of the required final information.

8.2 Recommendations

There is a need to develop methods to improve the accuracy of the merging and geo-referencing procedures. Extensive research should be performed by future students on those fields as well as the establishment of a set of accuracy standards that will provide a benchmark for measuring the quality of these operations.

It is also necessary to work in the field of sensor characterization, which includes the development of test protocols to verify TLS specifications such as accuracy (under various ranges, target reflectance and scan angles), scan speed and measurement repeatability. This activity also includes the identification and characterization of systematic errors for individual units. If a good test protocol is developed it will set the ground for an independent experiment to test and compare different makes and models of TLS units which can provide material for a great engineering paper.

The development of the Mobile Terrestrial Laser Scanning system must be accelerated, more students must be involved in the project and they can participate more actively in the integration of the different system subcomponents.

One of the lessons learned from this work is that the multidisciplinary background of the students from both the GSE and ASPL groups is an invaluable academic and research asset. However more actions have to be taken towards increasing the synergies between its members with respect to the application of MTLS to diverse scientific disciplines.

Networking activities must be undertaken within the UF academic community to identify potential partners that can use TLS systems in their research. Collaborative research projects should be started; the results can yield publishable material.

Some consideration should be given to develop a program such as NCALM that will make the M-TLS system and services available to scientific community. This program will not only increase system usage, but also increase the operator experience, the capability testing and provide more opportunities and material to publish.

Efforts should be made to participate in TLS related conferences such as the International Society for Photogrammetry and Remote Sensing Commission III on Photogrammetric Computer Vision and Image Analysis, where a great part of the published work refers to processing and interpretation of laser range data. Also an annual meeting from an engineering and industry perspective is organized by Spar Point Research LLC; this meeting focuses on advanced dimensional control, work processes and 3D laser scanning technologies. The participation in events of this sort will help UF researchers to keep on the leading edge of scientific and engineering applications of Terrestrial Laser Scanning systems.

APPENDIX
COMPARISON OF TERRESTRIAL LASER SCANNERS

A.1 Optech ILRIS 3D

This is a dual scanning mirror, pulsed infrared laser system with the highest range available on the market: from 3 m to beyond 1 km. It has an integrated megapixel digital camera and large-format LCD viewfinder. 40° x 40° instantaneous field of view. An optional Pan and Tilt base allows for a panoramic -20° to 90° x 360° scanning coverage. Web site Reference: http://www.optech.ca/i3dfeat-ilris.htm

Figure A-1. Optech ILRIS TOF TLS

A.2 Leica HDS3000

Leica High-Definition Surveying 3000, Nd:YAG frequency doubled pulsed laser, with a single mirror scanner, with a dual-window and rotating base that allows for a 360° x 270° field of view. Has an integrated Bore-sighted Single 24° x 24°, 1024 x 1024 digital camera for automatically calibrated photo overlays. Web site Reference: http://www.leica-geosystems.com/hds/en/lgs_5574.htm

Figure A-2. Leica HDS 3000 TOF TLS

A.3 Leica HDS4500 25 & 53m

The Leica HDS4500 is an ultra-high speed 690 nm laser, phase-based, short range scanner. Capable of scanning from 100,000 points/sec to 500,000 points/sec on a 360° x 310° field of view. Two different models are capable of 25 and 53 m ambiguous ranges. Web site Reference: http://www.leica-geosystems.com/hds/en/lgs_5572.htm

Figure A.-3. Leica HDS 4500 PD TLS

A.4 RIEGL LMS-Z420i

Designed as a High-Accuracy & Long-Range pulsed laser, single vertical line rotating polygon scanner with a 80° range. The azimuth scan is accomplished by a rotating base full 360°. An optional digital camera can be mounted for photorealistic textured point clouds. Range up to typ. 1000 m, precision up to 10 mm and scan rate up to 12 000 pts/s. Web site Reference: http://www.riegl.com/terrestrial_scanners/lms-z420i_/420i_all.htm

Figure A-4. Riegl LMS-Z420i TOF TLS

A.5 RIEGL LMS-Z390

Designed as a High-Accuracy & High Resolution pulsed laser, single vertical line rotating polygon scanner with a 80° range. The azimuth scan is accomplished by a rotating base full 360°. An optional digital camera can be mounted for photorealistic textured point clouds. Range up to typ. 300 m, precision up to 2 mm and scan rate up to 12 000 pts/s. Web site Reference: http://www.riegl.com/terrestrial_scanners/lms-z390_/390_all.htm

Figure A-5. Riegl LMS-Z390 TOF TLS

A.6 RIEGL LMS-Z210ii

Designed as a general purpose pulsed laser, single vertical line rotating polygon scanner with a 80° range. The azimuth scan is accomplished by a rotating base full 360°. An optional digital camera can be mounted for photorealistic textured point clouds. Range up to typ. 650 m, precision up to 10 mm and scan rate up to 12 000 pts/s. Web site Reference: http://www.riegl.com/terrestrial_scanners/lms-z210ii_/210ii_all.htm

Figure A-6. Riegl LMS-Z210ii TOF TLS

A.7 Trimble GS101

A single scan line pulsed green laser system, with an integrated digital camera, on a rotating base. It allows to scan in 60° vertical and 360° horizontal, up to a range of 200 -350 m, with a spot spacing of 32 µrad and a range resolution of 1.5 mm @ 50m and a scan rate of up to 5,000 pts/s. Web site Reference: http://www.trimble.com/gs200.shtml

Figure A-7. Trimble GS101 TOF TLS

A.8 Trimble GX 3D

A single scan line pulsed green laser system, with an integrated digital camera, on a rotating base. It allows to scan in 60° vertical and 360° horizontal, up to a range of 200 -350 m, with a spot spacing of 32 µrad and a range resolution of 1.5 mm @ 50m and a scan rate of up to 5,000 pts/s. Web site Reference: http://www.trimble.com/trimblegx.shtml

Figure A-8. Trimble GX 3D TOF TLS

A.9 Minolta VIVID 910

The VI-910 uses LASER triangulation. The entire area is captured in 2.5 seconds, and the surface shape is converted to a lattice of over 300,000 vertices (connected points). A (24-bit) color image is captured at the same time by the same triangulation CCD. The range is limited to 2.5 meters and the range resolution is in the order or 8 micrometers. Web site Reference: http://www.minolta3d.com/products/main-en.asp

Figure A-9. Minolta VIVID 910 OT TLS

A.10 Zoller-Frohlish IMAGER 5006

Is an ultra-high speed visible laser, phase-based, short range scanner. Capable of scanning from up to 500,000 points/s on a 360° x 310° field of view with an Ambiguity range up to 79 meters. Web site Reference: http://www.zf-laser.com/e_imager5006.html

Figure A-10. Zoller-Frohlish IMAGER 5006 PD TLS

A.11 IQSun 880

Is an ultra-high speed visible 785 nm laser, phase-based, single line short range scanner. Capable of scanning from up to 240,000 points/s on a 360° x 320° field of view with an Ambiguity range up to 76 meters.

Figure A-11. IQSun 880 PD TLS

A.12 Comparison of Terrestrial LASER Scanner Specifications

The specifications of commercial TLS units was compiled and presented in Table A-1.

Table A-1. Comparison of terrestrial laser scanner specifications

Manufacturer	Optech	Leica	Leica	Leica
Model	ILRIS 3D	HDS3000	HDS4500 25m	HDS4500 53m
Method of operation	Time of Flight	Time of Flight	Phase Difference	Phase Difference
Range [m]	3-1500 @80% 3-800 @20% 3-350 @4%	300 @90% 134 @18%	0.1-25.2	0.1-53.5
Range resolution [mm]	4	4	3	5
Azimuth, elevation resolution [°]	0.00115	0.00022918	20.0535228	20.0535228
IFOV [Ver° X Hor°]	40 x 40			
Aux FOV [Ver° X Hor°]	-20 to 90 x 360	270 x 360	310 x 360	310 x 360
Laser type/color	Infrared	Visible Green	Visible Red	Visible Red
Laser wavelength [nm]	1500	532	690	690
Scan rate [points/s]	2,000	4,000	500,000	500,000
Beam divergence [°]	0.00974	0.00687549	0.02864789	0.02864789
Texture	Intensity & RGB	Intensity & RGB		
Weight [kg]	12	17		
Dimensions (LxWxH) [cm]	32 × 32 × 22	26.5 x 37 x 51	18 x 30 x 35	19 x 30 x 35
Power Supply	24 VDC	36 V, AC or DC	24V DC 90 - 260V AC	24V DC 90 - 260V AC
Power consumption [W]	75	80	50-70	50-71

Table A-1. Continued

Manufacturer	RIEGL	RIEGL	RIEGL	Trimble
Model	LMS-Z420i	LMS-Z390	LMS-Z210ii	GS101
Method of operation	Time of Flight	Time of Flight	Time of Flight	Time of Flight
Range [m]	2-1000 @80% 2-350 @10%	1-300 @80% 1-100 @10%	4-650 @80% 4-200 @10%	2-200
Range resolution [mm]	10?	6?	15?	1.4-6.5
Azimuth, elevation resolution [°]	0.002, 0.0025	0.001	0.005	1.83346494
IFOV [Ver° X Hor°]	80 x 0.014	80 x 0.014	80 x 0.15	
Aux FOV [Ver° X Hor°]	80 x 360	80 x 360	80 x 360	60 x 360
Laser type/color	Near Infrared	Near Infrared	Near Infrared	Green
Laser wavelength [nm]				
Scan rate [points/s]	8,000-12,000	8,000-11,000	8,000-12,000	5,000
Beam divergence [°]	0.014	0.014	0.15	0.00343775
Texture	Intensity & RGB	Intensity & RGB	Intensity & RGB	Intensity & RGB
Weight [kg]	14.5	14.5	13	12.8
Dimensions (LxWxH) [cm]	21 x 21 x 46.3	21 x 21 x 46.3	21 x 21 x 43.7	34 x 27 x 42
Power supply	12-18 VDC	12-18 VDC	12-18 VDC	90-240 VAC 24 VDC
Power consumption [W]	78-98	78-98	78-98	

Table A-1. Continued

Manufacturer	Trimble	Trimble	Minolta	Zoller-Frohlish
Model	GS200	GX 3D	VIVID 910	IMAGER 5006
Method of operation	Time of Flight	Time of Flight	Optical Triangulation	Phase Difference
Range [m]	2-350	350 @90%	0.6 -2.5	79
Range resolution [mm]	1.4-6.5	7	0.008	0.1
Azimuth, elevation resolution [°]	0.00171887	0.00343775		0.0018
IFOV [Ver° X Hor°]				
Aux FOV [Ver° X Hor°]	60 x 360	60 x 360		310 x 360
Laser type/color	Green	Green	Visible Red	Visible
Laser wavelength [nm]		532	690	
Scan rate [points/s]	5,000	5,000	120,000-256,000	500,000
Beam divergence [°]	0.00343775	0.00343775		0.01260507
Texture	Intensity & RGB	Intensity & RGB	none	
Weight [kg]	12.8	13	11	14
Dimensions (LxWxH) [cm]	35 x 27 x 42	32.3 x 34.3 x 40.4	21.3 x 27.1 x 41.3	28.6 x 19 x 37.2
Power supply	90-240 VAC 24 VDC	90-240 VAC 24 VDC	100 to 240 VAC	24V DC
Power consumption [W]		100	60	50

LIST OF REFERENCES

Baltsavias, E.(1999) Airborne laser scanning: existing systems and firms and other resources. ISPRS Journal of Photogrammetry & Remote Sensing 54, 164–198.

Baltsavias, E.P. (1999) Airborne laser scanning: basic relations and formulas. ISPRS Journal of Photogrammetry & Remote Sensing 54, 199–214.

Bellian, J.A.; Jennette, D.C.; Kerans, C.; Gibeaut, J.; Andrews, J.; Yssldyk, B.; Larue, D. (2002) 3-Dimensional Digital Outcrop Data Collection and Analysis Using Eye-safe Laser (LIDAR) Technology. Published by AAPG/Datapages, Inc., 1444 South Boulder, Tulsa, OK, 74119, USA Retrieved March, 2007 from http://www.searchanddiscovery.com/documents/beg3d/index.htm.

Bender, Currie, Dickey, Eckhardt, Faller, Kaula, Mulholland, Plotkin, Poultney, Silverberg, Wilkinson, Williams, Alley. (1973). The Lunar Ranging Experiment. Science, New Series, 182, (4109), 229-238.

Bennett, W.R., 2000. Background of an Inversion: The First Gas Laser. IEEE Journal on Selected Topics In Quantum Electronics, 6 (6), 869-875.

Beraldin, J-A; Blais, F; Rioux, M; Domey, J; Gonzo,L; De Nisi,F; Comper,F; Stoppa, D; Gottardi, M; Simoni,A.(2003) Optimized Position Sensors for Flying-Spot Active Triangulation Systems. Proceedings of the Fourth International Conference on 3-D Digital Imaging and Modeling (3DIM'03), October 06 - 10, 2003, Banff, Canada. 2003, 28- 36.

Bureau of Beaches and Coastal Systems (BBCC). Florida Department of Environmental Protection (2004) Monitoring Standards for Beach Erosion Control Projects. Tallahassee, Florida. Retrieved March, 2007 from http://www.dep.state.fl.us/beaches/.

Burkard, R.K. (1983). Geodesy for the Layman (Fourth Revision). Defense Mapping Agency Technical Report TR-80-003. St. Louis, Missouri.

Callens, M., Verhoest, N.E.C. and Davidson, M.W. J.. (2006) Parameterization of Tillage-Induced Single-Scale Soil Roughness from 4-m Profiles. IEEE Transactions on Geoscience and Remote Sensing. 44 (4), 878 – 888.

Carter, W. (1973). The Lunar Laser Ranging Pointing Problem. Unpublished doctoral dissertation, University of Arizona, Tucson.

Carter, W. & Shrestha, R. (1997). Airborne laser swath mapping: Instant snapshots of our changing beaches. In Proceedings of the Fourth International Conference Remote Sensing for Marine and Coastal Environments, Environmental Research Institute of Michigan (ERIM), Ann Arbor, Michigan. p. 298–307.

Carter, W., Shrestha, R., Slatton, K.C., Cossio, T., Shrestha, K. (2005) Geodetic Laser Scanning: Refractive Optics Offer Wide Variety of Scan Patterns. Poster at the American Geophysical Union, Fall Meeting 2005, San Francisco, California.

Cheves, M. (1999). Geodimeter—The First Name in EDM. Professional Surveyor, 19 (2).

Cheves, M. (2002).In the Air, On the Ground: Laser-based Technology from Optech. Professional Surveyor, 22 (10).

Curless, B.; Levoy, M. (1995). Better Optical Triangulation through Spacetime Analysis. Procedings of the Fifth International Conference on Computer Vision (ICCV 95), June 20-23, 1995, Massachusetts Institute of Technology, Cambridge, Massachusetts, USA., 987-994.

Davidson, M.W.J., Toan, T.L., Mattia, F., Satalino, G., Manninen, T., Borgeaud, M. (2000). On the Characterization of Agricultural Soil Roughness for Radar Remote Sensing Studies. IEEE Transactions on Geoscience and Remote Sensing, 38 (2), 630-640.

Defense Mapping Agency (DMA) (1991) Error Theory as applied to Mapping Charting and Geodesy. DMA Technical Report 8400.1, Fairax, Virginia, USA.

Drake, D.R. (2002) Applications of Laser Scanning and Imaging Systems. Unpublished Masters Thesis, University of Florida, Gainesville.

Ewing, Clair & Mitchell, Michael (1970). Introduction to Geodesy. Elsevier North Holland Publishing Company, Inc, New York, New York, USA.

Flood, M. (2001) Laser Altimetry: From Science to Commercial LIDAR Mapping. Journal of The American Society for Photogrammetry and Remote Sensing, 67 (11), 1209-1211.

Fröhlich, C., Mettenleiter, M.(2004). Terrestrial Laser Scanning – New Perspectives In 3d Surveying. Proceedings of the ISPRS working group 8/2 'Laser-Scanners for Forest and Landscape Assessment', Freiburg, Germany, October 3-6, 2004, 7-13.

Guenther, G., Goodman, L., Enabnit, D., Swift, R., Thomas, R.. (1978). Laser Bathymetry for Near Shore Charting Application (Preliminary Field Test Results). Oceans, 10, 390- 396.

Hickman, D., Hogg, J. (1969) Application Of An Airborne Pulsed Laser For Near Shore Bathymetric Measurements Remote Sensing Of Environ, 1 (1), P 47-58.

Hopkinson,C.; Chasmer, L.; Young-Pow, C.; Treitz, P. (2004) Assessing forest metrics with a ground-based scanning LIDAR. Canadian Journal of Forest Research. 34, 573–583.

Iavarone, A (2002) Laser Scanner Fundamentals. Professional Surveyor Magazine, 24 (5).

Institute of Electrical and Electronics Engineers (IEEE). (N.D.). Theodore H. Maiman. Published by the IEEE Virtual Museum, New Brunswick, New Jersey, USA. Retrieved March, 2007, from http://www.ieee-virtual-museum.org/collection/people.php?id=1234591&lid=1.

Institute of Electrical and Electronics Engineers (IEEE). (N.D.). Charles H. Townes. Published by the IEEE Virtual Museum, New Brunswick, New Jersey, USA.Retrieved March, 2007, from http://www.ieee-virtual-museum.org/collection/people.php?id=1234588&lid=1

Institute of Electrical and Electronics Engineers (IEEE). (N.D.). Arthur L. Schawlow. Published by the IEEE Virtual Museum, New Brunswick, New Jersey, USA.Retrieved March, 2007, from http://www.ieee-virtual-museum.org/collection/people.php?id=1234585&lid=1

Javan,A., Bennett, W.R., Herrott, D.R. (1961) Population inversion and continuous optical maser oscillation in a gas discharge containing a He–Ne mixture. Phys. Rev. Lett., 6, 106–110.

Jenkins, J.C.; Chojnacky, D.C.; Heath, L.S.; Birdsey, R.A. 2003. National-scale biomass estimation for United States tree species. Forest Science. 49(1), 12-35.

Kern, J. (2001) Mapping Groud Zero. Professional Surveyor, November 2001, 21 (10)

Kim, H; Cervenka, P; Lankford, C. (1975) Development of an Airborne Laser Bathymeter, NASA Techincal Note D-8079, NASA Wallops Flight Center, Wallops Island, Virginia, USA.

Kraus, N.C. & Galgano, F.A. (2001) Beach Erosional Hot Spots: Types, Causes, and Solutions. US Army Engineer Research and Development Center/Coastal Hydraulics Laboratory. Coastal and Hydraulics Engineering Technical Note ERDC/CHL CHETN-II-44. Vicksburg, Mississippi, USA.

Kaufman, C.C., Batts, E.L., Levine, N.S., Doyle, B.C. (2005) Beach Erosion Mapping Using LIDAR and a 3D Laser Scanner: Folly Beach, South Carolina. Poster presentation at the Geological Society of America (GSA) Annual Meeting 2005, Salt Lake City, Utah, October 16–19, 2005, paper 59-14

Lefsky,M.; Cohen, W.; Parker, W.; & Harding, D. (2002) LIDAR Remote Sensing for Ecosystem Studies. BioScience, 52 (1), 19-30.

Lefsky, M.A.; Cohen, W.B.; Acker, S. A.; Spies, T.A.; Parke3, G.G.; Harding, D. (1998), LIDAR Remote Sensing of Forest Canopy Structure and Related Biophysical Parameters at the H.J. Andrews Experimental Forest, Oregon, USA. Geoscience and Remote Sensing Symposium Proceedings, 1998. IGARSS '98, Seattle, WA, USA. 6-10 Jul 1998, 3, 1252-1254.

Lichti, D.D.; Gordon, S.J. & Stewart, M.P.. (2002). Ground-based laser scanners: operation, systems and applications. Geomatica, 56, 22–33.

Maling, D. H. (1992). Coordinate Systems and Map Projections (2nd Edition). Pergamon, Oxford, United Kindom.

Marino, R.; Davis, W.R. (2005) Jigsaw: A Foliage-Penetrating 3D Imaging Laser Radar System. Lincoln Laboratory Journal, 15 (1), 23-36.

Martel, S.J. (2006) Effect of topographic curvature on near-surface stresses and application to sheeting joints: Geophysical Research Letters, 33 (1) pg:L01308.

Mattia, F.; Davidson, Malcolm W.J.; Toan, Thuy Le; D'Haese, Christophe M. F.; Verhoest, Niko E.C.; Gatti, Anna Maria; Borgeaud, Maurice. (2003) A Comparison Between Soil Roughness Statistics Used in Surface Scattering Models Derived From Mechanical and Laser Profilers. IEEE Transactions on Geoscience and Remote Sensing, 41 (7), 1659-1671.

McClung, F.J. and Hellwarth, R.W. (1962): "Giant optical pulsations from ruby". Journal of Applied Physics, 33 (3), 828-829.

McGarry, Jan; Zagwodzki, Tom. (2005) A Brief History of Satellite Laser Ranging: 1964 – present*. Published by the Crustal Dynamics Data Information System (CDDIS), NASA Goddard Space Flight Center, Greenbelt, Maryland. Retrieved October, 2005, from http://cddis.nasa.gov/slr2000/docs/gsfcslr_jm0504.pdf.

Mitchell, R (N.D.) AOL History - WFF AOL. Published by the Hydrospheric and Biospheric Sciences Laboratory, NASA GSFC/Wallops Flight Facility, Wallops Island, Virginia, USA Retrieved March, 2007, from http://aol.wff.nasa.gov/index.php?module=pagemaster&PAGE_user_op=view_page&PAGE_id=3&MMN_position=3:3.

Næsset, E & Gobakken, T. (2005) Estimating forest growth using canopy metrics derived from airborne laser scanner data. Remote Sensing of Environment 96, 453 – 465.

National Aeronautics and Space Administration (NASA). (N.D.) National Space Science Data Center Apollo Laser Altimeter Experiment. Published by the NASA Goddard Space Flight Center, Greenbelt, Maryland. Retrieved March, 2007, from http://nssdc.gsfc.nasa.gov/database/MasterCatalog?sc=1971-063A&ex=5.

National Oceanic and Atmospheric Administration (NOAA), (N.D.). Distance Measurement Tools, AGA Geodimeter NASM-2A. Published by the NOAA the Office of Public Affairs, Washington, D.C., USA. Retrieved March, 2007, from http://celebrating200years.noaa.gov/distance_tools/0411.html.

National Oceanic and Atmospheric Administration (NOAA), (N.D.). Distance Measurement Tools, Tellurometer. Published by the NOAA the Office of Public Affairs, Washington, D.C., USA.Retrieved March, 2007, from http://celebrating200years.noaa.gov/distance_tools/tellurometermra1.html.

National Oceanic and Atmospheric Administration (NOAA), (N.D.). Distance Measurement Tools, Ranger III and Rangemaster III. Published by the NOAA the Office of Public Affairs, Washington, D.C., USA.Retrieved March, 2007, from http://celebrating200years.noaa.gov/distance_tools/ranger.html.

Oelze, Michael L.; Sabatier, James M.; Raspet, Richard (2003). Roughness Measurements of Soil Surfaces by Acoustic Backscatter. Soil Science Society of America Journal, 67, 241-250.

Parrish, C.E.; Tuell, G.H.; Carter,W.E. and Shrestha, R.L. (2005) Configuring an Airborne Laser Scanner for Detecting Airport Obstructions. Photogrammetric Engineering & Remote Sensing, 71 (1), 37–46.

Perron, Jay Taylor (2006). *Formation of Evenly Spaced Ridges and Valleys*. Unpublished doctoral dissertation, University of California, Berkeley.

Schawlow, A. L. & Townes, C. H. (1958) Infrared and Optical Masers. Physical Review, 112, 1940-1949.

Shrestha, Ramesh (1983). *Local Geodetical Networks Adjustments in Three Dimensions*. Unpublished doctoral dissertation, University of Wisconsin-Madison.

Shrestha,R.L., Carter,W.E., Sartori,M., Luzum, B.J., Slatton, K.C.(2005) Airborne Laser Swath Mapping: Quantifying changes in sandy beaches over time scales of weeks to years. ISPRS Journal of Photogrammetry & Remote Sensing, 59, 222–232.

Smith, James R. (1996). Introduction to Geodesy. John Wiley & Sons, Inc. New York, New York, USA.

Smithsonian National Museum of American History. Virtual Surveying Instrument Collection. (ND). EDM (Geodimeter Model 2A). Published by the Smithsonian National Museum of American History. Washington. D.C., USA. Retrieved March, 2007, from http://americanhistory.si.edu/collections/surveying/object.cfm?recordnumber=748815.

Smithsonian National Museum of American History. Virtual Surveying Instrument Collection. (ND). EDM (Tellurometer M/RA 1). Published by the Smithsonian National Museum of American History. Washington. D.C., USA. Retrieved March, 2007, from http://americanhistory.si.edu/collections/surveying/object.cfm?recordnumber=759173

Smithsonian National Museum of American History. Virtual Surveying Instrument Collection. (ND). EDM (Tellurometer M/RA 1). Published by the Smithsonian National Museum of American History. Washington. D.C., USA. Retrieved March, 2007, from http://americanhistory.si.edu/collections/surveying/maker.cfm?makerid=45

Smithsonian National Museum of American History. Virtual Surveying Instrument Collection. (ND). EDM (Geodolite). Published by the Smithsonian National Museum of American History. Washington. D.C., USA. Retrieved March, 2007, from http://americanhistory.si.edu/collections/surveying/object.cfm?recordnumber=748473

Taylor, Nick (2000). LASER: The inventor, the Nobel laureate, and the thirty-year patent war. Simon & Schuster. New York, New York, USA.

Thoma,D. P., Moran,M.S., Bryant,R., Rahman,M., Holifield-Collins,C.D., Sano,E.E., Slocum, K., Skirvin,S..(2006) Comparison of four models to determine surface soil moisture from C-band radar imagery in a sparsely vegetated semiarid landscape. Water Resources Research, Vol. 42, W01418

Watt, P. J. & Donoghue, D. N. M. (2005) Measuring forest structure with terrestrial laser scanning. International Journal of Remote Sensing, 26 (7), 1437–1446.

Wehr, A; Lohr U. (1999) Airborne Laser Scanning—An Introduction and Overview. ISPRS Journal of Photogrammetry & Remote Sensing 54, 68–82.

Zribi,M., Ciarletti, V., Taconet, O., Boissard, P., Chapron, M. and Rabin, B. (2000) Backscattering on soil structure described by plane facets. International Journal on Remote Sensing, 21 (1), 137-153.

BIOGRAPHICAL SKETCH

Juan Carlos Fernandez Diaz was born August 18, 1976, in Tegucigalpa, Honduras, to Venancio Fernandez and Ana Maria Diaz. His family is also composed by one sister: Maria Esther and two brothers David and Jose Venancio. Since a very young age he developed strong interest towards science and technology; especially to earth and space science, aviation, telecommunications and electronics. He was fortunate to attend an American school (Elvel School) from kindergarten to 11th grade, where the professors motivated his scientific curiosity. He graduated from High School in 1993 from a program that fulfills the requirements from both the American and Honduran academic curriculum. That same year he enrolled on the Electrical Engineering program of the Universidad Nacional Autonoma de Honduras (UNAH). When he did not find college challenging enough he decided to work full time while pursuing the B.S. degree. His first position was as an instructor of the university's astronomical observatory where he acquired knowledge and expertise related to the design, use and maintenance of astronomical instrumentation as well as astronomical data processing and analysis. During this period he also participated in a train ship at the European Space Agency Satellite Tracking Station in Villafranca del Castillo, Spain and received a Summer Undergraduate Research Fellowship (SURF) from the California Institute of Technology (CALTECH) to perform scientific research at the Jet Propulsion Laboratory. Soon after this experience he accepted a new position with the Honduras National Telecommunication Commission as a Spectrum Planning and Engineering technician. He obtained the BS degree in electrical engineering in June 2001 having not only the formal academic knowledge but also a great deal of experience in telecommunications, space science and technology.

From 2002 to 2005 he continued his career in telecommunications holding positions in a Wireless service provider were he performed functions as network planning engineer and quality

assurance chief. He also obtained a Master of business administration degree with a summa cum laude distinction from the Universidad Catolica de Honduras in 2005. During 2004 he applied for a Fulbright Scholarship to participate in a masters program in the fields of Satellite Applications (Navigation, Communications and Remote Sensing). He was fortunate to receive the scholarship and to be accepted to the University of Florida, Geosensing Systems Engineering graduate program.

Juan hopes to continue with his multidisciplinary education, continue to explore his interest in space science and technology and to contribute in some way to mankind progress, especially to the benefit of his fellow Hondureños.